Phase II Demonstration

September 28, 2012

ASCEM-SITE-2012-01

United States Department of Energy

M. Freshley, PNNL
S. Hubbard, LBNL
G. Flach, SRNL
V. Freedman, PNNL
D. Agarwal, LBNL
B. Andre, LBNL
Y. Bott, PNNL
X. Chen, PNNL
J. Davis, LBNL
B. Faybishenko, LBNL
I. Gorton, PNNL
C. Murray, PNNL
D. Moulton, LANL
J. Meyer, LBNL
M. Rockhold, PNNL
A. Shoshani, LBNL
C. Steefel, LBNL
H. Wainwright, LBNL
S. Waichler, PNNL

DISCLAIMER

Printed in the United States of America

Prepared for
U.S. Department of Energy

Authorization:

Mark Freshley, Pacific Northwest National Laboratory — September 28, 2012
ASCEM Site Applications Thrust Lead — Date

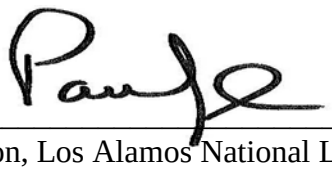

Dr. Paul Dixon, Los Alamos National Laboratory — September 28, 2012
Multi-Lab ASCEM Program Manager — Date

Concurrence:

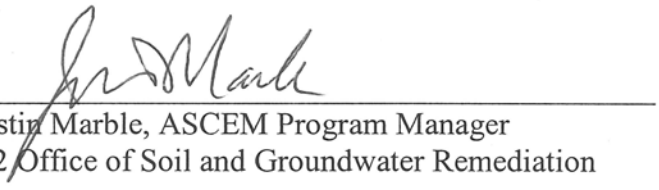

Dr. Justin Marble, ASCEM Program Manager — 09/28/2012
EM-12 Office of Soil and Groundwater Remediation — Date

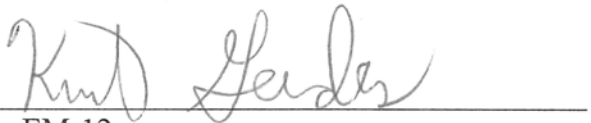

Kurt Gerdes, EM-12 — 9/28/2012
Director for Office of Soil and Groundwater Remediation — Date

This page intentionally left blank

Table of Contents

This page intentionally left blank

ACKNOWLEDGMENTS

Funding for this work was provided by the U.S. Department of Energy Office of Environmental Management. Special recognition is extended to Justin Marble and Kurt Gerdes in Soil/Groundwater Remediation for their support. The project team includes key contributors too numerous to list. These include the software development teams for Akuna and Amanzi as well as other individuals supporting the Site Applications teams.

This page intentionally left blank

LIST OF ABBREVIATIONS

AFRI	Applied Field Research Initiative
Akuna	Advanced Simulation Capability for Environmental Management Platform Toolset
Amanzi	Advanced Simulation Capability for Environmental Management High-Performance Computing Simulator Toolset
AMR	adaptive mesh refinement
AODMS	Advanced Simulation Capability for Environmental Management Observational Data Management System
ASCEM	Advanced Simulation Capability for Environmental Management
BER	Biological and Environmental Research
bgs	below ground surface
BTC	breakthrough curve
CBP	Cementitious Barriers Partnership
CDF	cumulative distribution functions
CEC	cation exchange capacity
CPT	cone penetrometer testing
DOE	U.S. Department of Energy
DS	Decision Support
DVZ	deep vadose zone
EM	U.S. Department of Energy Office of Environmental Management
FMB	Fourmile Branch
FY	fiscal year
GSA	General Separations Area
GUI	graphical user interface
HDF5	Hierarchical Data Format (Version 5)
HPC	high-performance computing
LANL	Los Alamos National Laboratory
LBNL	Lawrence Berkeley National Laboratory
LUTRA	lower aquifer zone of the Upper Three Runs Aquifer
MCL	maximum concentration level
MFD	Mimetic Finite Difference
MLE	maximum likelihood estimation
MNA	monitored natural attenuation
MPC	Multi-Process Coordinator
NERSC	National Energy Research Scientific Computing Center

ORNL	Oak Ridge National Laboratory
PA	Performance Assessment
PE	Parameter Estimation
Platform	Advanced Simulations for Environmental Management Platform and integrated toolsets thrust
PNNL	Pacific Northwest National Laboratory
RA	Risk Assessment
SA	Sensitivity Analysis
SFA	Scientific Focus Area
SR	Simulation Run
SRNL	Savannah River National Laboratory
SRS	Savannah River Site
STOMP	Subsurface Transport Over Multiple Phases
TCCZ	Tan Clay Confining Zone
TIC	total inorganic carbon
UQ	Uncertainty Quantification
UUTRA	upper aquifer zone
Vis	Visualization using VisIt
WMA	Waste Management Area
XDMF	extensible data model and format

URL REFERENCES TO OPEN-SOURCE SOFTWARE AND LIBRARIES

ASCEM	http://esd.lbl.gov/research/projects/ascem/
FLOT	http://code.google.com/p/flot/
Google Maps	http://code.google.com/apis/maps/documentation/javascript/
HDF5 format	http://www.hdfgroup.org/HDF5/doc/H5.intro.html
Mediawiki (Velo)	http://www.mediawiki.org
MOAB	http://trac.mcs.anl.gov/projects/ITAPS/wiki/MOAB
PEST	http://www.sspa.com/pest
PostegreSQL	http://www.postgresql.org/
Python	http://www.python.org/
Semantic Mediawiki	http://semantic-mediawiki.org
Stk_Mesh	http://trilinos.sandia.gov/release_notes-10.2.html
Subversion	http://subversion.apache.org
Trilinos	http://trilinos.sandia.gov/
VisIt	https://wci.llnl.gov/codes/visit/ and http://www.llnl.gov/visit

This page intentionally left blank

EXECUTIVE SUMMARY

In 2009, the National Academies of Science (NAS) reviewed and validated the U.S. Department of Energy Office of Environmental Management (EM) Technology Program in its publication, *Advice on the Department of Energy's Cleanup Technology Roadmap: Gaps and Bridges.* The NAS report outlined prioritization needs for the Groundwater and Soil Remediation Roadmap, concluded that contaminant behavior in the subsurface is poorly understood, and recommended further research in this area as a high priority. To address this NAS concern, the EM Office of Site Restoration began supporting the development of the Advanced Simulation Capability for Environmental Management (ASCEM). ASCEM is a state-of-the-art scientific approach that uses an integration of toolsets for understanding and predicting contaminant fate and transport in natural and engineered systems. The ASCEM modeling toolset is modular and open source. It is divided into three thrust areas: Multi-Process High Performance Computing (HPC), Platform and Integrated Toolsets, and Site Applications. The ASCEM toolsets will facilitate integrated approaches to modeling and site characterization that enable robust and standardized assessments of performance and risk for EM cleanup and closure activities.

During fiscal year 2012, the ASCEM project continued to make significant progress in capabilities development. Capability development occurred in both the Platform and Integrated Toolsets and Multi-Process HPC Simulator areas. The new Platform and Integrated Toolsets capabilities provide the user an interface and the tools necessary for end-to-end model development that includes conceptual model definition, data management for model input, model calibration and uncertainty analysis, and model output processing including visualization. The new HPC Simulator capabilities target increased functionality of process model representations, toolsets for interaction with the Platform, and model confidence testing and verification for quality assurance.

The Platform and HPC capabilities are being tested and evaluated for EM applications through a suite of demonstrations being conducted by the Site Applications Thrust. In 2010, the Phase I Demonstration focused on testing initial ASCEM capabilities. The Phase II Demonstration, completed in September 2012, focused on showcasing integrated ASCEM capabilities. For Phase II, the Hanford Site Deep Vadose Zone (BC Cribs) served as an application site for an end-to-end demonstration of ASCEM capabilities on a site with relatively sparse data, with emphasis on integration and linkages between the Platform and HPC components. Other demonstrations included in this Phase II report included addressing attenuation-based remedies at the Savannah River Site F-Area, to exercise linked ASCEM components under data-dense and complex geochemical conditions, and conducting detailed simulations of a representative waste tank.

This report includes descriptive examples developed by the Hanford Site Deep Vadose Zone, the SRS F-Area Attenuation-Based Remedies for the Subsurface, and the Waste Tank Performance Assessment working groups. The integrated Phase II Demonstration provides test cases to accompany distribution of the initial user release (Version 1.0) of the ASCEM software tools to a limited set of users in 2013. These test cases will be expanded with each new release, leading up to the release of a version that is qualified for regulatory applications in the 2015 time frame.

This page intentionally left blank

1 INTRODUCTION

The U.S. Department of Energy's (DOE) Office of Environmental Management (EM), Office of Soil and Groundwater is supporting development of the Advanced Simulation Capability for Environmental Management (ASCEM) Initiative. ASCEM is an emerging state-of-the-art scientific approach and software infrastructure for understanding and predicting contaminant fate and transport in natural and engineered subsurface remediation systems. The modular and open-source High-Performance Computing (HPC) tool will facilitate integrated approaches that enable standardized assessments of performance and risk for DOE-EM cleanup and closure decisions. The project is organized into three main technical thrust areas (Figure 1.1):

1. Platform and Integrated Toolsets (called Akuna)
2. Multi-Process HPC Simulator (called Amanzi)
3. Site Applications.

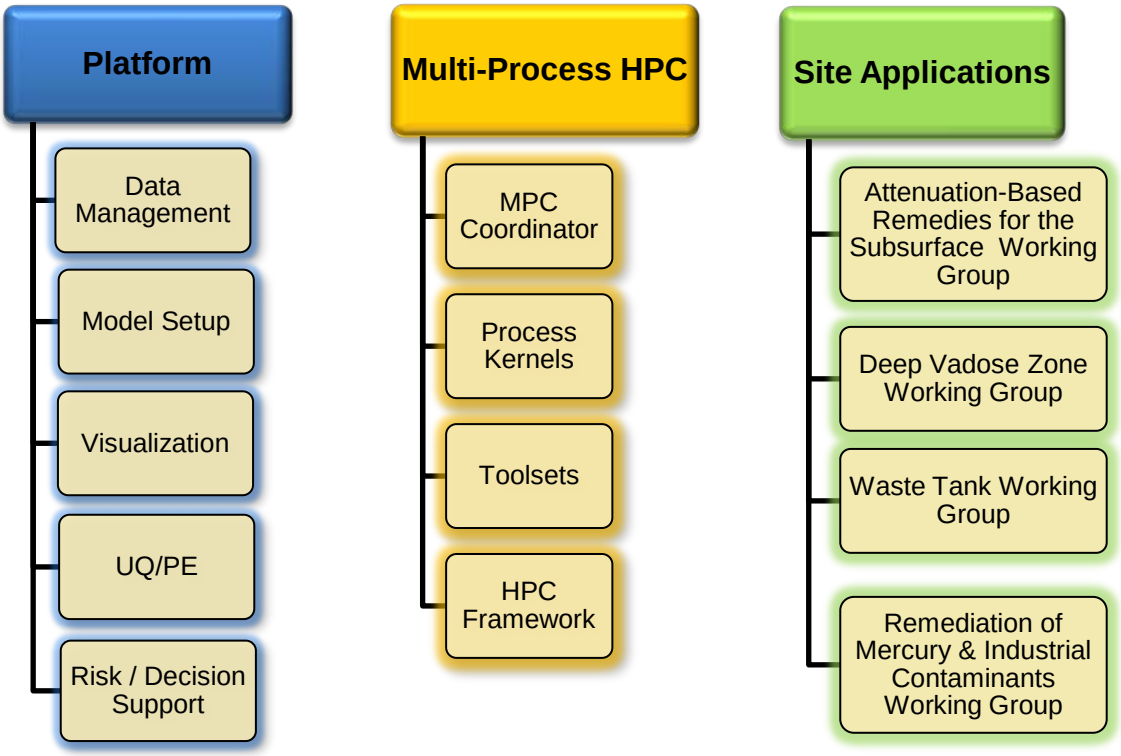

Figure 1.1. ASCEM project organization.

As part of the development process, demonstrations are conducted to test and highlight ASCEM components, engage end users in applications, and provide feedback to software developers. The overall approach for ASCEM demonstrations consists of testing

components and integrated capabilities at an increasing number of DOE sites and with disparate data sets over time.

General goals for the phased demonstrations over the first few years of the ASCEM project are as follows:

- Phase I (2010): Demonstrate selected ASCEM components.
- Phase II (this report): Demonstrate capability to use several ASCEM components in an "end-to-end" mode and to more extensively exercise particular components.
- Phase III (next year): Demonstrate ability to use ASCEM to explore remediation and end-state strategies at DOE sites and engage site personnel in testing capabilities and modeling toolsets.

To perform the Phase II demonstrations, several working groups were formed:

1. Hanford Site Deep Vadose Zone (DVZ) Working Group
2. Savannah River Site (SRS) F-Area Attenuation-Based Remedies for the Subsurface Working Group (hereafter referred to as the SRS F-Area Working Group)
3. Waste Tank Performance Assessment Working Group.

The SRS F-Area Attenuation-Based Remedies for the Subsurface and DVZ working groups both link to Applied Field Research Initiatives (AFRIs). A fourth ASCEM working group has been formed at Oak Ridge, Tennessee, to address the problem of mercury contamination at Oak Ridge National Laboratory (ORNL). This ORNL group has to date focused on initial planning for activities that will start in 2014. These working groups reside in the Site Application Thrust Area but rely on close interactions with developers, end users, and collaborators (including those associated with the EM AFRIs, the Biological and Environmental Research Scientific Focus Areas [SFAs], and the Cementitious Barriers Partnership [CBP]).

The Phase I Demonstration provided an early assessment of advances associated with four specific components of ASCEM: Data Management, Visualization, Uncertainty Quantification (UQ), and HPC. The Phase I Demonstration was conducted over a relatively short time period (4 months) and at an early stage of ASCEM development. As a result, the software development teams performed the bulk of implementation and analyses. For the Phase I Demonstration, the Data Management component adapted and implemented open-source, web-based tools to allow users to easily import, browse, filter, graph, query, and output data sets common to environmental remediation investigations. Visualization capabilities were developed to allow users of the data sets to visualize the information, including depositional and hydrostratigraphic surfaces and the evolution of contaminant plumes. To allow a user to perform uncertainty analyses using a variety of analysis approaches through a graphical user interface, UQ capabilities were developed and tested on the SRS F-Area.

Within ASCEM, the Multi-Process HPC Simulator, called Amanzi, and prototypes of selected toolsets were developed and tested on laptops, desktops, and on several supercomputers. Both unstructured and structured mesh approaches were used to simulate geochemical and hydrological processes using the SRS F-Area data and information. Two supplementary efforts were also initiated to advance new ASCEM capabilities and engage different end-user communities. These advances include implementation of an adaptive mesh refinement approach to more efficiently and accurately simulate potential release from waste tanks, as well as development of several different approaches to quickly visualize simulation and uncertainty output from the waste tank performance assessment example. A graphics viewer, part of the ASCEM Model Setup tool, was developed using data from the Hanford Site DVZ. The graphics viewer allowed the user to visualize conceptual models without the need for third-party software.

The purpose of the Phase II Demonstration is to highlight integration of ASCEM capabilities and continue advancement of the following specific components: Data Management, Visualization, UQ, and HPC. The demonstrations also showcase how ASCEM toolsets can be used to address DOE-EM problems. The DVZ Working Group efforts are focused on a conceptual model scenario that facilitates a complete end-to-end demonstration of ASCEM capabilities with emphasis on integration and linkage between components. The SRS F-Area Working Group and Waste Tank Performance Assessment Working Group efforts focused on demonstrating how some linked components performed under conditions of increased data density and geochemical complexity. The Waste Tank Performance Assessment Working Group exercised HPC using parallel processing to demonstrate adaptive mesh refinement for resolution of fine-scale features in engineered systems.

The Phase II Demonstration followed a major development phase and relied on the Site Applications Thrust Working Group for testing developing capabilities, providing feedback to developers on the relative priority and implementation of new capabilities in association with the three demonstrations. The Phase I and Phase II approach and results were widely presented at meetings, conferences, and workshops, and published in scientific journals and books. A list of publications stemming from the ASCEM project is provided in Appendix A.

In Section 1.1, a brief overview is provided of the Platform and Integrated Toolsets (called Akuna) and the Multi-Process HPC Simulator (called Amanzi); details about each of these ASCEM components are provided in Gorton et al. (2010) and Moulton et al. (2011).

1.1 Overview of Akuna Structure and Capabilities

Development of the Akuna capabilities in the Phase II Demonstration targeted a level of functionality defined by case studies developed by the DVZ, SRS F-Area, and the Waste Tank Performance Assessment Working Groups. These examples defined the primary functionality for the Core Platform, Model Setup and Analysis, Data Management, Parameter Estimation (PE), UQ, and Visualization toolsets. The overall Platform requirements are defined in a specification of system requirements (Gorton et al. 2010). A summary of the current Akuna capabilities is included in Appendix B in Table B.1.

The Akuna Toolset is a collection of Java-based desktop graphical user interfaces (GUIs) to support a complete modeling workflow, from model setup to simulation execution and analysis. The toolset is an open-source, platform-independent user environment that is designed to perform basic model setup, Sensitivity Analysis (SA), inverse modeling PE, UQ, launching and monitoring simulations, and visualization of both model setup and simulation results. Features of the model setup tool include visualizing wells and lithologic contacts, generating surfaces or loading surfaces produced by other geologic modeling software (e.g., EarthVision 2012; Petrel 2012), and specifying material properties, initial and boundary conditions, and model output. The model setup tool uses LaGrit (2012) for generation of both structured and unstructured model simulation grids. Integration with WorldWind (2012) also enables a user to develop a model based on the initial visualization of the site surface topography and geomorphic features.

After creating the model, the Akuna Toolset facilitates launching forward runs to perform a SA, PE, UQ, and visualization of results. Automated job launching and monitoring capabilities allow a user to submit and monitor simulations. Visualization of large outputs can be performed without moving the data back to local resources. These capabilities make HPC accessible to the users, who might not be familiar with batch queue systems and usage protocols on different supercomputers and clusters.

The Akuna Toolset supports a common workflow for developing and applying a numerical model in support of environmental management. Many workflow elements are repeatedly and iteratively performed as part of the modeling process. Figure 1.2 provides a simplified workflow chart. In general, a conceptual understanding of the system to be analyzed is gained from site characterization efforts and monitoring data. This conceptual understanding is then translated into a mathematical model and further implemented in a numerical model. The Akuna Model Setup Toolset supports the development of a numerical model by describing the model domain with its salient hydrogeochemical features, associated material properties, initial and boundary conditions, and forcing terms, as well as information on how space and time are discretized for numerical simulations.

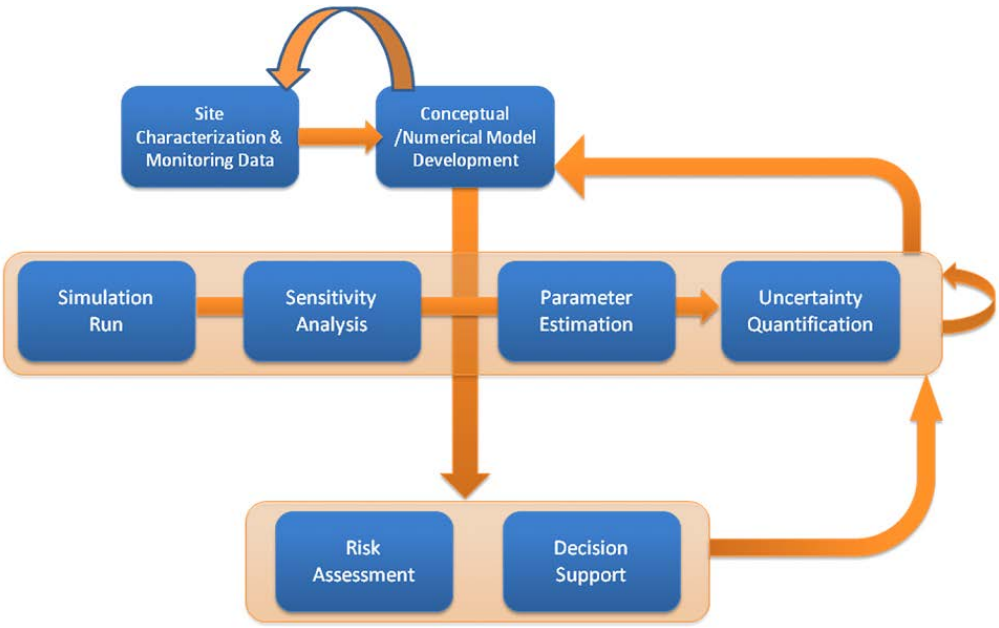

Figure 1.2. Schematic of analysis workflow and supporting Akuna toolsets.

Once an initial numerical model has been developed, the Simulation Run (SR) Toolset is used to launch and monitor a single simulation, the results of which can be analyzed and visualized. In the next step, the Akuna SA Toolset is used to perform a SA to identify parameters that most strongly influence the system behavior, and to examine output variables that are sensitive to model input parameters. These parameters may include material properties, initial and boundary conditions, and generally any aspect of the conceptual model that can be suitably parameterized. The Akuna PE Toolset can be used to automatically calibrate the model using field measurement results. This step not only provides effective parameter values that can be considered consistent with the data collected at the site but also provides estimates of the uncertainty with which these parameters were determined. This information can then be used in the Akuna UQ Toolset to evaluate the uncertainty of model predictions. The Akuna's Risk Assessment (RA) Toolset (future capability) can be used for subsequent assessment of environmental and health risks. As a final step, based on the information from these model analyses, the Akuna Decision Support (DS) Toolset (future capability) can be used to evaluate and optimize performance measures to help manage DOE's legacy sites.

The toolsets integrated in Akuna are transparent and can be flexibly invoked to accommodate any application's particular workflow. Several major components comprising the Akuna architecture are shown in Figure 1.3 and are briefly described below.

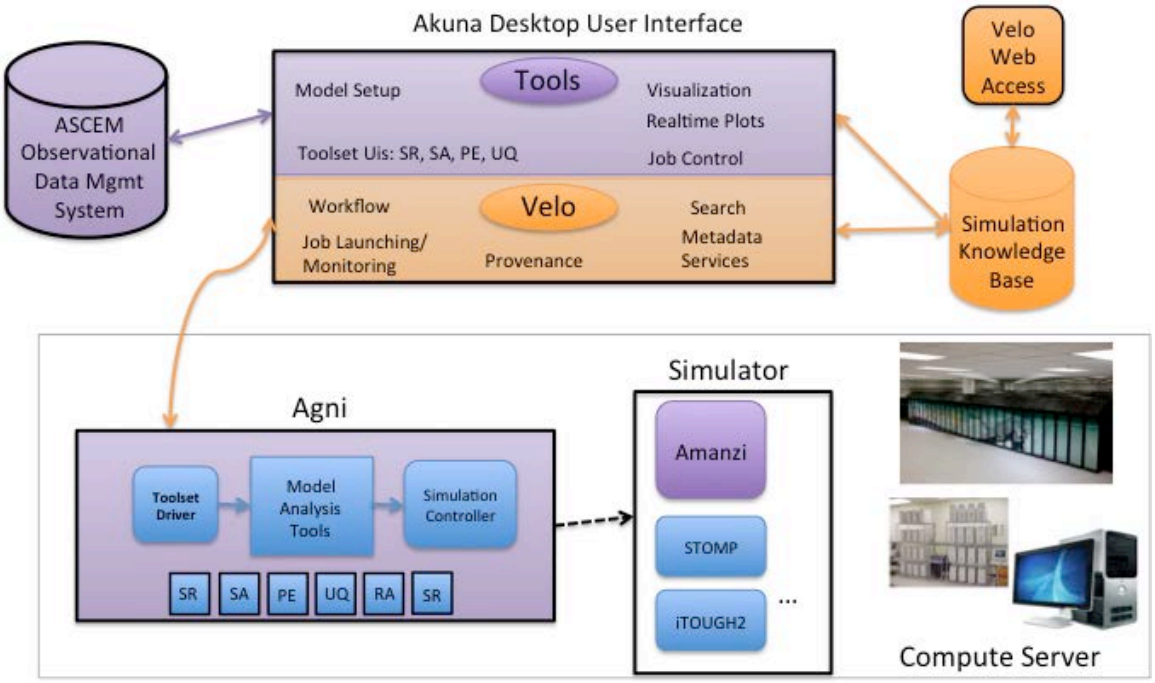

Figure 1.3. Akuna architecture.

The Akuna user interface provides a front end to the simulation workflow. The cross-platform user interface is written in Java and is built on the Velo (Gorton et al. 2011) knowledge management framework. The user interface includes a data browser that provides access to all data, metadata, provenance, and tools associated with the workflow. The VisIt (2012) visualization tool has been integrated to support remote visualization of large-scale outputs. A robust open-source content management system is used to manage workflow data and metadata (Gorton et al. 2011). Shared and private workspaces are supported to enable collaborative modeling.

Agni software—located on the computer server—takes modeling requests from the Akuna client, executes them, and reports information back to the user interface. Agni includes a component for controlling local execution of the simulator as well as the analysis toolsets for SA, UQ, and PE. In the future, tools for risk assessment and decision support will be added.

Amanzi is the main simulator supported by the Akuna platform. However, Akuna and Agni are designed to accommodate other simulators that can be plugged in using a set of defined interfaces. Additional support was provided for several existing simulators, including Subsurface Transport Over Multiple Phases ([STOMP] White and Oostrom 2000, 2006) and TOUGHREACT (Xu 2006, 2012).

The ASCEM Observational Data Management System (AODMS) provides data management capabilities to import, organize, retrieve, and search across various types of observational data sets needed for environmental site characterization and numerical modeling. The AODMS framework provides capabilities to organize, interactively browse on maps, search by filters, select desired data, plot graphs, and save selected data for subsequent use in the modeling process. Figure 1.4 depicts the AODMS design.

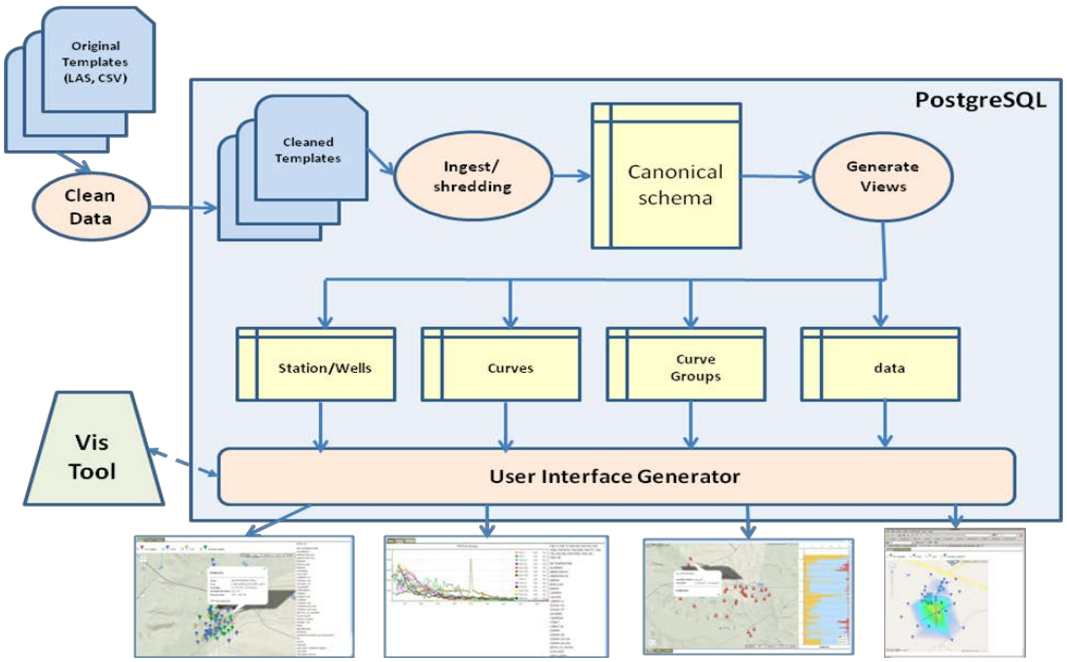

Figure 1.4. Schematic diagram of the Observational Data Management System implementation with examples of the user-interface displays in the bottom row.

As part of the Phase II Demonstration, new visualization templates for VisIt were developed to automate the process of generating meaningful visualizations of structured and unstructured meshes, of model setup and PE results, and for generating two-dimensional and three-dimensional animations from large-scale HPC simulations for selected analytes. The templates, written in Python, enable a user to generate complex visualizations with a single-button click in the Akuna GUI. The templates automatically scale and label axes, select intuitive color schemes and camera angles, and generate animations of time-varying data sets. These data can be viewed in an interactive mode, which allows the user to modify the initial visualization provided by the template to adjust variables, color schemes, and camera angles. The visualization can also be created in the background; for instance, to generate an animation using a large number of simulation output time steps. In this case, when the execution of the parallel rendering code is complete, the resulting images and video animations are returned to the Akuna user interface and displayed as a thumbnail image.

1.2 Overview of Amanzi Structure and Capabilities

The Multi-Process HPC Simulator, named Amanzi, provides a flexible and extensible simulation capability for ASCEM. Amanzi supports a wide range of process complexity in flow and reactive transport models and supports the graded and iterative approach to performance and risk assessment required by EM. Amanzi is designed, developed, and has been tested on a range of computer architectures, from laptops to supercomputers, to ensure that advanced computational power is effectively utilized when it is accessed. A summary of the current Amanzi capabilities is included in Appendix B in Table B.2.

To ensure Amanzi's design and capabilities support the wide range of conceptual models developed by Akuna, a high-level requirements document focused on the underlying complete mathematical formulations of the models was developed first (Steefel et al. 2011). After prototyping key high-level concepts for the Phase I Demonstration (Hubbard et al. 2010), a high-level design document was developed for Amanzi (Moulton et al. 2011). During Phase II development of Amanzi, significant advances were made toward accomplishing this design and establishing capabilities that ASCEM needs in the future. Some of these advances, which are discussed in more detail in this section, include transient saturated/unsaturated flow; the van Genuchten and Brooks–Corey water retention models; a flexible high-level model representation and input specification; a wide variety of geochemical processes, including surface complexation, aqueous speciation, and several sorption models; parallel input/output for visualization and restarts; and a hierarchical verification and validation testing framework. Amanzi has performed parallel 3-D single runs on over 1000 processors using the Hopper Cray XE6 at the National Energy Research Scientific Computing Center (NERSC) and is readily driven by Akuna/Agni for UQ and PE studies.

The Multi-Process HPC Simulator takes as input a conceptual model, which describes a set of coupled processes such as flow and reactive transport. The conceptual model is expressed mathematically by a system of differential and algebraic equations that represent the relevant conservation laws, constitutive laws, equations of state, and reactions. Various parameters required for the model are specified, along with initial and boundary conditions. To represent this system of equations on a computer, a mesh (grid) is provided with the model. A mesh may be thought of as a collection of discrete cells or grid blocks that fill the domain of interest. For a given mesh, a relationship between variables (e.g., pressure), parameters (e.g., permeability), and mesh geometry is developed. This process is referred to as discretization and gives rise to a system of equations that represent the model. This discretized system of equations is often nonlinear and must be iteratively solved to determine the quantities of interest, such as the concentration of particular contaminants.

The hierarchical and modular design of the Multi-Process HPC Simulator reflects the steps in translating a conceptual model to a numerical model producing output for analysis. At the highest level, the Multi-Process Coordinator (MPC) and the Process Kernels represent the conceptual model (Figure 1.5). The Process Kernels are high-level objects that represent processes such as flow, transport, and reactions. Mathematically, a Process Kernel represents a specific set of differential and algebraic equations. The MPC manages the coupling of all the Process Kernels that comprise the conceptual model as well as the data associated with the conceptual model.

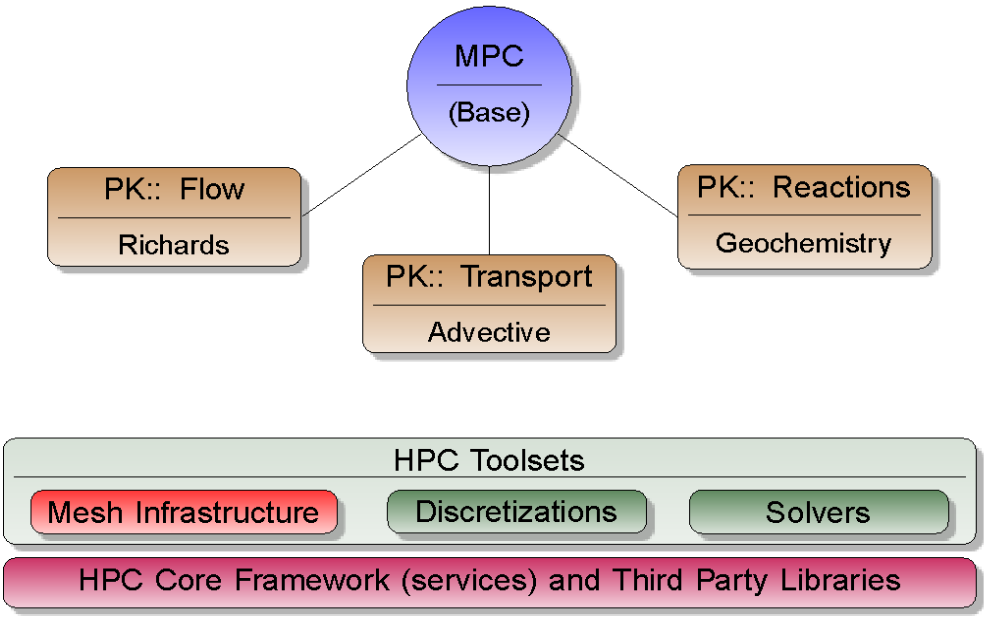

Figure 1.5. Schematic showing a base Multi-Process Coordinator that has instantiated Process Kernels (PK) for flow, transport, and reaction modeling.

At the next level of design, the HPC toolsets include Mesh Infrastructure, Discretization, Reactions, and Solvers. The Mesh Infrastructure Toolset provides interfaces and supporting routines to leverage existing mesh representation libraries. The Discretization Toolset provides procedures that generate the discrete system of equations from a given continuum model on a mesh. The Reaction Toolset implements geochemical reactions such as aqueous speciation and sorption. At the lowest level, the HPC Core Infrastructure provides low-level services such as data structures to operate on parallel computers, input and output, and error handling.

The Phase II Demonstration provided an excellent test-driven environment for the prioritization, development, and testing of new Amanzi features. At the highest level, Process Kernels have been added or their capabilities have been enhanced to support these demonstrations. In addition, new capabilities have been added to the MPC to manage these processes during simulation, control output for observations and visualization, and initiate input and output associated with parallel restarts. These high-level capabilities have been supported by significant advances in the underlying HPC toolsets (e.g., mesh infrastructure, discretization, reactions), as well as the HPC Core Framework. The following high-level input specifications ensure that a user can focus on the model description in geologic and geometric terms without being overly concerned with the underlying computational approach:

- Execution control: This feature enables Process Kernels to be easily turned off or on, readily isolating flow, transport, or reactive transport for verification and benchmarking studies, or to select only the processes needed for the given conceptual model.
- Regions: This feature provides a convenient way to label any part of the model domain, including volumes, areas, segments, and points. After regions are defined, boundary

conditions, material properties, and other elements can be defined on them. Regions are defined either in the unstructured mesh file or by geometric descriptions in the input file (e.g., a box with low, high corners).

- Materials: This feature provides a convenient section of the input to give working names to the common materials in the domain, and assign them the properties needed by the model. For example, a material could be named "Sandy Loam," and then its flow properties, including its water-retention model, could be assigned to it. Each material property has a list of regions to which it applies.
- Boundary conditions/initial conditions: These conditions are assigned to regions and may use polynomial functions in space and time as well as standard tabular input. The most commonly used function is a constant in space over a specified time interval.
- Output: The most common output is for visualization, which writes out values of a particular field quantity over the whole domain in parallel, and for observations corresponding to specific data (location and times) that are used for PE and UQ studies. To accommodate these and other types of output, macros have been created that allow the user to give a name to a desired time sequence so it can be used in all types of output and for all fields.
- Restarts: The data file for restarting Amanzi from a previously simulated time plane is output at user-specified times. This enables restarting simulations from a previously calculated condition that can be used as a common starting point for multiple scenarios (e.g., UQ studies) or to re-enter a simulation just before an unexpected failure occurred for debugging purposes. Checkpoint files for restarts, as well as output for visualization, are written in parallel using Amanzi's extensible data model and format (XDMF)/Hierarchical Data Format (HDF5) capabilities.

In addition, a portable build system has been developed to enable the use of Amanzi on a wide variety of modern architectures. Automatic builds and tests run nightly and are documented to provide quality assurance.

2 PHASE II DEMONSTRATION

Unlike the Phase I Demonstration, Phase II working group efforts were performed sequentially rather than in parallel. This approach allowed developers to focus on advances needed to meet specific objectives of one demonstration at a time. The approach also allowed each demonstration to build on previously developed capabilities. The focus of the DVZ Working Group was to demonstrate a simple but complete beginning-to-end demonstration of ASCEM capabilities. The SRS F-Area Working Group demonstration focused on implementing some of the linked ASCEM capabilities under conditions of dense and complex environmental data, including reactive chemistry, source-term uncertainty, and linked vadose zone and saturated flow. The waste tank demonstration emphasized visual analysis tools for model sensitivity as well as HPC.

The following sections provide a summary of goals and highlights of the Phase II Demonstration for the three working groups.

2.1 Deep Vadose Zone Working Group

The DVZ AFRI at the Hanford Site provides an opportunity to demonstrate ASCEM capabilities needed to evaluate innovative treatment technologies for recalcitrant contaminants. For example, a technology currently under evaluation at the BC Cribs waste site is soil desiccation, an approach that minimizes technetium-99 movement in the vadose zone by removing pore water via the injection of dry air and vapor extraction. The first step in using modeling to evaluate possible technologies for implementation is an analysis of contaminant transport. Future demonstration phases will include explicit representation of soil desiccation as well as other remediation approaches, such as foam delivery or ammonia gas treatment of uranium. These remediation technologies are being developed by the DVZ AFRI or by the DOE Richland Operations Office (the Hanford Site DOE field office).

The primary objective of the Hanford Site DVZ Phase II Demonstration is to illustrate end-to-end integration of Platform and HPC components, from the Data Management and Model Setup and Analysis toolsets to PE and UQ. The Platform Toolset was executed to import and manage data from the BC Cribs waste site, visualize multiple conceptual models, facilitate PE and uncertainty analysis, and set up and execute Amanzi simulations. In the end-to-end demonstration, integration of Platform and HPC components is demonstrated through the model setup, execution, and analysis of Amanzi simulations that evaluate flow and transport at the DVZ site. Additional simulations were performed with eSTOMP, the scalable implementation of STOMP (White and Oostrom 2000, 2006). Simulations using eSTOMP were used to benchmark Amanzi and also permitted testing of the Akuna Toolsets while Amanzi was still under development. The results from executing eSTOMP are presented in Section 2.1.4, which discusses uncertainty in future recharge rates with respect to multiple realizations of the geological conceptual model. The use of parallel processing in the HPC toolset makes execution of multiple simulations feasible, and the Akuna Toolset streamlines this process. Illustrative examples of the toolsets are included in this section of the report.

2.1.1 Background and Problem Description

From 1943 through 1989, the primary mission of the Hanford Site was the production of nuclear materials for national defense. The BC Cribs are located in the 200-East Area of the Central Plateau; their location is part of a larger area known as the BC Cribs and Trenches (Figure 2.1). The BC Cribs area includes six relatively small cribs (12.2 m^2 at the bottom) that received scavenged waste from uranium and ferrocyanide recovery processes that occurred from 1956 to 1958. This waste is described as "scavenged" because most of the highly radioactive cesium-137 was chemically removed. Discharges to these liquid waste disposal sites were limited to avoid exceeding the estimated capacity of the soil to retain the liquid above the water table. These sites received waste in large quantities (~42,000 L at a time) from a siphon tank that—when full—automatically flushed its contents through a pipe to the crib (DOE 1992). This practice resulted in elevated technetium-99 and nitrate concentrations in the 107-m thick vadose zone. To date, the contamination has migrated to approximately 70 m below ground surface (bgs), and has the potential to contaminate groundwater in the future. Groundwater protection is a primary goal of remediation; therefore, intervening strategies are being evaluated.

Contaminant remediation in the DVZ poses unique challenges because conventional remediation technologies (such as pump and treat) are ineffective, and excavation and removal of the contaminated sediments is impractical. The heterogeneous nature of the Central Plateau vadose zone also confounds contaminant distribution and extent in the subsurface. Because the affected vadose zone is more than 100 m thick, thorough characterization using traditional sampling is cost and resource prohibitive. At the BC Cribs, characterization data are sparse, and one of the major geological units—the Hanford formation—is known to contain relatively thin fine-textured lenses that could enhance lateral spreading of water and contaminants and reduce the vertical movement of contaminants (Ward et al. 2009). Because flow and transport in variably saturated porous media is determined by its structure—especially the connectivity of heterogeneous unsaturated conductivities—this factor presents a source of uncertainty in the conceptual model at the BC Cribs waste site.

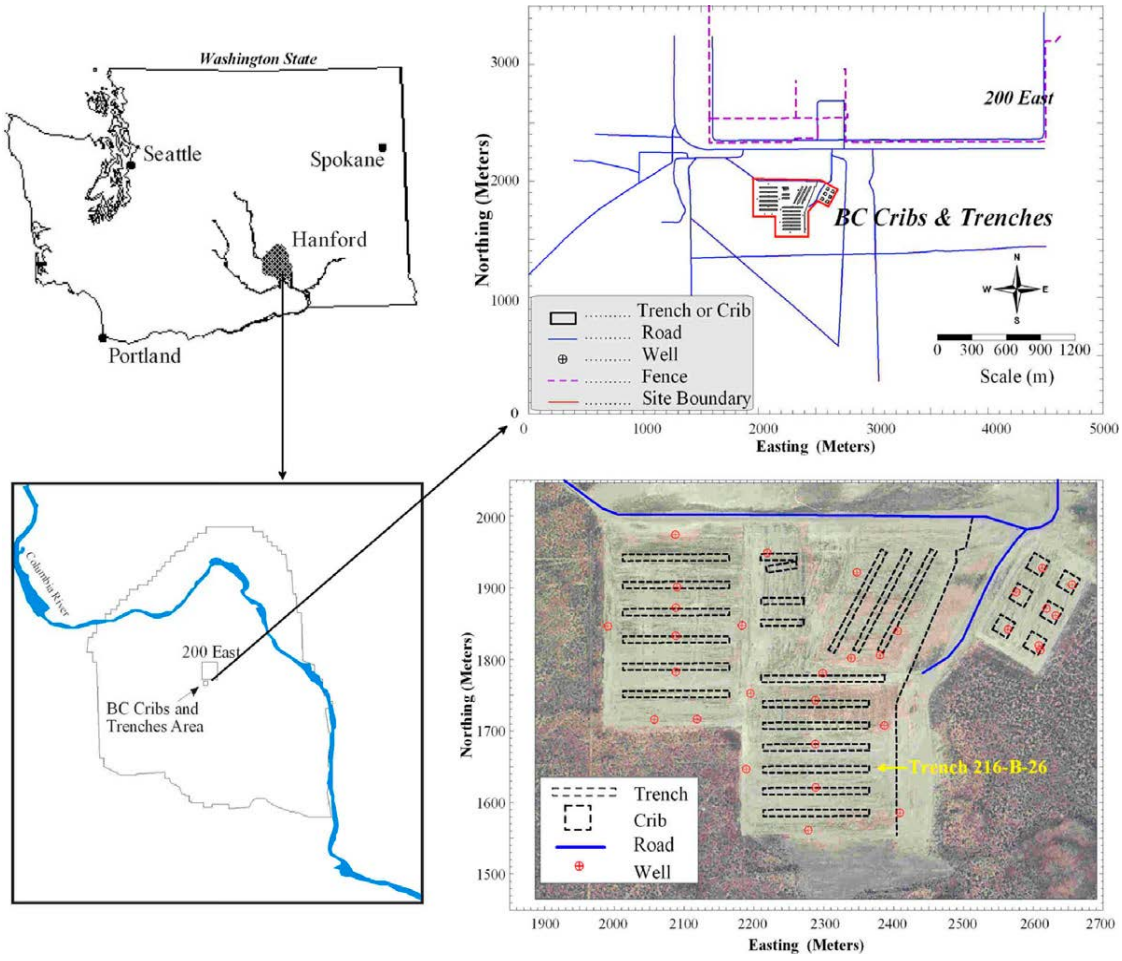

Figure 2.1. BC Cribs and Trenches Waste Management Area at the Hanford Site (from Rucker and Fink 2007).

The primary contaminant of concern, technetium-99, is a long-lived radionuclide with a half-life of 2.13×10^5 years. The Hanford Site vadose zone is oxidizing, so the presumed technetium species is a pertechnetate anion, TcO_4^-, which exhibits high mobility under these

conditions (Icenhower et al. 2008). The complexity of the vadose zone and the conservative transport and recalcitrant nature of technetium-99 combine to make the Hanford Site DVZ a challenging remediation problem.

Soil desiccation is at the forefront of potential remediation technologies that could be deployed at the BC Cribs waste site. Desiccation applied to the DVZ has the potential of minimizing downward contaminant migration of water and contaminants toward the water table. The technology consists of injecting dry air and withdrawing an equal volume of wet air in an array of wells. In combination with surface flux control such as surface barriers, the technology can be used to immobilize contamination by reducing aqueous-phase transport (Ward et al. 2008; Truex et al. 2011).

2.1.2 Deep Vadose Zone Conceptual Model

A cross-section of the stratigraphy at the BC Cribs and Trenches Waste Management Area (WMA) is in Figure 2.2a and Figure 2.2b, which shows the WMA in plan view, with the eastern portion of B-B' extending into the BC Cribs area. The cross-section shows the area consists of various sand and gravel units of the Hanford formation to a depth of about 73 m. From 73 m to 107.5 m, the layers consist of are sand and gravel units of the Hanford formation and/or Cold Creek Unit. Within the saturated zone are sediments of the Ringold Formation that overlie the Columbia River Basalt Group.

Within the Hanford formation, multiple beds of fine- to coarse-grained sand can exist up to several meters thick. These beds of sand may grade back and forth between coarse sand to fine sand multiple times, with the finer-grained materials retaining more moisture retention due to the stronger capillary forces within these finer sediments (Serne et al. 2009). At the BC Cribs, hydraulic conductivity varies strongly with moisture content and is highly anisotropic.

In outcrops of the Hanford formation, fine-grained facies generally appear to be continuous and can be traced laterally for hundreds of meters (Serne et al. 2009). However, it is difficult to correlate individual beds from one borehole to another. Because heterogeneities likely exert important controls over flow patterns, they need to be captured in models used for predicting flow and transport. Hence, a stochastic method was used to develop a facies-based geologic conceptual model at the BC Cribs. The lithofacies used in mapping the BC Cribs area were identified based on analysis of the spectral gamma ray data from four deep wells in the BC Cribs area. Three lithofacies were identified by clustering thorium-232 and potassium-40 data. Facies one was identified as dominantly sand, facies two as sandy gravel, and facies three as muddy sand. Details on the development of the lithofacies model and geostatistical generation of the conceptual model realizations are described in Appendix C.

One hundred realizations of the geologic conceptual model were generated. Ten models were sampled from the full suite of 100 realizations and used in the Phase II Demonstration to estimate the variability in system response. Block diagrams that demonstrate the extent of the variability in the lithofacies distribution are shown in Figure 2.3. These diagrams demonstrate that the large-scale features are maintained, but small-scale differences in the lithofacies distributions vary between the different realizations of the conceptual model.

a)

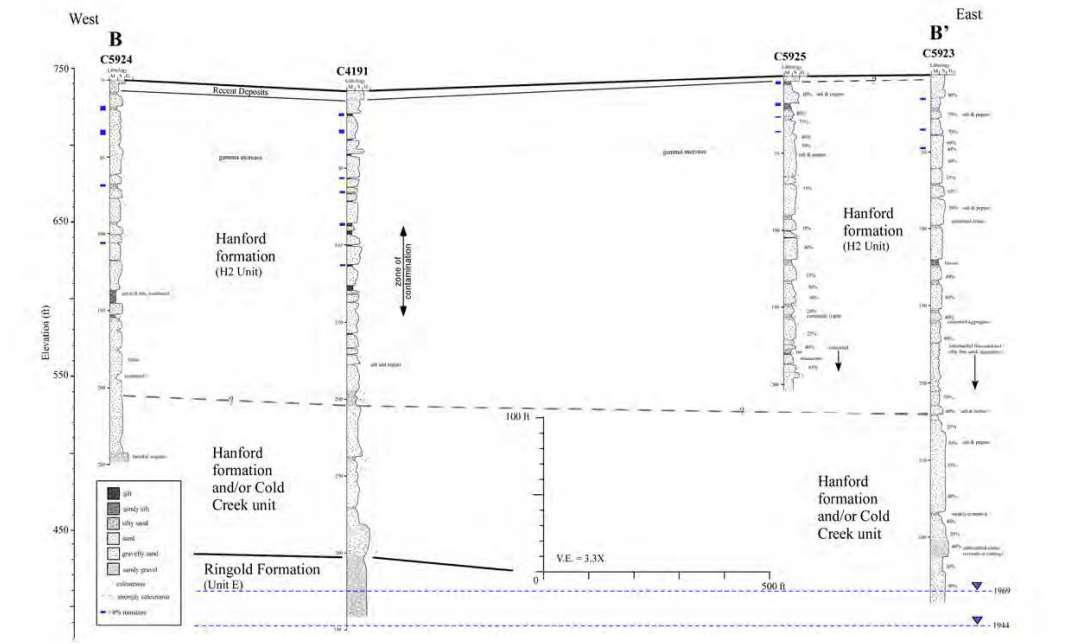

b)

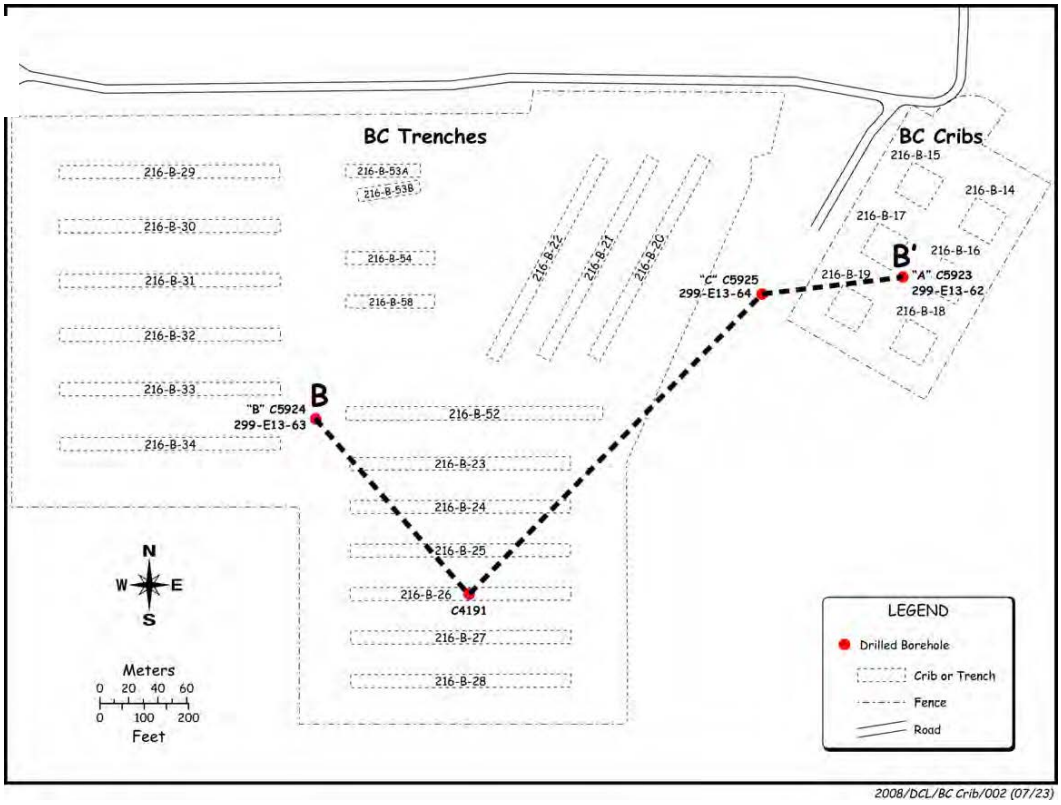

Figure 2.2. a) Cross Section B-B' BC Cribs and b) BC Cribs and Trenches Area Map (from Serne et al. 2009).

The simulation domain extended to 320 m in the X-direction and 280 m in the Y-direction. The grid was discretized at a 5-m resolution in both horizontal directions and at a 1.0-m resolution in the vertical. This yielded a total of 383,488 nodes in the simulation domain.

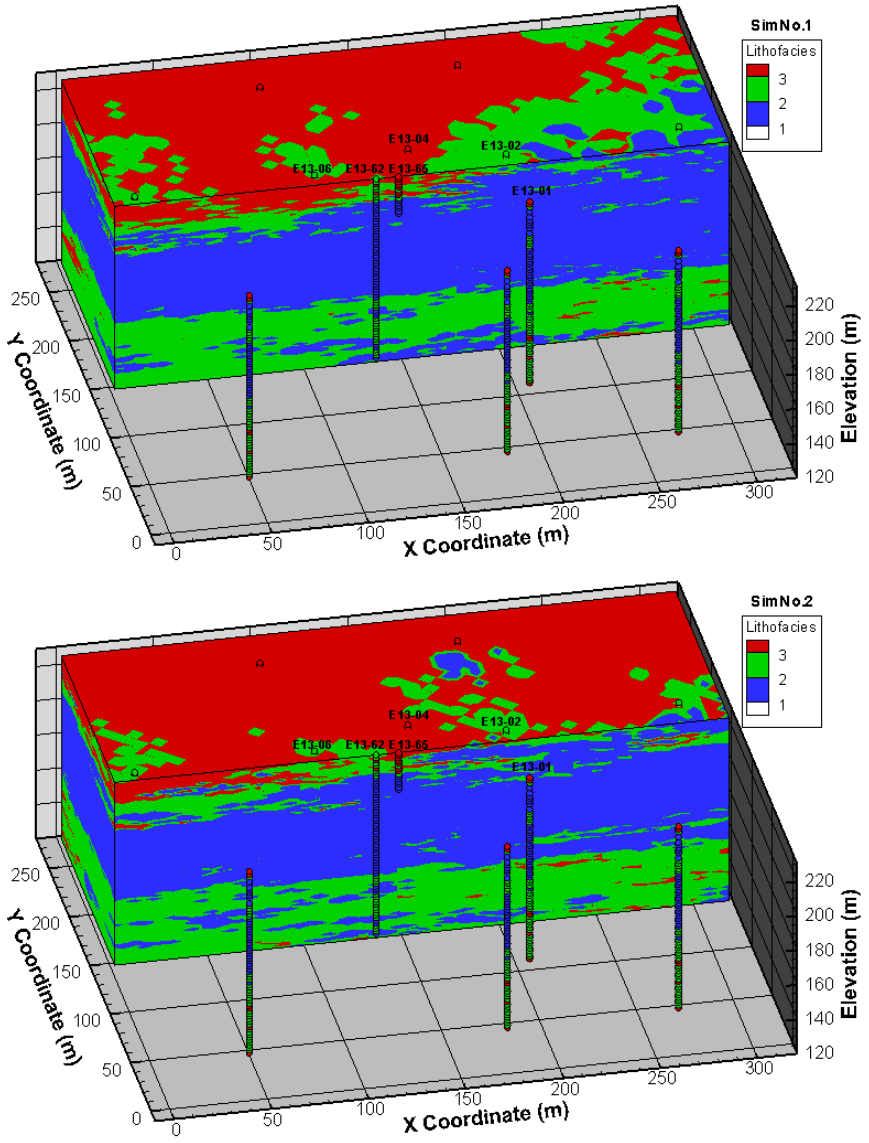

Figure 2.3. Transect near Wells 299-E13-62 and 299-E13-65 of the first two realizations of lithofacies distributions.

2.1.3 End-to-End Demonstration Results

The Phase II Demonstration for the DVZ Working Group includes integration of the Core Platform, Data Management, Model Setup and Analysis, PE, UQ, Visualization, and HPC toolsets. This integration is demonstrated by showing each step of the modeling process for one of the geostatistical realizations of the BC Cribs conceptual model. This section presents a general description of model setup and execution using Akuna without describing the simulation results. An analysis of the results is provided in Section 2.1.4 with respect to UQ for all 10 of the conceptual model realizations.

2.1.3.1 High-Performance Computing and Amanzi

The DVZ Working Group worked with the Amanzi development team to ensure that the simulator had the capabilities needed to perform simulations at BC Cribs for the end-to-end demonstration. Specifically, an ability to simulate variably saturated flow and conservative solute transport was needed for the demonstration. Because of the highly nonlinear nature of the unsaturated hydraulic properties at BC Cribs, the Brooks and Corey water retention model with Burdine permeability were incorporated into the simulator in addition to the van Geunuchten water retention and Mualem permeability models. Anisotropic hydraulic conductivity was also incorporated in the Amanzi simulator. A critical factor in simulating flow and transport at BC Cribs is the representation of small-scale heterogeneities. The ability to read the geology specification from an external input file was included to satisfy this requirement.

The DVZ Working Group also performed testing of Amanzi's transient Richards Equation Process Kernel, including benchmark simulations with STOMP. These studies used a simple three-layer model that included some of the key problem characteristics, such as the computation of an initial steady-state flow and saturation field and subsequent time event control for piece-wise constant boundary conditions. Adaptive time-stepping algorithms were improved with testing on the DVZ problem.

The end-to-end demonstration was initially performed in two dimensions using a synthetic data set, which provided a case for testing the Akuna Toolset and linkages with Amanzi. A realistic depiction of flow and transport at BC Cribs, however, requires a three-dimensional domain. Amanzi was used to simulate the historical releases at each of the six cribs in three dimensions, as described in the following sections. Time event controls were used for each of the six crib discharge periods. This three-dimensional problem, which has a total of 383,488 cells, was run on 192 cores of Hopper (Cray XE6 at NERSC). Typical run times were between 1.5 and 4 hours depending on the input parameter values (e.g., permeability of the facies and infiltration rates).

2.1.3.2 Akuna

The Akuna Toolset applied by the DVZ Working Group included the Core Platform, Data Management, Model Setup and Analysis, Simulation Execution, PE, Visualization, and UQ.

2.1.3.3 Core Platform

Akuna provides the primary user interface for accessing data, and executing the Core Platform. In the BC Cribs example, the Akuna Core Platform provided access to a data server that has both a private and public workspace (Figure 2.4). This workspace allows the user to organize and manage projects, or simulations and data that support them, in a data tree structure, which is displayed on the left-hand side of Figure 2.4. In Figure 2.4, the right-hand side shows that BC Cribs simulations were executed using the job launching and monitoring tools. A forward run (named 001 in Figure 2.4) was launched on the NERSC system (Hopper) and successfully completed.

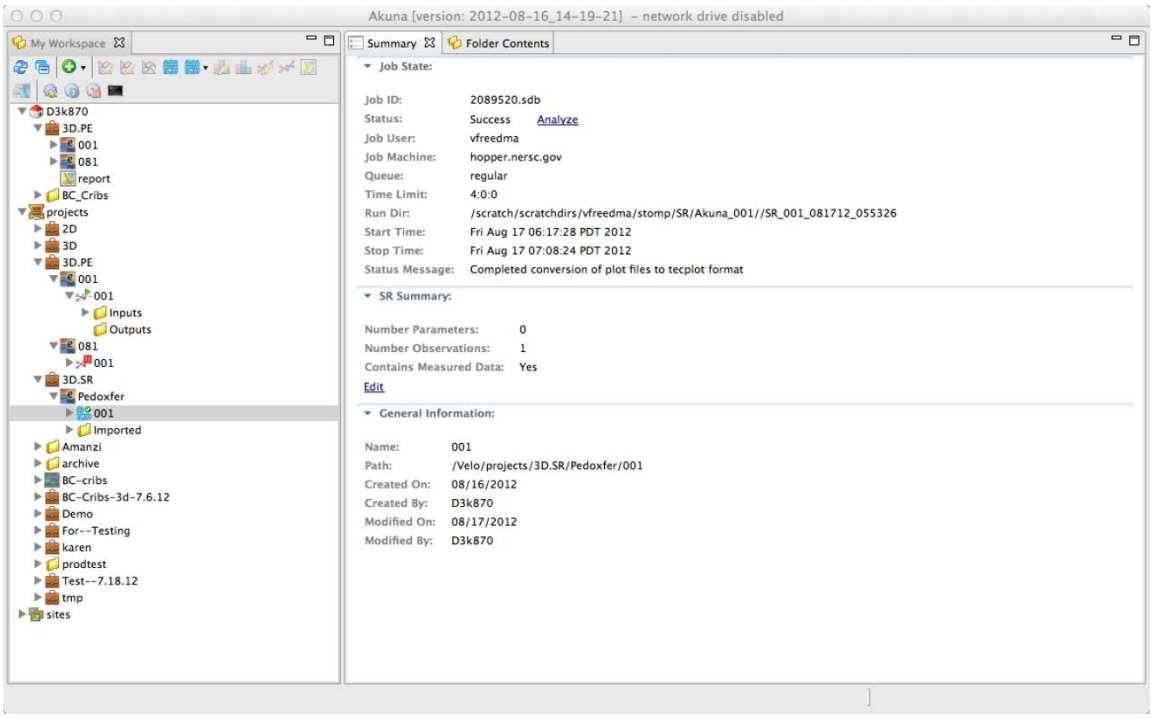

Figure 2.4. Screenshot showing directory structure and summary information for a Simulation Run.

Within the directory structure, simulation input and output data can be stored. The user interface gives the user options for creating either a project or a folder. Once a project is created, a new model is created. That model can then be used to launch other parts of the Akuna Toolset, such as PE, UQ, SA, or a forward SR.

2.1.3.4 Data Management

Environmental data often originate from a variety of different sources and in disparate formats and scales. The Data Management Toolset provides a state-of-the-art database platform from which to integrate, organize, and access these data. The BC Cribs and Trenches WMA has a sparse data set. The Data Management Toolset was used to collect and organize gravimetric water content and concentration data available for Boreholes A, B and C. A plan view of the BC Cribs Site in Model Setup and Analysis using Google Maps® is shown (Figure 2.5). Note that Borehole B is located near the trenches at some distance from the cribs, and is not within the BC Cribs simulation domain (Figure 2.6). Only Boreholes A and C were extracted from the database and used in the BC Cribs modeling.

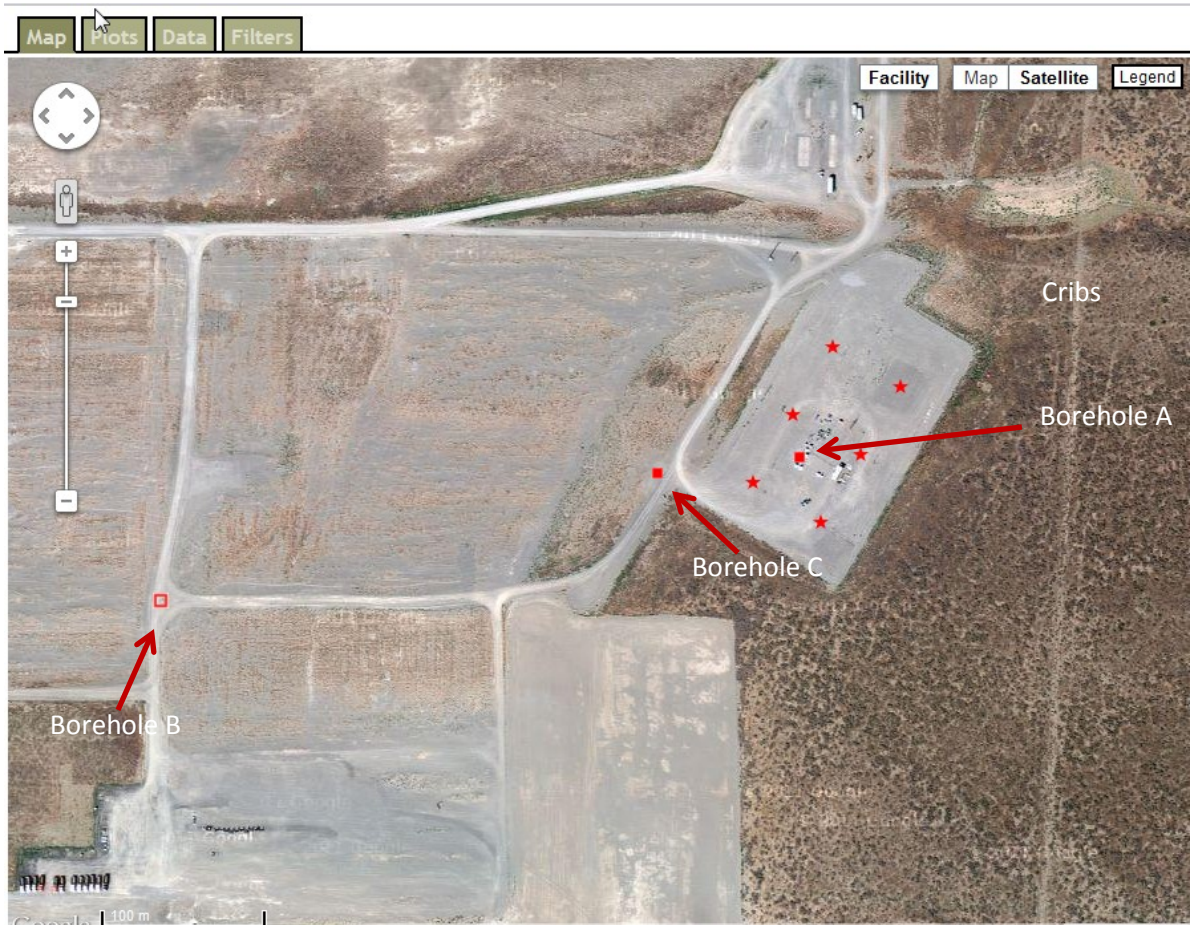

Figure 2.5. BC Cribs and Trenches site with crib locations marked with stars and boreholes with squares.

The borehole locations in Figure 2.5 are links that provide access to the data of interest. Data from more than one borehole can be accessed simultaneously. Figure 2.7 shows a graph of moisture content and technetium-99 concentration with depth at Boreholes A and C. These data can be exported from the data management system in user-specified formats. For the BC Cribs analysis, data were exported in a comma-delimited file format compatible with the measured data format in Akuna needed for performing the model calibration.

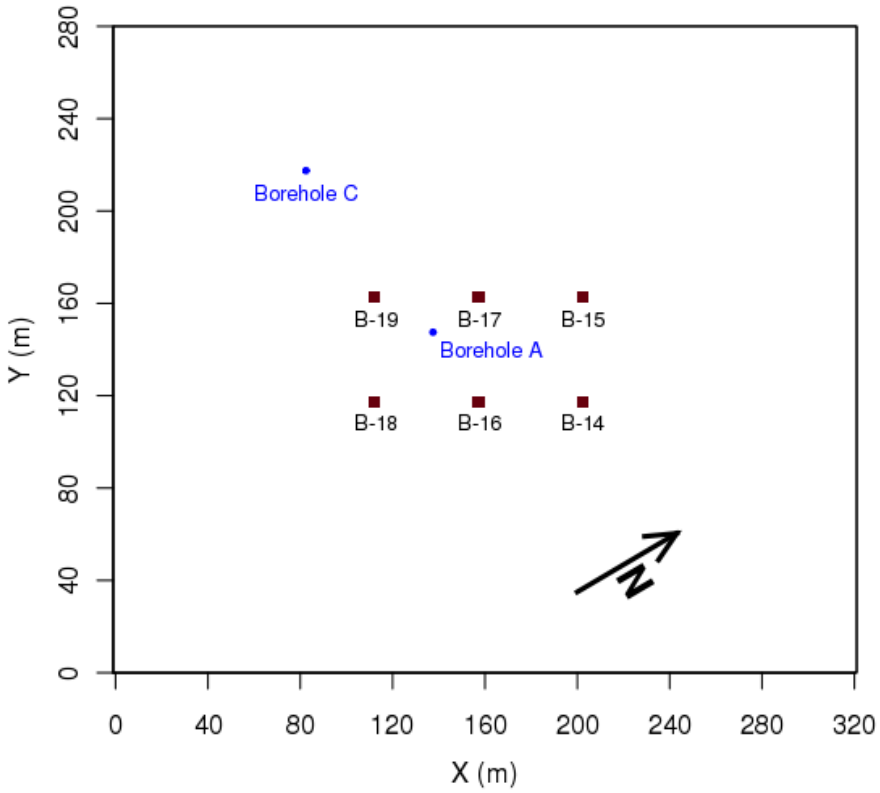

Figure 2.6. Map of the BC Cribs and boreholes used in the analysis.

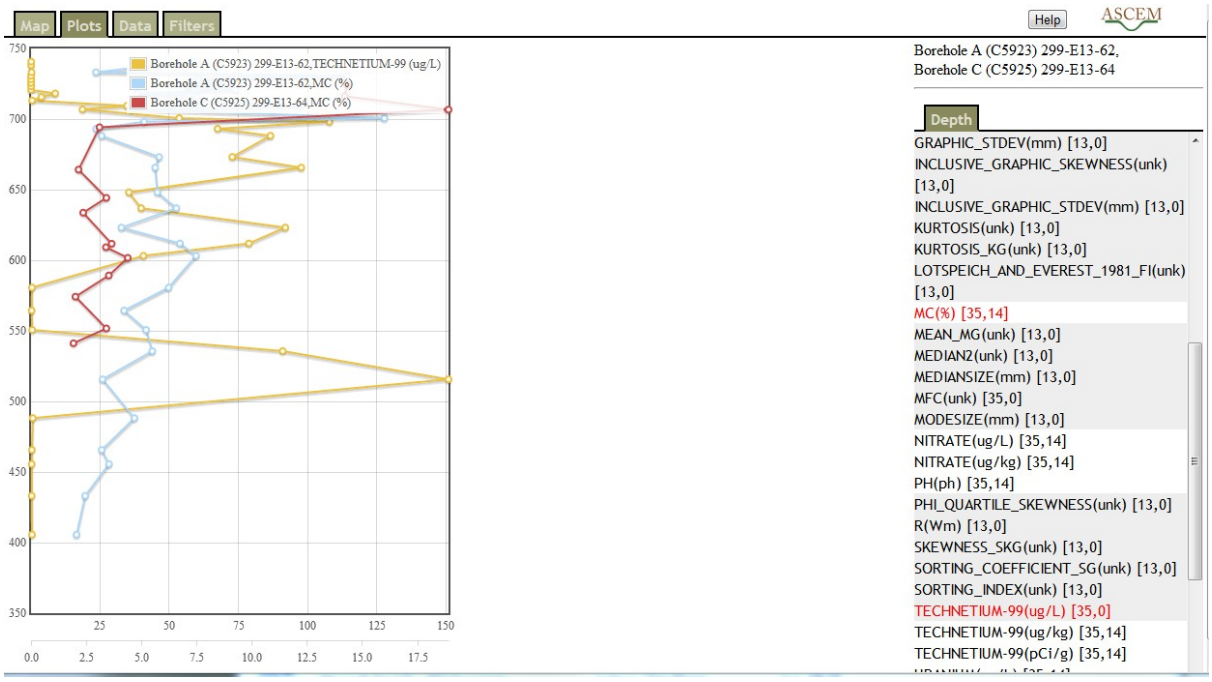

Figure 2.7. Plot of moisture content and technetium-99 concentrations for Boreholes A and C through the Akuna Data Management tool.

2.1.3.5 Model Setup and Analysis

The Model Setup and Analysis Toolset allows simulation input file generation in a fast and user-friendly way. When a new model is created in Akuna, the user is led through steps to define 1) a Geologic Model (e.g., domain extent and geologic layers); 2) Inputs (e.g., material properties, boundary and initial conditions); 3) Outputs (e.g., checkpoint and visualization data); and 4) Execution Controls (e.g., solver parameters, time-step control periods). The geologic conceptualization of the BC Cribs involved multiple conceptual models generated outside of Akuna (as described in Section 2.1.2 and Appendix C) and lithofacies were assigned on a cell by cell basis via a file read (Figure 2.8). The other option for defining the geologic model involves defining stratigraphic layers (surfaces) and the Model Setup and Analysis Toolset fills in regions of the model in between the surfaces.

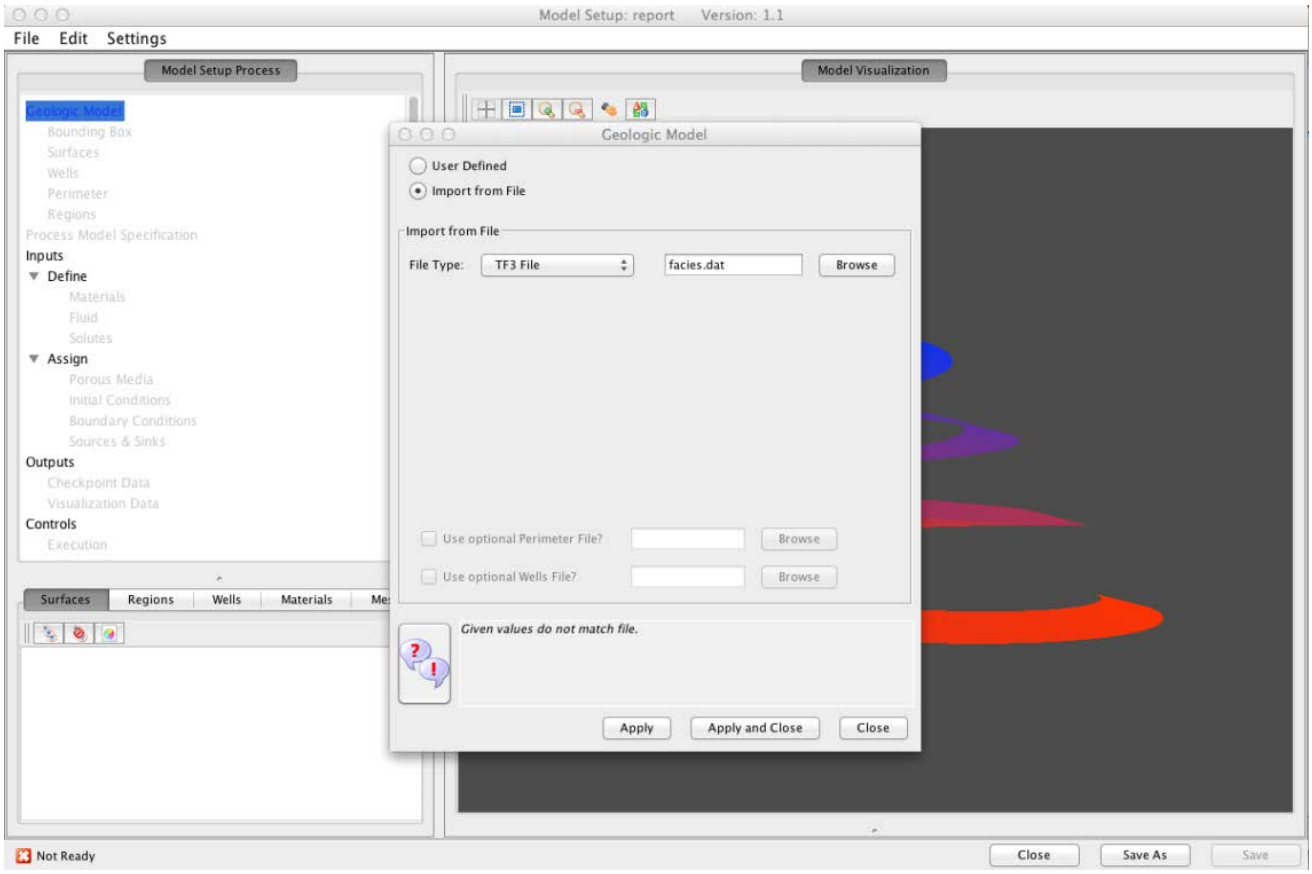

Figure 2.8. Akuna Model Setup and Analysis Tool.

Regions were defined to represent the locations of the six cribs using the Regions tab shown in Figure 2.8. Operational discharges to each of the cribs were represented as a flux boundary for flow and a fixed concentration boundary for technetium-99. Time-averaged water flux and technetium-99 concentrations were input into the Model Setup Tool as shown in Figure 2.9. A screenshot from Model Setup and Analysis (Figure 2.10) shows the locations of the six cribs and two boreholes in plan view.

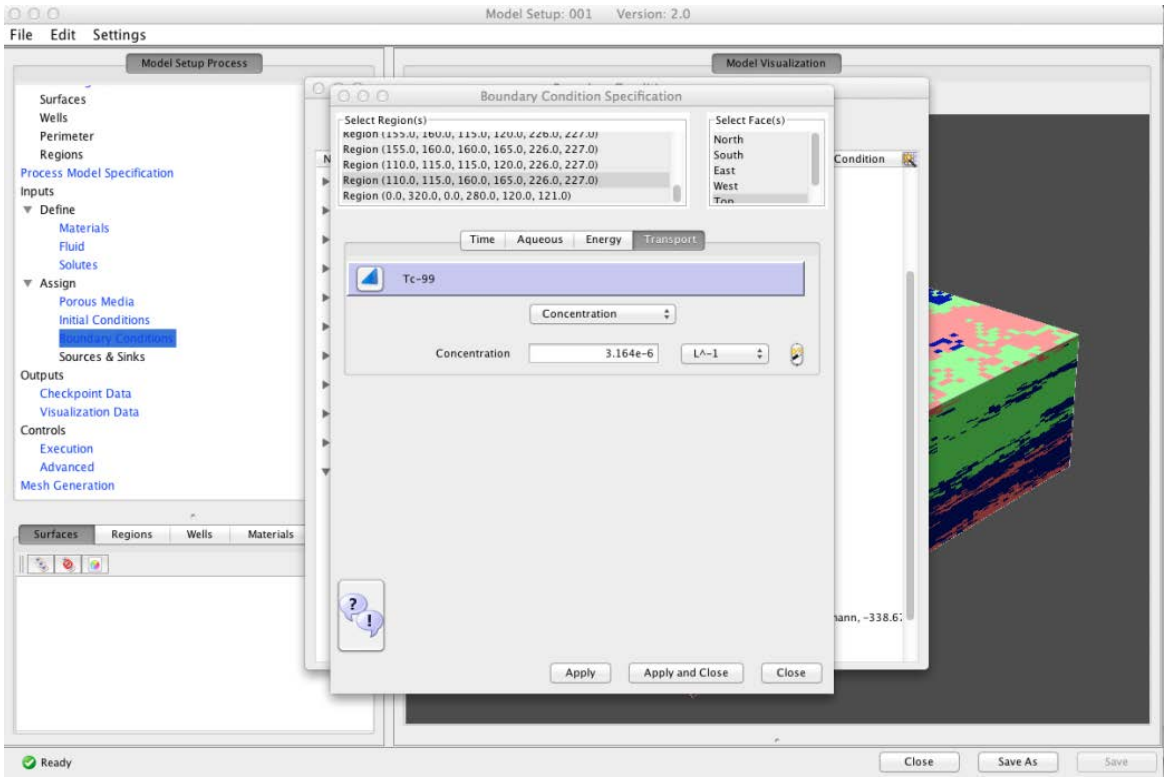

Figure 2.9. Boundary condition assignment in the Model Setup and Analysis Toolset.

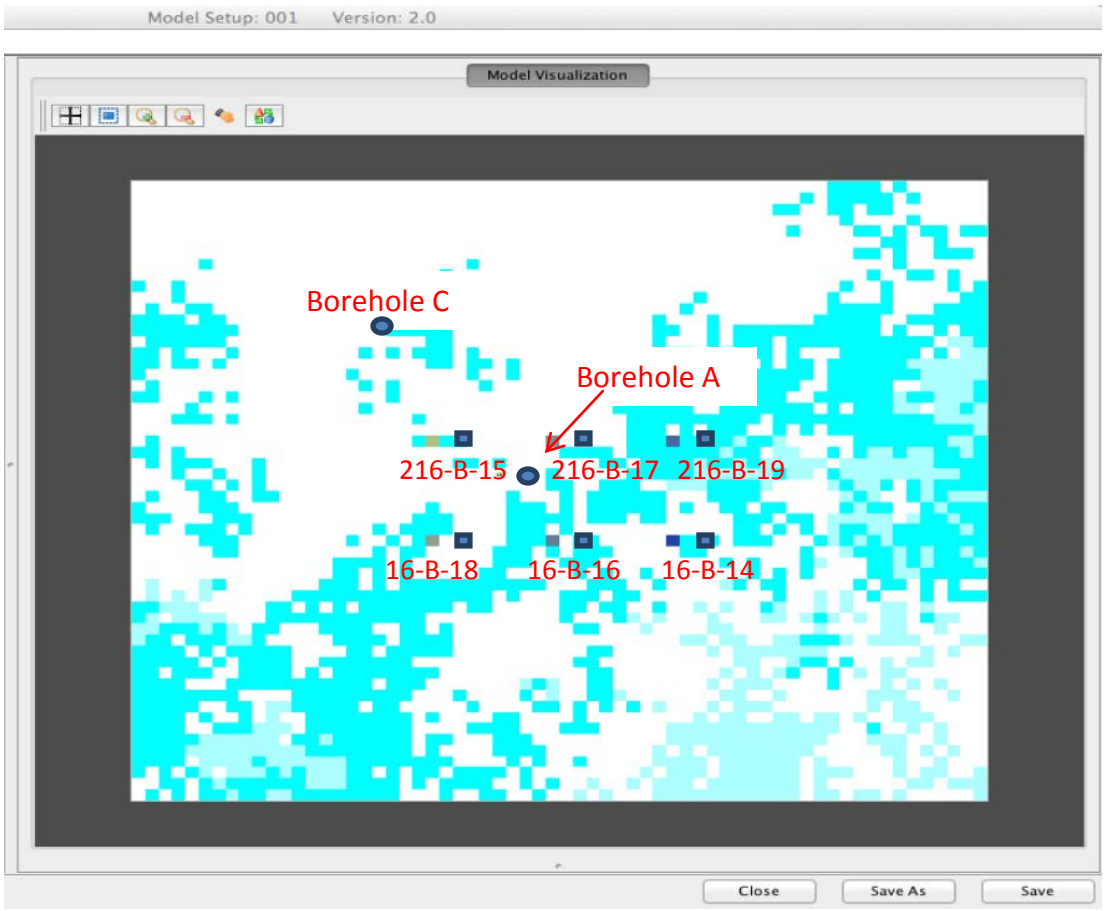

Figure 2.10. Plan view of the six cribs and borehole locations in the Model Setup and Analysis Toolset.

After hydraulic properties are identified, they are assigned to each of the lithofacies through the Model Setup and Analysis Toolset. The structured grid for the BC Cribs domain was generated using Gridder, a structured mesh tool associated with the Akuna Toolset. Once the domain extent has been defined, the Mesh Generation window allows the user to create a structured mesh from the discretization and domain extents that have been defined. The grid can be toggled on and off in the visualization window. The domain can also be interrogated using slices, as shown in Figure 2.11.

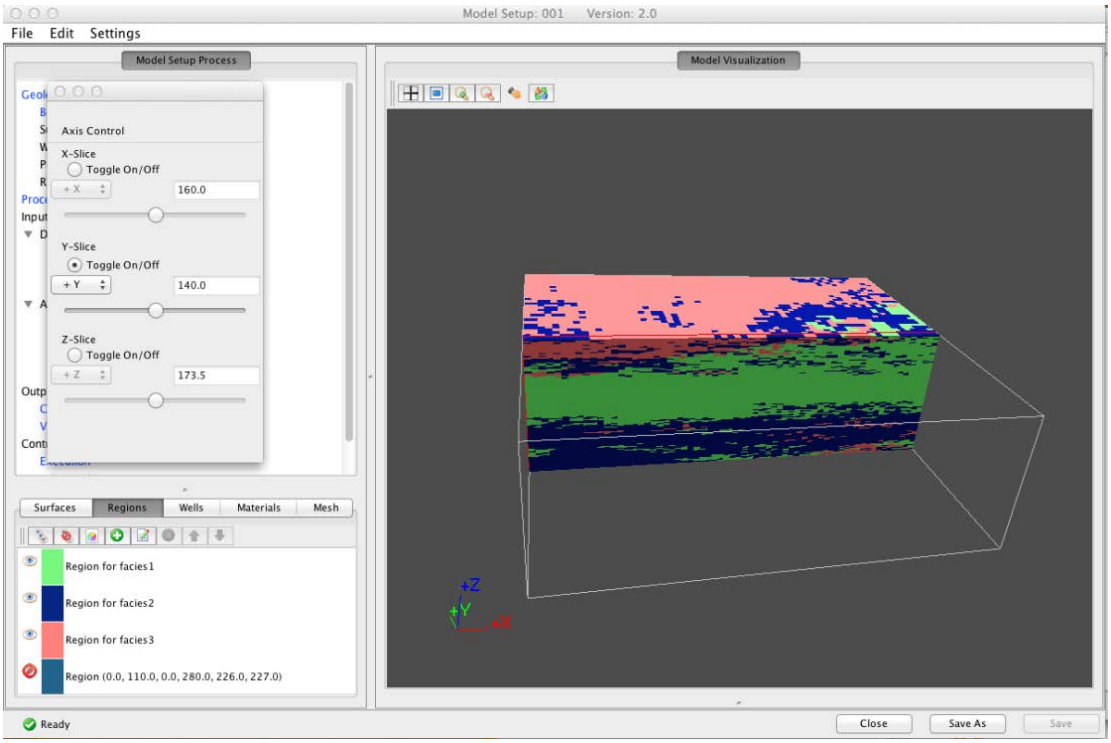

Figure 2.11. Viewer window in the Model Setup and Analysis Tool showing the distribution of lithofacies in the model.

2.1.3.6 Simulation Run

Once model setup is complete, simulations are executed. Simulations can be performed as a forward SR, SA, PE, or UQ. In the BC Cribs Phase II Demonstration, a SR was first executed to validate the model setup and to compare the simulated results with the measured data at Boreholes A and C before performing a PE. Parameter estimates were assigned from pedotransfer functions prior to the initial SR. The Model Setup and Analysis Toolset creates an input file and launches the simulator, as shown in Figure 2.12.

Akuna provides ongoing status of simulations (e.g., submitted, running, and completed). When the simulation completes successfully, a small green check mark appears next to the SR directory in the Akuna viewer window. In the BC Cribs Phase II Demonstration, the SR completed using the initial values from the pedotransfer functions showed a mismatch between simulated and measured data, as shown for concentrations in Borehole A (Figure 2.13). This indicated the need for model calibration.

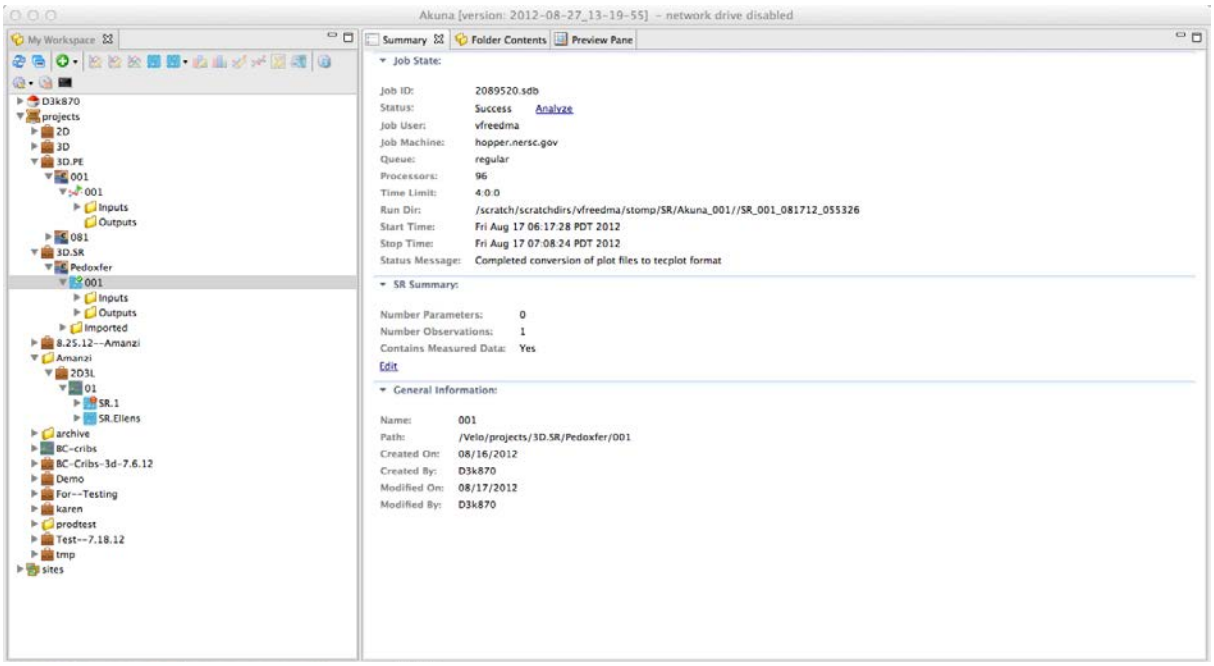

Figure 2.12. Viewer window showing a successful Simulation Run execution.

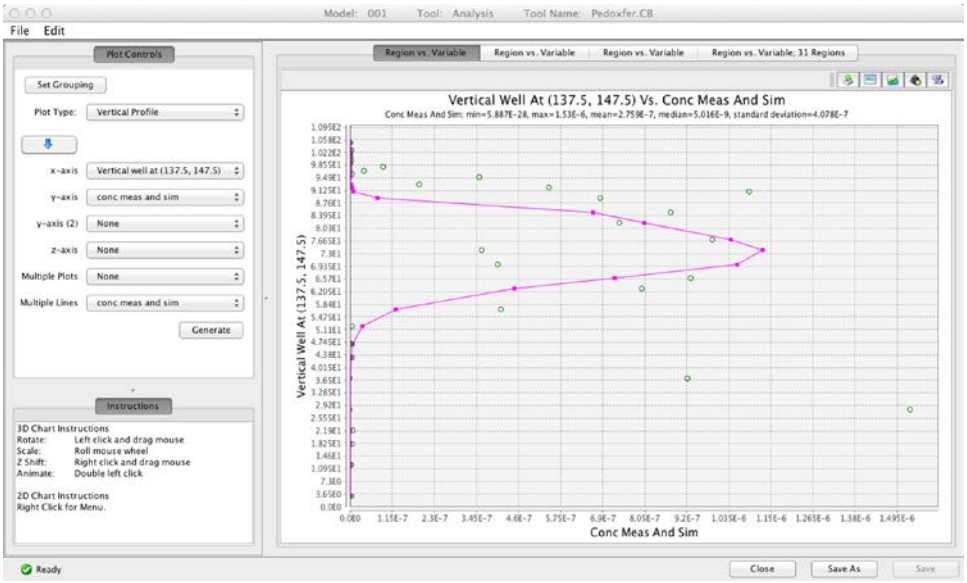

Figure 2.13. Comparison of simulated and observed concentration data at Borehole A.

2.1.3.7 Parameter Estimation

One objective of PE is to minimize differences between the observed data and simulated values through model calibration. In general, a model is considered calibrated when it reproduces historical data within some arbitrary level of accuracy. When the match is poor, several sources of error could contribute, and it may be difficult to distinguish between them. For example, sources of error may include 1) errors in the conceptual model, 2) errors in the numerical solution, or 3) a poor set of parameter values. Even when a good match to

measured data occurs, the model may still fail to predict future responses accurately, especially under a new set of stresses that differ from those experienced during the calibration period (Konikow and Bredehoeft 1992).

To perform PE, the user first selects the conceptual model that has been set up using the Model Setup and Analysis Toolset. For the BC Cribs demonstration, the same conceptual model defined in Model Setup and Analysis was used for both SR and PE. The screen shots in this section are based on PE simulations performed with eSTOMP. Parameters to be optimized are selected as shown in Figure 2.14. If parameters need to be estimated as a function of another parameter (e.g., horizontal and vertical permeability), then both parameters are highlighted and the user defines the multiplier in the *Transformation* column in the user interface.

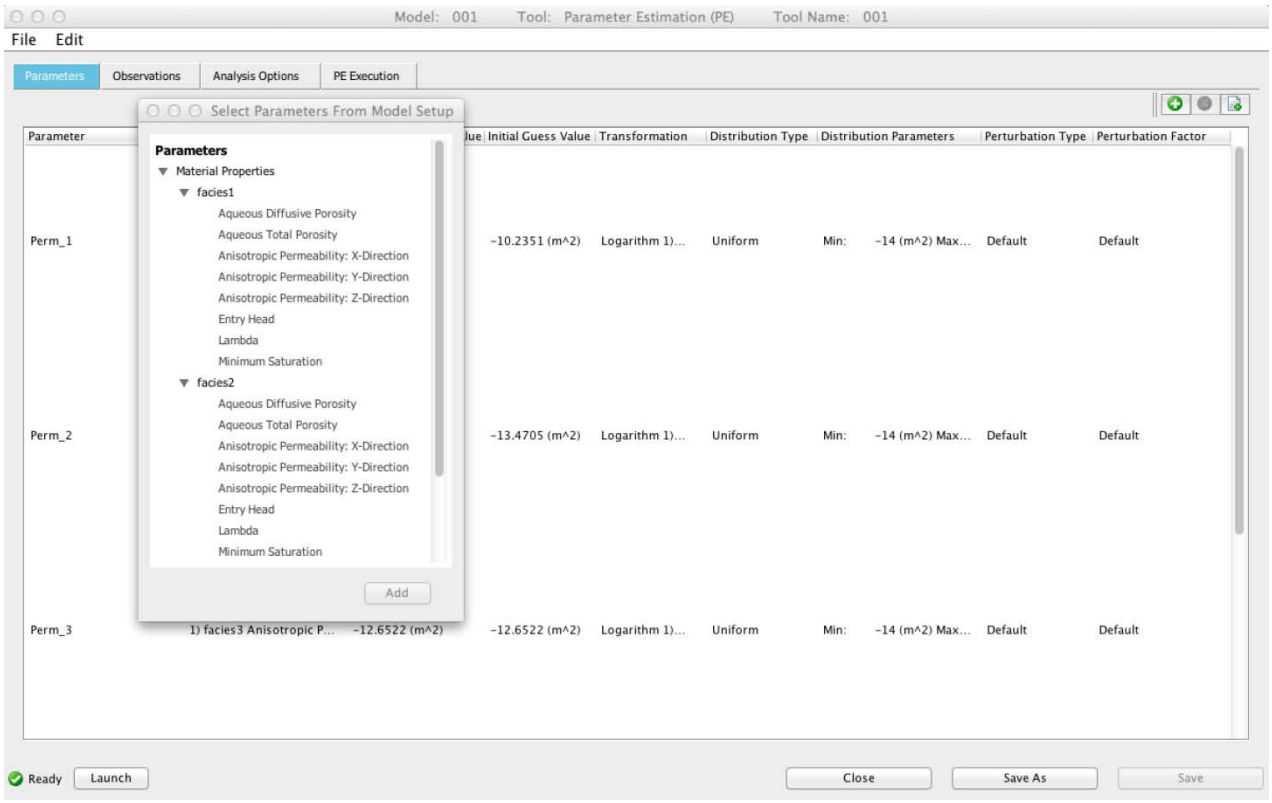

Figure 2.14. Parameters tab in the PE Toolset.

Measured field data (moisture content and concentration) are established as observations (Observations tab in the PE Toolset). In Akuna, an observation is defined as a monitoring point within the simulation domain. In the BC Cribs demonstration, the moisture content and concentration data from Boreholes A and C were extracted from the database and read by Akuna. Translations in the three coordinate directions can be performed if needed, so that measured data locations align with the simulation grid. This was required for the BC Cribs demonstration because the simulation grid used a zero-based Cartesian coordinate system in the X and Y directions, and the database coordinates were stored in latitude and longitude coordinates. Akuna assigns grid locations for observation data using a nearest-neighbor approach (spatial interpolation will be added in a future release).

The user selects different options for PE execution control,,such as algorithm selection, stopping criteria, and tolerances, through the Analysis Options tab as shown in Figure 2.15. This includes defining parameters such as the maximum number of iterations and tolerances. Launching a PE simulation requires the user to define both the total number of parallel processors required and the number of processors per task. For the BC Cribs PE demonstration, each simulation was executed on 192 processors, requiring a total of 576 processors because three simulations were executed simultaneously, one for each parameter being estimated. As with a single SR, Akuna provides status monitoring for PE execution.

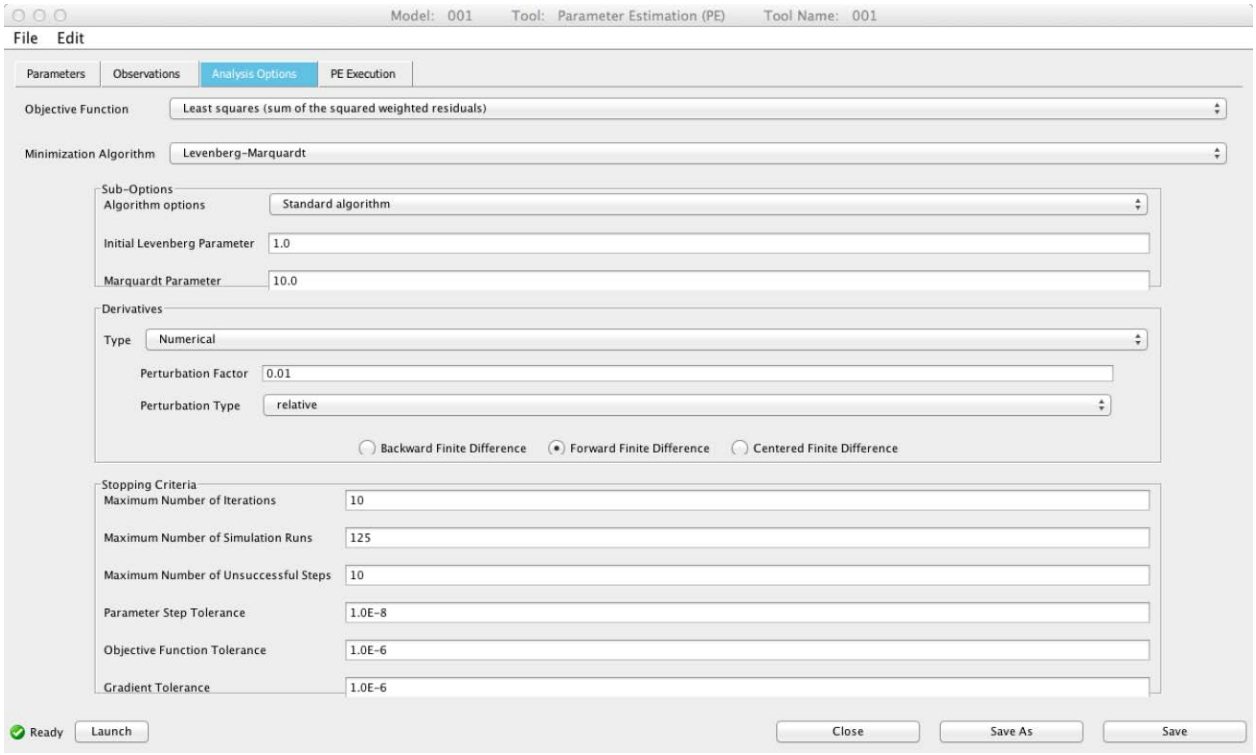

Figure 2.15. Parameter Estimation analysis tab.

Upon successful completion of a PE simulation, the user is presented with options for examining the results, including the following:

1. General summary
2. Tabular summary of parameter estimates
3. Plot of the objective function versus iteration (Figure 2.16)
4. Plot comparing measured and simulated data (Figure 2.17)
5. Plot of elevation versus error.

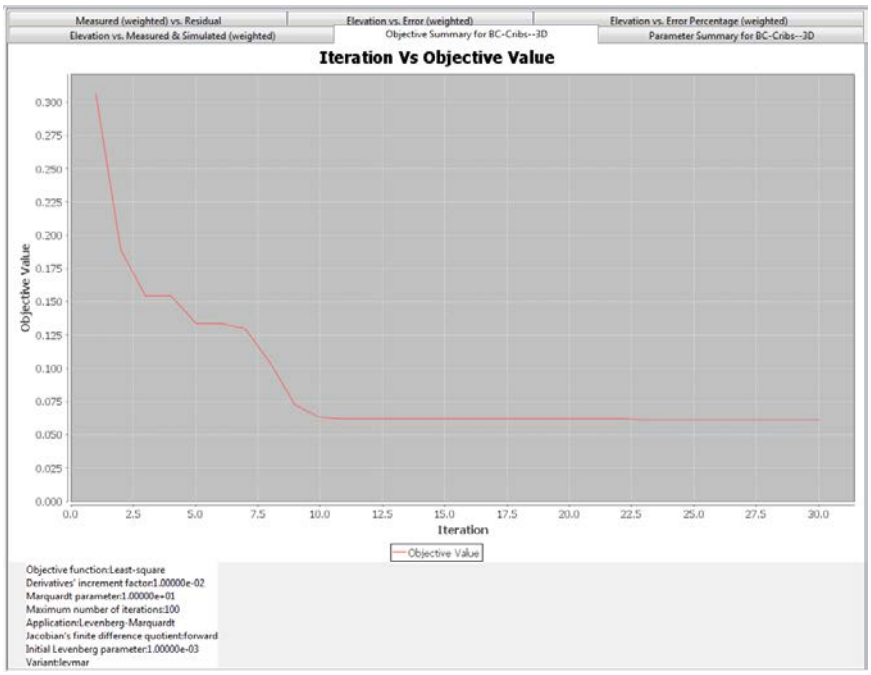

Figure 2.16. Objective function versus iteration.

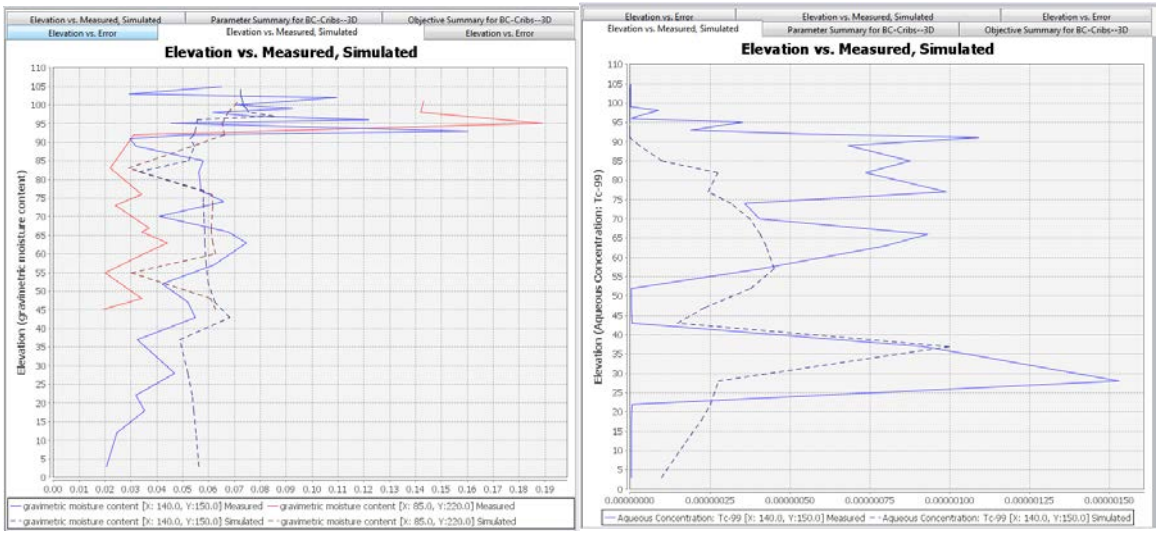

Figure 2.17. Elevation versus measured and simulated data; the discrepancy is for one of the iterations, and the objective is to minimize the difference.

2.1.3.8 Visualization

Understanding the spatial distribution of contaminants is important to identifying potential remedial actions at the BC Cribs. Visualizing the spatial distribution of technetium-99 also contributes to an understanding of how heterogeneities impact contaminant transport simulations. When a simulation (or set of simulations) has successfully completed, the Visualization Toolset using VisIt is launched from Akuna. For the BC Cribs demonstration, the spatial distribution of technetium-99 after the discharges to the cribs terminated (1960) is

shown in Figure 2.18. Horizontal cross-sections through each row of cribs, as well as a vertical cross-section through Borehole A, are also shown in Figure 2.18.

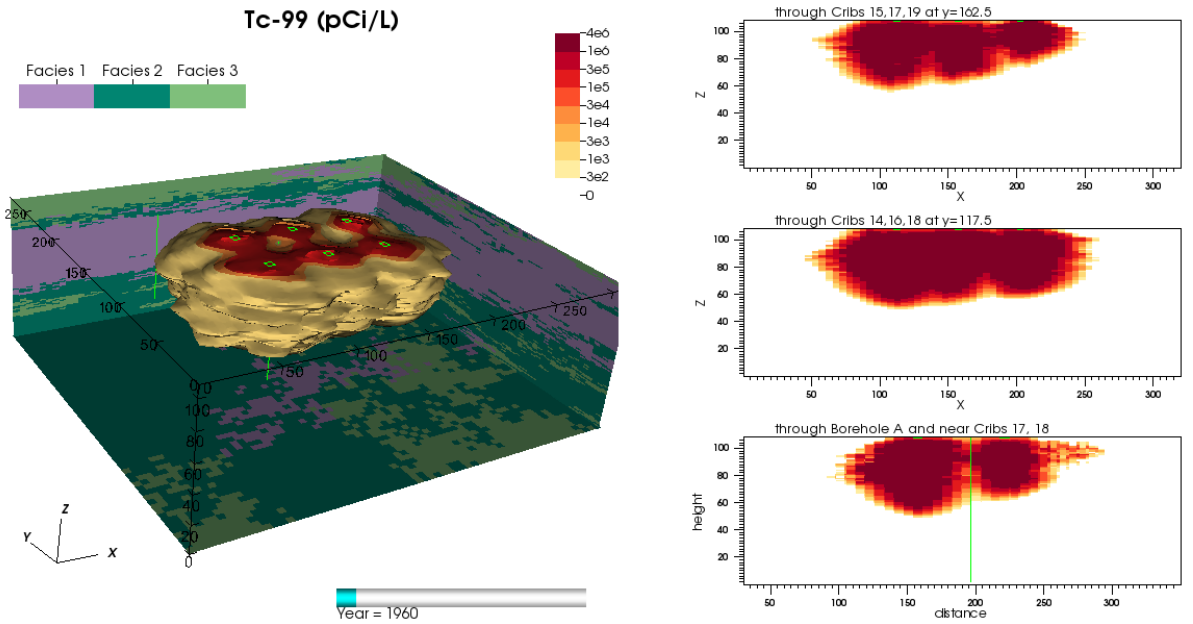

Figure 2.18. Spatial distribution of technicium-99 after the releases from the cribs using VisIt software.

2.1.3.9 Uncertainty Quantification

Flow and transport models are frequently used to evaluate uncertainties and how they impact decisions about potential remedial actions. In the BC Cribs demonstration, the UQ Toolset is implemented to examine uncertainty in future net infiltration (recharge) conditions. This future condition was defined for the years 2012 to 3000, with a constant yet uncertain recharge rate that ranged from 0.1 to 75 mm/yr. This range was assumed to represent impacts from management actions that influenced the net infiltration rate, such as the emplacement of a barrier (lower recharge rates) or monitored natural attenuation (MNA) (higher recharge rates). Use of the UQ Toolset is illustrated in this section.

The setup for performing UQ is similar to PE, as described in Section 2.1.3.7, except in this case the results were generated with Amanzi. The user first selects the conceptual model that has been set up using the Model Setup and Analysis Toolset, and can either choose a new UQ from the pull-down menu, or define a UQ analysis using the best parameter estimates from the PE. The demonstration included simulations to the year 3000 and Monte Carlo analysis. For the analysis, 100 values of recharge were randomly sampled from a uniform distribution. The UQ Toolset displaying the histogram of the samples is shown in Figure 2.19.

In Akuna, a UQ simulation is launched in a manner similar to PE. The BC Cribs demonstration UQ was launched using a total of 9600 cores with 96 cores per task. When the UQ is complete, Akuna's job monitoring capability shows a green check mark in the viewer window next to the name of the UQ analysis. In addition to histograms, the user can generate breakthrough curves, histograms and scatter plots to help interpret results of the

analysis. Figure 2.19 shows a screen shot from Akuna that plots the mean and 95% confidence intervals for technetium-99 over time. Multiple peaks appear because the maximum concentration at each point in time is plotted for all the simulations, which demonstrates that peak concentrations occur at different times depending on the magnitude of the recharge rate. The relationship between peak concentration and recharge rate is shown in Figure 2.20 (recharge is shown as "unnamed parameter"), and a histogram showing the time to reach the peak concentration is shown in Figure 2.21.

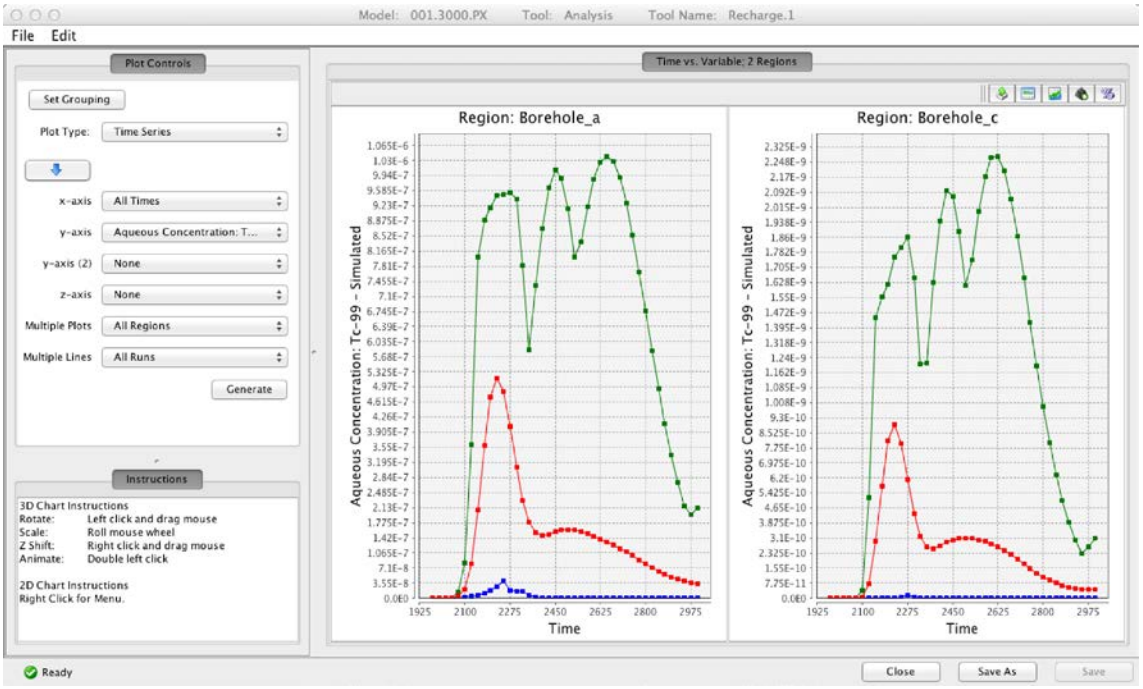

Figure 2.19. Screen shot from Uncertainty Quantification Toolset showing mean and 95% confidence intervals for the technetium-99 breakthrough curve at a monitoring location beneath Borehole A.

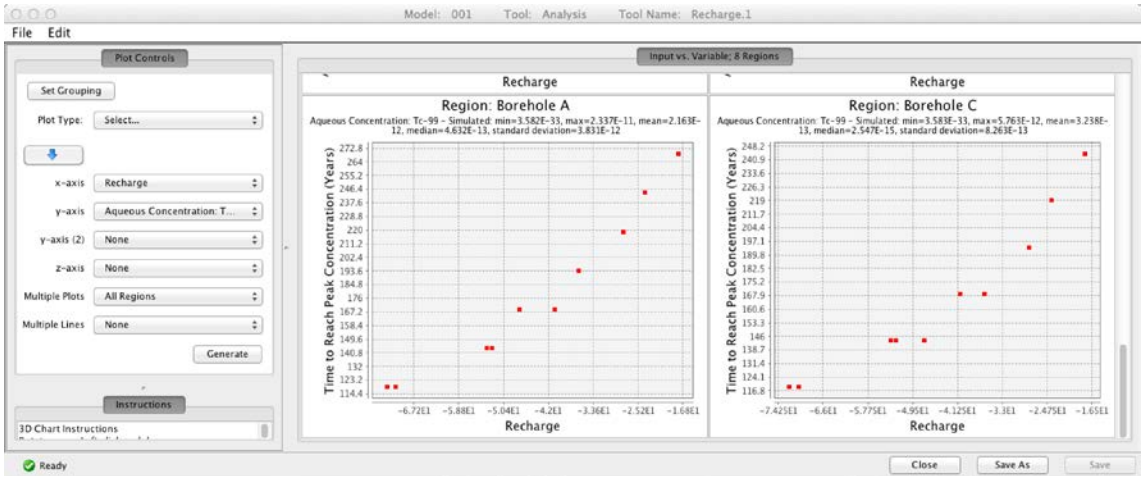

Figure 2.20. Screen shot from Uncertainty Quantification Toolset showing scatter plot for recharge rate ("Unnamed Parameter") and peak concentration at a monitoring location (Borehole A).

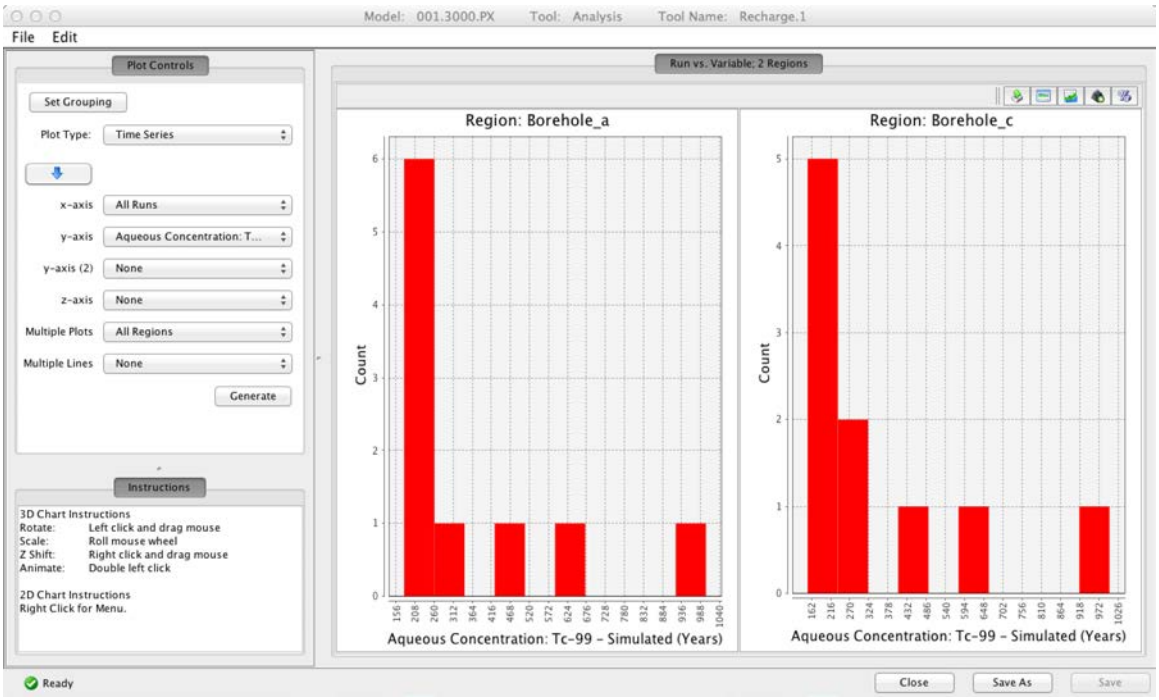

Figure 2.21. Screen shot from Uncertainty Quantification Toolset showing a histogram for time to reach the peak concentration at a monitoring location beneath Borehole A.

2.1.4 BC Cribs Uncertainty Analysis Results

The end-to-end demonstration for BC Cribs in Section 2.1.3 presented results for a single realization of the conceptual model using Amanzi. In this section, a summary of results for an additional nine realizations are presented using eSTOMP, which was used for testing Akuna and benchmarking Amanzi. One of the primary advantages of massively parallel processing available with Amanzi is the reduction in computational time, which means that multiple models can be analyzed. In this analysis, multiple representations of subsurface heterogeneities were used to represent conceptual model uncertainty. However, prediction uncertainty at BC Cribs is also due to parameter uncertainty, as well as crib release volumes, mass, and timing. Future analyses will examine the individual contributions of conceptual model and parameter uncertainty.

As presented in Section 2.1.3, parameter uncertainty is considered for a future recharge rate. The focus in this analysis is on demonstrating that the use of multiple conceptual models provides a more suitable range of prediction uncertainty than is provided when a single conceptual model is used.

To represent uncertainty in the future recharge rate, metrics related to technetium-99 concentration in the groundwater were examined at two points at the bottom of the domain, in the capillary fringe. These "observation" points were located directly beneath Boreholes A and C and represent a vadose zone concentration. Consequently, concentrations are much higher than they would be if concentrations were diluted by groundwater.

Typically, maximum concentration levels (MCLs) are used at downgradient groundwater wells as a metric for compliance. If groundwater levels remain below the MCL, the risk of exposure to the contaminant is considered to be low. Because groundwater was not represented in the BC Cribs simulations, the use of an MCL would be unfairly applied to the results of the BC Cribs analysis. However, Akuna has tools to address this analysis. As a result, vadose zone concentration predictions were still analyzed within the context of a *threshold* concentration, which is a metric analogous to an MCL. Because the analysis was based on vadose zone concentrations, a value of 100,000 pCi/L was arbitrarily selected as the threshold concentration to demonstrate the graphical analysis capabilities in Akuna.

2.1.4.1 Parameter Estimation

The Akuna Toolset was used to calibrate each of the 10 realizations of the geological conceptual models. Cross-sections of the facies distributions for all 10 realizations of the conceptual model are shown in Figure 2.22. The cross-sections show commonality in the locations and thicknesses of the three different facies but also demonstrate that subtle differences exist between the different realizations. The end-to-end demonstration in Section 2.1.3 is based on realization 001 (R001). The additional realizations examined in this section were arbitrarily selected from the set of 100 realizations.

To execute the PE in a systematic manner, six parameters (porosity and permeability for each facies) were estimated using the moisture content and concentration data at Boreholes A and C. Analysis options were the same among all realizations as were starting values for the parameters. Figure 2.23 shows the match between measured and simulated data for all 10 realizations of the conceptual models. Significant variability occurs for the permeability estimates for both facies 1 and 2 (Table 2.1). For facies 1, two orders of magnitude difference occur, whereas for facies 2, the estimates vary by nearly four orders of magnitude. The large variability in permeability estimates for facies 2 is likely due to its insensitivity to the existing data. This facies is primarily located at the bottom of the domain, but the bulk of the cribs' releases had not yet reached this depth by the year 2008 when the measurements occurred. This is an example of the observed data being too sparse to uniquely determine hydraulic parameters and underscores the importance of considering uncertainty in predictions of mass transport at the BC Cribs.

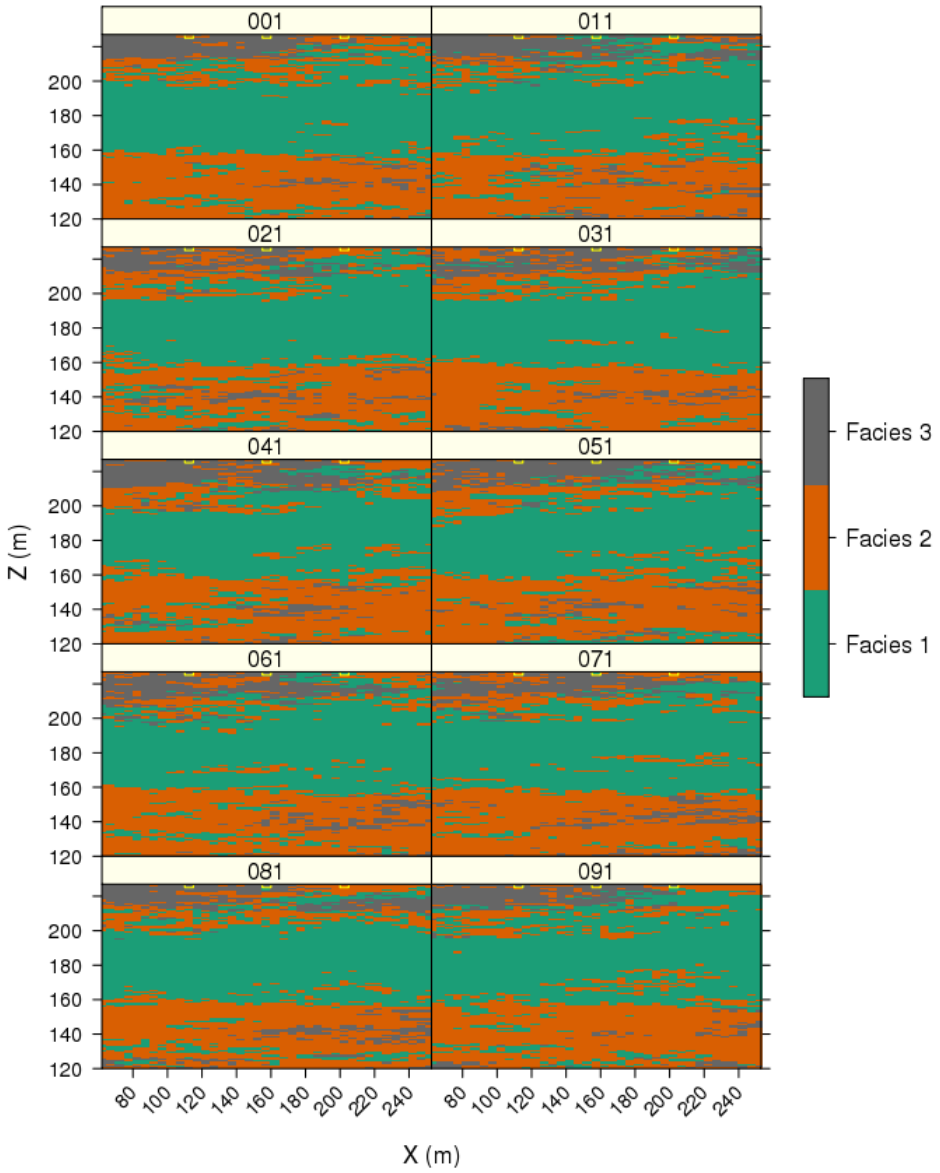

Figure 2.22. Geologic cross-sections for all 10 realizations of the conceptual model through Cribs 26-B-19, 216-B-17 and 216-B-15.

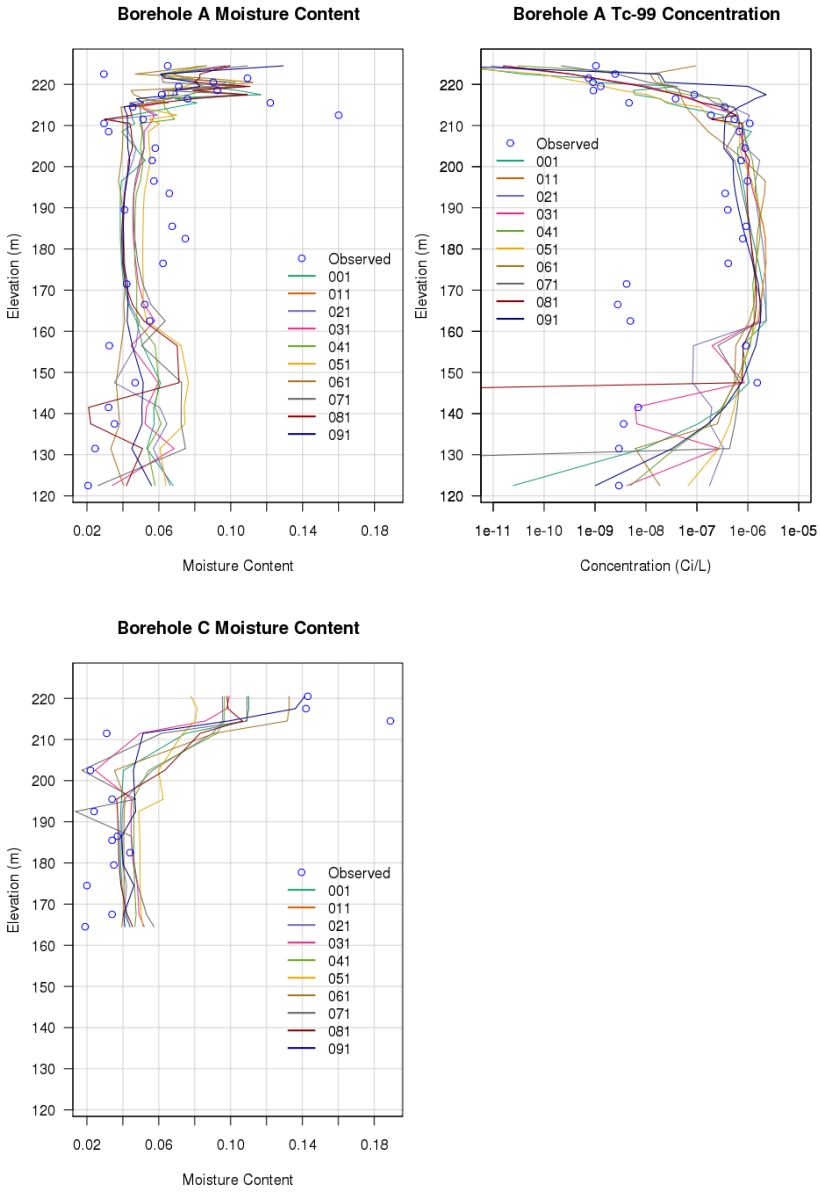

Figure 2.23. Simulated and measured moisture contents and concentrations at Boreholes A and C for all 10 realizations of the conceptual model.

Table 2.1. Parameter estimates ranges among the different conceptual model realizations.

Parameter	Min	Max
Permeability – Facies 1	1.68e-12 m^2	1.38e-10 m^2
Permeability – Facies 2	1.17e-14 m^2	1.89e-10 m^2
Permeability – Facies 3	1.00e-14 m^2	1.45e-13 m^2
Porosity – Facies 1	0.1319	0.2659
Porosity – Facies 2	0.1648	0.2832
Porosity – Facies 3	0.2427	0.3419

2.1.4.2 Uncertainty Quantification

In this section, histograms and scatter plots were generated outside Akuna because the ability to analyze results across realizations of the conceptual model does not currently exist in the toolset. Plots of cumulative distribution functions (CDFs), were also generated for all 1000 simulations (10 models, 100 simulations per model), as well as for the single conceptual model (100 runs). These were also generated outside Akuna because the ability to generate CDFs does not yet exist in the toolset but is planned for future release.

To analyze the uncertainty results across realizations of the conceptual model, the breakthrough curves (BTCs) for all runs are compared to the BTCs shown for a single realization (R001). This comparison (Figure 2.24) shows the 95% confidence intervals are wider when all 10 realizations are considered. For example, the upper bound on the confidence interval is approximately 85% higher at Borehole A for all 10 models than just for R001. A similar increase in the 95% confidence interval is shown for Borehole C.

The variability across all runs is also noted in the scatter plot depicting the number of years that technetium-99 is above the arbitrary threshold concentration of100,000 pCi/L (Figure 2.25). The number of years is calculated from the time of the first releases to the cribs (1956) to the time the threshold concentration is first exceeded. At Borehole A, the trend demonstrates that lower recharge rates increase the amount of time the concentrations are above the threshold concentration, whereas higher recharge rates generally translate into shorter periods of time that exceed the threshold concentration. In some cases, like CM001 at Borehole C, the post-2012 recharge rate has no impact on the number of years to exceedance. Even with recharge rates close to zero (e.g., < 10 mm/yr), the plume is close enough to the water table in the year 2012 that the threshold concentration is exceeded within 50 years. With other conceptual model realizations, a lower recharge rate increases the number of years required to exceed the threshold concentration. This has important implications for remediation technologies that reduce the recharge rate, such as soil desiccation. A reduction in the recharge rate may delay the arrival of peak concentrations to the water table, but it may also prolong the duration at which the concentrations are above the threshold concentration.

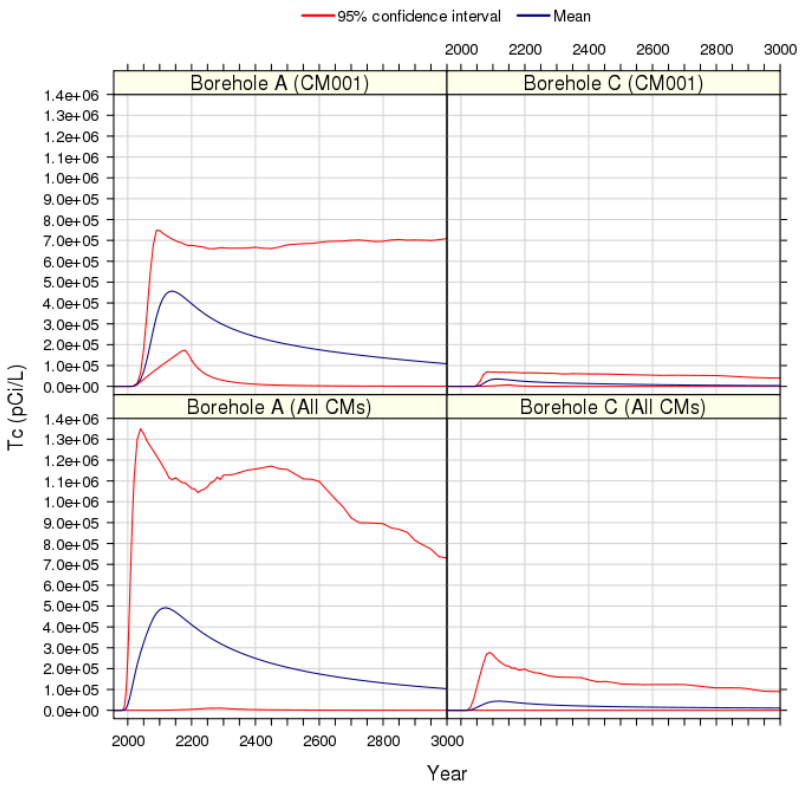

Figure 2.24. Breakthrough curves showing mean and 95% confidence intervals at Boreholes A and C.

As noted in the breakthrough curves in Figure 2.24, there is wider variability across all runs for the time of exceedance of the threshold value at both Boreholes A and C. The histogram depicted in Figure 2.26 compares the number of years of exceedance for the single and multiple realizations and the scatter plot in Figure 2.27 shows the time to reach peak concentration versus recharge rate. A greater variability occurs at both locations, although the variability is more significant for shorter periods of exceedance at Borehole C and more significant for longer periods of exceedance at Borehole A.

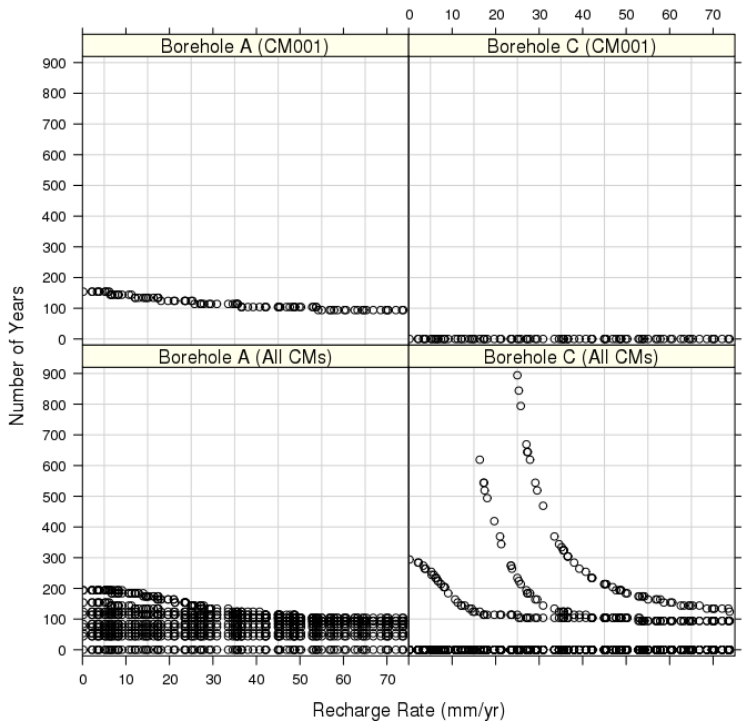

Figure 2.25. Scatter plot of time to reach the peak concentration at Boreholes A and C.

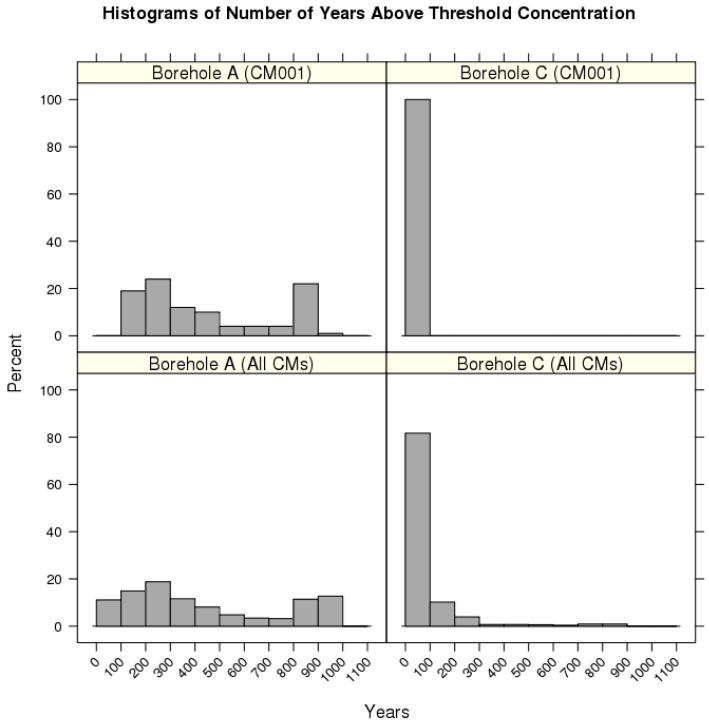

Figure 2.26. Comparison of the number of years the threshold value is exceeded for the single and multiple realizations of the conceptual model.

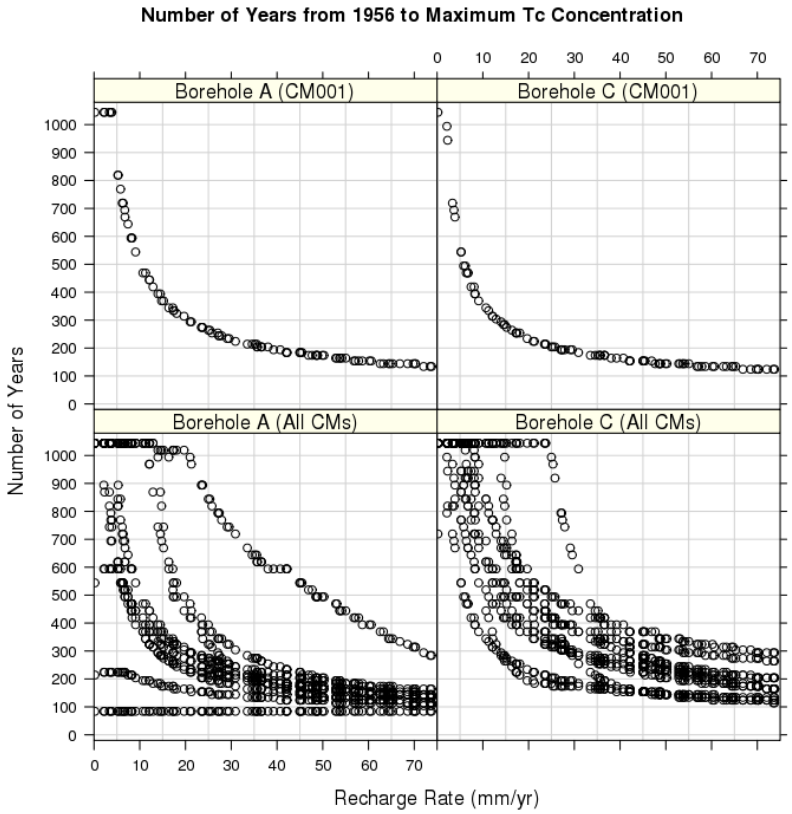

Figure 2.27. Scatter plot of time to reach peak concentration versus recharge rate at Boreholes A and C.

While breakthrough curves, scatter plots and histograms are useful for examining trends in an uncertainty analysis, CDFs can provide useful summary views by mapping prediction quantities to their percentile rank in a distribution. CDFs were generated based on the number of years to reach the peak concentration and the threshold concentration, and the time period above the threshold concentration (Figure 2.28). One notable distinction between the two figures is that the number of years to reach the threshold concentration (red line) is vertical for R001 at Borehole A but is a curved line for all realizations. The vertical line indicates the number of years (approximately 60) to reach the peak concentration is the same for all recharge rates, whereas across all realizations of the conceptual model, much greater variability occurs at Borehole A (approximately 60–1000 years). At Borehole C, the red line representing the number of years above the threshold concentration is 0 and does not appear in the plot because the number of years to the threshold concentration is also 0 (green line).

A similar trend is noted between the two plots for the number of years above the threshold concentration (green line). At Borehole C, for example, R001 predicts the concentrations never exceed the threshold concentration. Across all runs, 50% of the runs predict exceedance of the threshold concentration between 100 and 1000 years. Because the variable recharge rate is being used as a surrogate for potential remedial actions, this demonstrates subsurface heterogeneities need to be considered in the uncertainty analysis of potential impacts at the site.

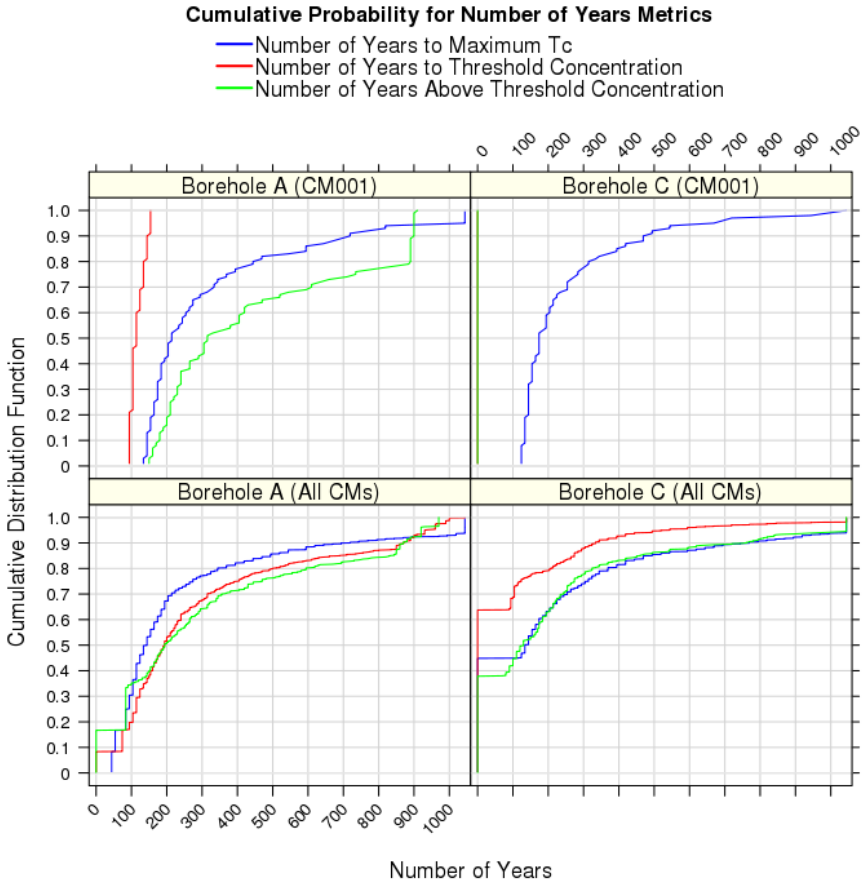

Figure 2.28. CDF for time to reach peak concentration, time to reach threshold concentration, and the time period above the threshold concentration.

Both CDFs show that significant variability in the number of years to reach the peak concentration (blue line). However, the shapes of the curves differ and yield different predictions for the single and multiple realizations of the conceptual model.

2.1.5 Deep Vadose Zone Discussion

In general, the main advantage of the Akuna modeling framework lies in its ease for model setup, execution, and analysis, from PE through uncertainty analysis. The use of HPC allows the user to select a suite of models to adequately capture a range of lithofacies distributions, parameter distributions, and boundary conditions, depending on the scope of the analysis. For the BC Cribs Phase II Demonstration, the focus was on illustrating how the ASCEM Toolset works for an end-to-end demonstration. In addition, the demonstration provides insights on the relative roles of recharge rates and lithofacies distributions using Monte Carlo-based simulations.

The Phase II Demonstration represents the first modeling effort using ASCEM at the BC Cribs site and was used to establish baseline conditions expected under a "no-action" alternative. Because small-scale subsurface heterogeneities are known to be a major factor

influencing transport at the site, heterogeneous lithofacies distributions were considered in this analysis. Although the PE effort provided a less than perfect match between measured and simulated values of moisture content and concentration, the new parameter estimates showed a significant improvement in matching historical data over the initial estimates. Modeling is an iterative process, and improvements in historical data matching are expected as the conceptual model is revised (e.g., boundary conditions, lithofacies distributions) and new capabilities are incorporated into the Akuna tools. These capabilities could include tools such as global search algorithms and the use of pilot points for PE and optimization.

The results of the Phase II Demonstration show the importance of examining uncertainty with respect to subsurface heterogeneities, as well as any other sources of uncertainty that may impact mass transport to the water table. Using Akuna to generate breakthrough curves, histograms, and scatter plots for UQ facilitated a rapid analysis and identification of trends.

2.2 Attenuation-Based Remedies for the Subsurface Working Group

The Attenuation-Based Remedies for the Subsurface Working Group demonstration at the SRS F-Area provides an opportunity to implement linked ASCEM capabilities, including those applied during the Phase II Demonstration by the DVZ Working Group, under complex geochemical conditions and using large, dense, and disparate heterogeneous data sets. Specific information about the F-Area site geology, hydrogeology, geochemistry, contaminants, available data, leveraging activities, and early advances in the development of ASCEM components can be found in Hubbard et al. (2010). Building on previous advances, additional ASCEM capabilities are needed to help DOE-EM provide an efficient and cost-effective transition from active to passive cleanup of uranium-contaminated groundwater, using MNA and enhanced attenuation. For example, the site currently operates a base-injection remediation treatment but lacks the technical underpinning needed to quantify the duration that this treatment is necessary or if other treatment delivery strategies or natural attenuation would be equally or more effective.

The Phase I Demonstration at the SRS F-Area site focused on predicting reactive geochemistry that governs uranium mobilization in saturated, layered sediments in a shallow groundwater system. The Phase II Demonstration incorporates source zone loading, infiltration through the vadose zone, and complex geochemistry. Of particular interest was the impact of the uncertain input parameters on trailing uranium plume concentration gradients, which are drivers for the remedial treatments at the site. As such, the Phase II Demonstration activities focused on using UQ tools to assess how uncertainty associated with recharge, contaminant source characteristics, and geochemical reactions affect long-term predictions of plume transport to the base injection barrier. This topic is generally of interest because recharge and basin seepage are common components of many DOE contaminated sites, but their effects on groundwater plume mobility are rarely considered in a quantitative manner. In addition to the emphasis on UQ, data management, HPC and visualization components of ASCEM were expanded and implemented during the Phase II Demonstration using the large, dense heterogeneous F-Area data sets. The demonstration was designed to highlight the utility of Amanzi for gaining a predictive understanding of long-term plume transport in complex systems, as is needed to guide remediation decisions and closure strategies.

2.2.1 SRS F-Area Conceptual Model

2.2.1.1 General Information and Modeling Domains

The SRS is located in south-central South Carolina, near Aiken, approximately 100 miles from the Atlantic Coast. It covers about 800 km^2 (300 mi^2) and contains facilities constructed in the early 1950s to produce special radioactive isotopes (e.g., plutonium and tritium) for the U.S. nuclear weapons stockpile. The SRS has approximately 172×10^6 m^3 of groundwater, soil, and debris contaminated with metals, radionuclides, and organics as a result of onsite disposal practices. Figure 2.29 depicts the large-scale model domain, encompassing the Upper Three Runs Creek and Fourmile Branch watersheds, the intermediate-scale domain, including a General Separations Area (GSA), and a small-scale domain, covering the plume from the SRS F-Area Seepage Basins.

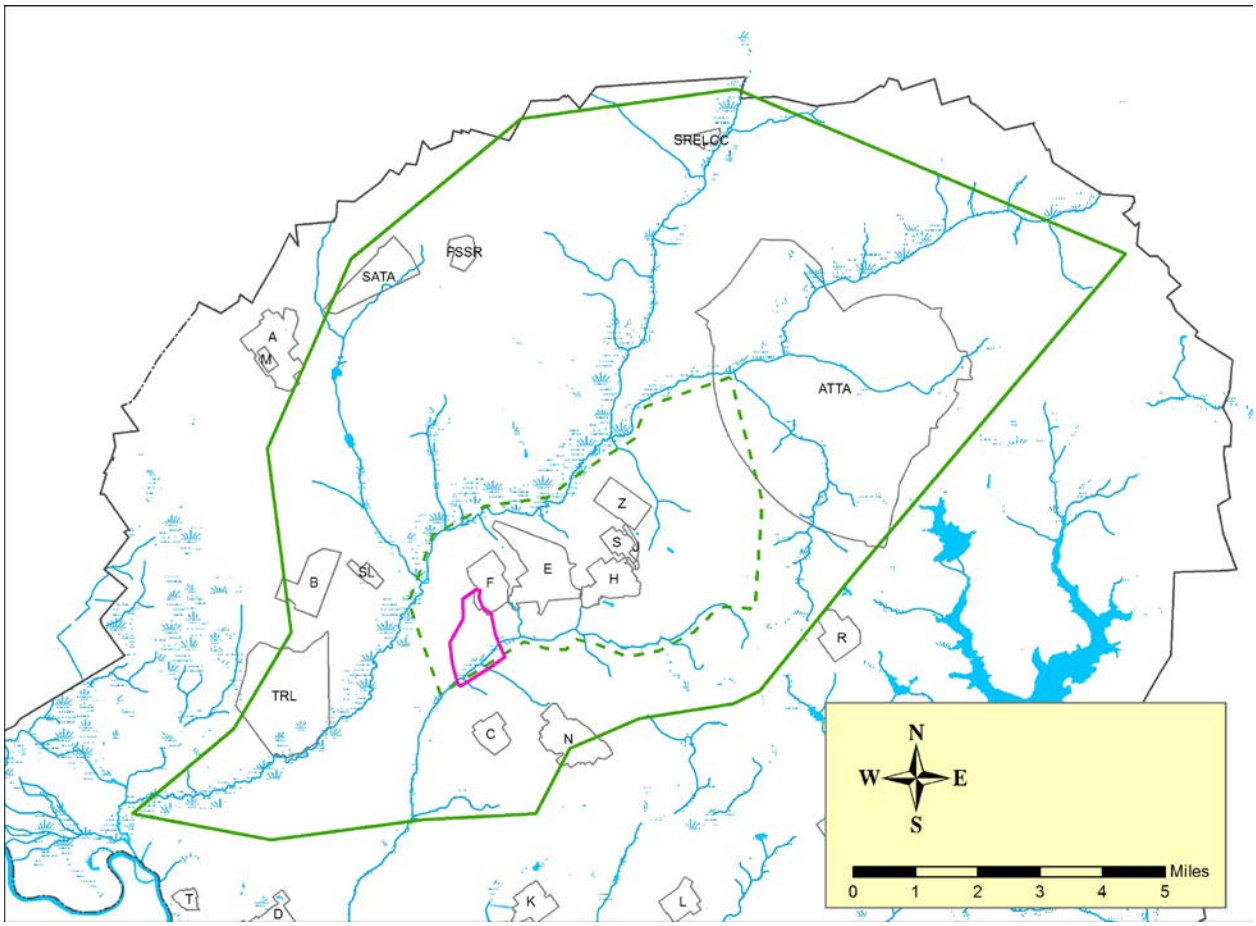

Figure 2.29. SRS map showing the boundaries of the domains: solid green—the area where the data were collected as part of the Phase II Demonstration Data Management activities; dashed green—the SRS General Separations Area modeling domain, and fuchsia—the Phase II modeling domain of the F-Area plume.

The SRS F-Area seepage basins were constructed as unlined, earthen surface impoundments that received approximately 7.1 billion L of acidic, low-level waste solutions from the processing of irradiated uranium in the F-Area Separations facility from 1950 through 1989. Basin F-1 received 3.9 million L, Basin F-2 received 7.4 million L, and Basin F-3 received 53 million L. As the largest basin, Basin F-3 is considered the primary source of groundwater contamination in the F-Area (Millings et al. 2012).

Based on extensive monitoring observations, the acidic uranium plume extends from the basins approximately 600 m downgradient (Figure 2.30). The plume contains various radionuclides—uranium isotopes, strontium-90, iodine-129, technetium, and tritium, as well as nitrate. The basins were closed and capped in 1991. A pump-and-treat remediation system began operation in 1997 and was replaced in 2004 by a hybrid funnel-and-gate system installed about 300 m upgradient from the Fourmile Branch stream (Figure 2.30). Because uranium mobility is greatly influenced by pH (higher pH values increase uranium sorption), alkaline solutions are now being injected periodically into the gates in an attempt to neutralize the acidic groundwater and immobilize uranium before it reaches the stream. MNA is a desired closure strategy for the site, assuming that rainwater will eventually increase pH of the plume and stimulate natural immobilization of uranium. If the natural pH neutralization upgradient is insufficient, additional enhanced neutralization will be required. Critical to assessing the impact of in situ treatments over long time frames is the improved understanding of the long-term pH evolution and uranium sorption processes at the site. To address this aspect, this demonstration focuses on illustrating that ASCEM can be used to identify key controls on plume transport, from the source to the location of the base injection region.

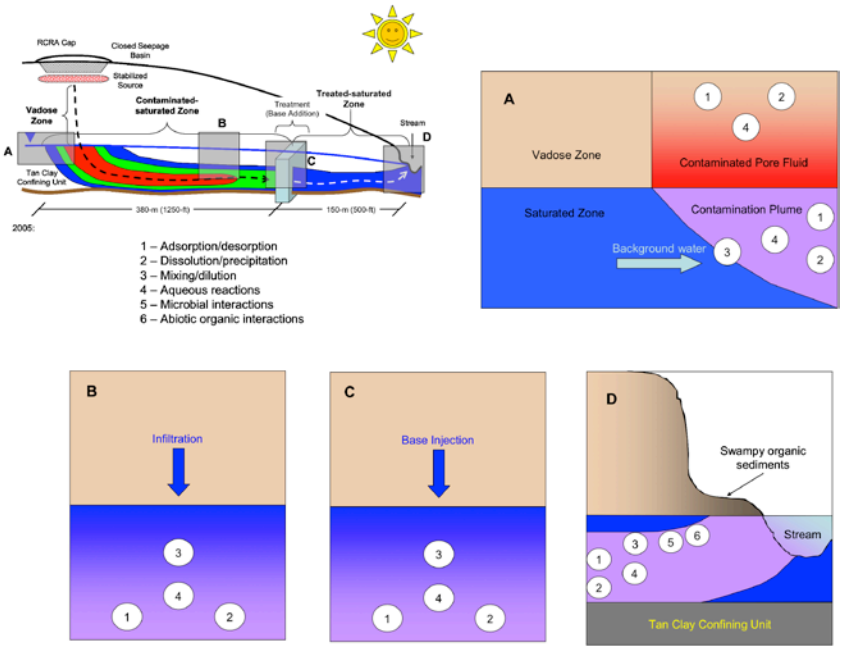

Figure 2.30. Conceptual model of uranium attenuation processes in the entire F-Area Seepage Basins plume, including 1) adsorption/desorption; 2) dissolution/precipitation; 3) mixing/dilution; 4) aqueous reactions; 5)

microbial interactions; and 6) abiotic organic interactions. (Note that microbial and organic interactions are not part of the Phase II Demonstration).

2.2.1.2 Hydrostratigraphic Boundaries and Flow Domain

The hydrostratigraphy at the site consists of the Atlantic Coastal Plain unconsolidated and semi-consolidated sands and clays. The shallowest aquifer at the F-Area is the Upper Three Runs Aquifer, which consists of an upper aquifer zone (UUTRA), a Tan Clay Confining Zone (TCCZ), and a lower aquifer zone (LUTRA). Beneath the LUTRA is the Gordon confining unit and under that, the Gordon aquifer. Figure 2.31 shows the location of the seepage basins in the F-Area of the SRS and the hydrostratigraphic units defined for the F-Area (Fenimore and Horton 1973; Killian et al. 1986; Strom and Kaback 1992; Flach 2004).

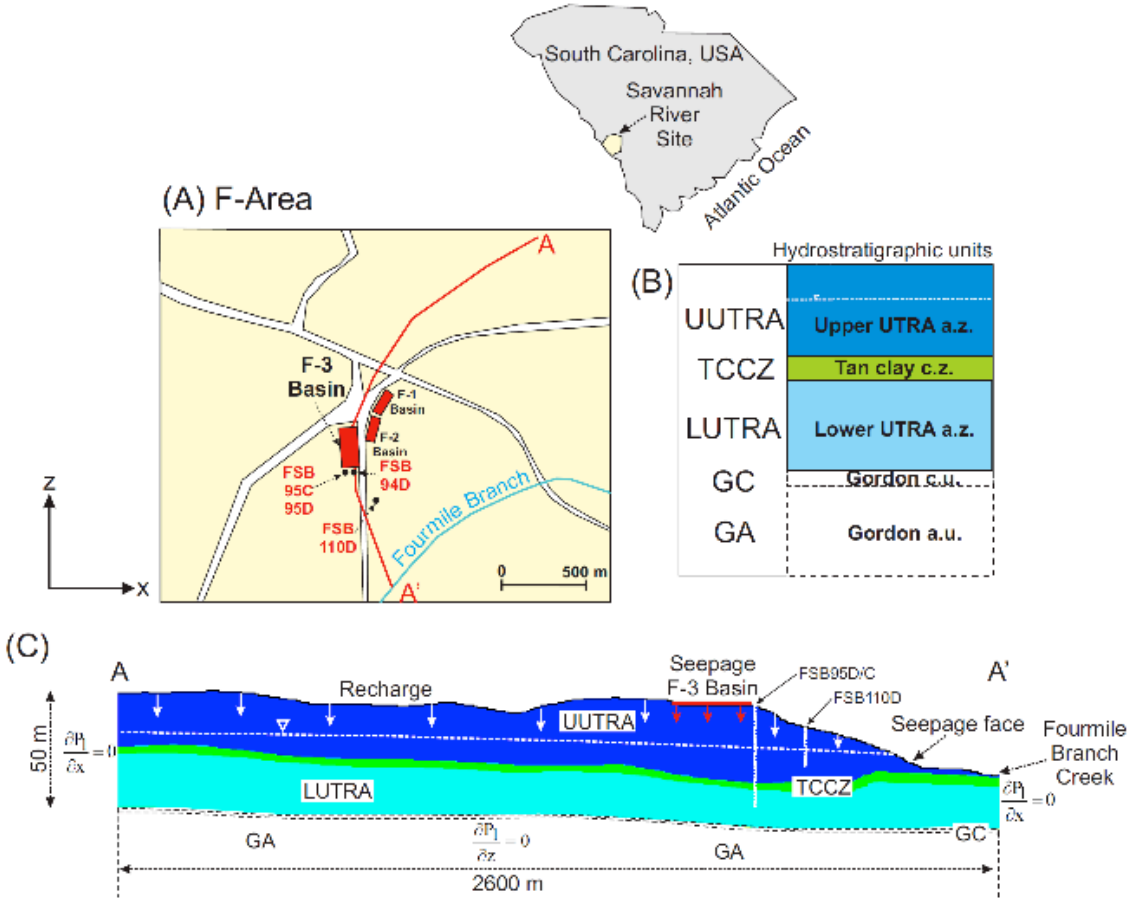

Figure 2.31. a) Location of seepage basins in the F-Area of the Savannah River Site; b) hydrostratigraphic units defined for the F-Area (e.g., Fenimore and Horton 1973; Killian et al. 1986; Strom and Kaback 1992; Flach 2004); c) two-dimensional cross section model domain.

A geostatistical approach was used to estimate the distribution of the hydrostratigraphic units, using borehole and cone penetrometer testing (CPT) data. This approach was based on the nonstationary variogram model and the maximum likelihood estimation (MLE) method in the R:geoR package (Diggle and Ribeiro 2006). Although the LBNL SFA research has

demonstrated that heterogeneity within larger units exists and plays a role in plume migration (Sassen et al. 2012), for simplicity this Phase II Demonstration assumed that each hydrostratigraphic unit was hydrologically homogeneous.

The two-dimensional modeling cross-section, which is shown by a red line *A-A'* on Figure 2.31a, extends from the watershed divide (shown by a symbol *A*) to the Fourmile Branch Creek (shown by the symbol *A'*). No-flow boundary conditions were assigned at the bottom of LUTRA and along the two vertical boundaries of the two-dimensional cross section, which are consistent with the groundwater divides of the watershed (Flach 2004). At the top boundary, a constant average seepage rate (4 m/yr) was assigned at Basin 3 during the waste discharge (Flach 2004), whereas a constant recharge rate from precipitation and runoff (0.14 m/yr) is assumed elsewhere (see Appendix D, Table D.1). The seepage-face boundary condition was assigned along the Fourmile Branch (FMB) stream to control the outflow from the modeling domain. The unsaturated-saturated groundwater flow was modeled based on the Richards equation, with unsaturated flow parameters given for the van Genuchten model. Because of the high groundwater flow velocity at the F-Area (on the order of 100 m/year), advective transport is dominant so that diffusion transport processes are assumed negligible. Initial flow conditions were computed before starting the numerical simulations, imposing a hydrostatic pressure distribution throughout the modeled domain. The simulations performed during the Phase II Demonstration did not include the engineered treatments that have occurred at the site, including pump-and-treat and pH manipulation remediation strategies; these treatments will be included in the Phase III Demonstration. The demonstration also did not include the redox chemistry that is prevalent in the wetlands downgradient from the pH injection barrier. As such, our simulation validations are performed using wellbores located upgradient from the barrier, including one well close to the basin and one directly upgradient from the barrier.

2.2.1.3 Geochemical Processes

The geochemical processes modeled in the Phase II Demonstration include equilibrium aqueous complexation, kinetically controlled mineral dissolution and precipitation, and adsorption/desorption described with a nonelectrostatic surface complexation and ion exchange model considered to be at equilibrium. The primary geochemical system consists of 13 reactive chemical components and 8 minerals, which were defined based on Lawrence Berkeley National Laboratory (LBNL) SFA research by Bea et al. (2012). A detailed list of reactions and geochemical parameters is included in Appendix E. Amanzi's implementation of the individual geochemical processes and solution of the full geochemical system were verified through a series of benchmarks against other existing codes, including TOUGHREACT (Xu et al. 2006, 2012), PFLOTRAN (Hammond et al. 2012), and CrunchFlow (Steefel. 2012).

The sorption model used in Amanzi is based on a single-site equilibrium, pH-dependent surface complexation model, which provides the principal control on the uranium migration rate. An ion exchange model includes reactions involving the major cations (Ca^{2+}, Na^{+}, and Al^{3+}, along with H^{+}) and provides primary pH buffering along with the mineral reactions. The nonelectrostatic model used here is applied to the bulk sediment rather than to specific pure mineral phases that serve as sorbents in the conventional electrostatic model.

Additionally, the nonelectrostatic model does not assume the presence of well-defined mineral phases (Davis et al. 1998).

The uranium mobility is controlled largely by a single sorption reaction, with the only significant effect on the stability of the surface complexation being the solution pH and carbonate activity. The pH has an effect directly through the surface complexation reaction:

$$>SOH + UO_2^{2+} \rightleftharpoons >SOUO_2^{+} + H^{+}$$

where $>SOUO_2^{+}$ refers to the uranium-bearing surface complex developed on the sediment grain surfaces. To determine the reaction stoichiometry and associated equilibrium constant for the reaction, LBNL SFA researcher J. Davis carried out a fit of U(VI) sorption data collected on six samples of contaminated sediments from the SRS F-Area. The model averages the pH-dependent U(VI) adsorption behavior of 36 separate contaminated sand samples from the F-Area. Only the samples from the pH 3–6 range were used to calibrate the log K (equilibrium constant) for the reaction. The effect of carbonate concentration on the strength of the uranium surface complex (and thus the mobility of the uranium) enters indirectly through the various (calcium)-uranium-carbonate complexes that form as a function of carbonate activity and pH. At the F-Area, a significant mass of the H^{+} ion is sorbed on the mineral surfaces. This effect is treated with a set of cation exchange reactions that represent the pH buffering via sorption on mineral surfaces (in addition to pH buffering by mineral dissolution and precipitation reactions) by the following:

$$Na\text{-}X \rightleftharpoons Na^{+} + X^{-};\ \log K = 0.0$$

$$Ca\text{-}X_2 \rightleftharpoons Ca^{2+} + 2X^{-};\ \log K = -0.5$$

$$H\text{-}X \rightleftharpoons H^{+} + X^{-};\ \log K = -1.60$$

In essence, these ion exchange reactions, along with the single uranium surface complexation reaction, capture much of the pH and carbonate activity effects on uranium mobility and have the additional advantage that they involve a much smaller list of adjustable parameters than is included by other LBNL SFA research (i.e., Bea et al. 2012; Dong et al. 2012;). The important result for the Phase II Demonstration is that the geochemical system behavior can be investigated by carrying out a UQ analysis on only two adjustable geochemical parameters: the total site concentration of nonelectrostatic surface complexation sites (total >SOH) and the cation exchange capacity (CEC). The total concentration of surface complexation sites implicitly includes site density (in units of moles sites per surface area sediment) and sediment surface area.

2.2.1.4 Summary of Uncertain Input Parameters used for HPC and Uncertainty Quantification Modeling

An important task of the F-Area Phase II Demonstration was the use of the HPC and UQ toolsets to define the key parameters that control overall plume behavior and to determine how the uncertainty of these parameters may affect predictions of pH and uranium concentration over space and time. The initial UQ analysis was conducted using

Agni-TOUGHREACT simulations, while the Amanzi code was still under development. TOUGHREACT (Xu et al. 2012) is a multiphase simulator that has been extensively used for subsurface remediation problems. The results of Agni-TOUGHREACT simulations were then used for benchmarking of Agni-Amanzi UQ simulations. UQ simulations were carried out to assess geochemical parameters (kaolinite and goethite reactive and specific surface areas), hydraulic parameters (groundwater recharge, permeability, porosity, and van Genuchten parameters), and source term parameters (basin seepage rate and waste chemistry), which are summarized in Appendix D. The hydraulic and source-term parameter reference values and their uncertainty ranges are based largely on previous studies (Phifer 1991; Flach 2001; Cook et al. 2002; Balakrishnan et al. 2003; Flach 2004; Phifer et al. 2006; Phifer et al. 2007). The geochemical parameters are based on the geochemical dataset described in Section 2.2.1.3 and in Appendix E.

As part of the Phase II Demonstration effort, large initial uncertainty in waste composition was reduced through data analysis to identify key geochemical factors that control overall SRS basin water chemistry (Millings et al. 2012). The mixing model of the archetype waste streams indicated the overall basin system would likely remain acidic much of the time. This analysis also showed that the short-term treatments (e.g., base addition) did not change the waste chemical composition of Basin F-3, which is the primary source of groundwater contamination at the SRS F-Area.

2.2.2 Demonstration Results

2.2.2.1 Data Management

Goals of the Data Management component of the Phase II Demonstration for the SRS F-Area were to expand the Phase I Demonstration database to include the data sets needed to perform the UQ-HPC simulations and to provide automated access. The extended dataset incorporated during Phase II included the area of the Upper Three Runs and Fourmile Branch watersheds (see Figure 2.29). The majority of the SRS data came from two databases: 1) the Landmark depositional database (Smits et al. 1997), which contains information about lithology, well coordinates, well depths, screened zones, depths of stratigraphic units, particle size distribution, and depositional environments, as well as CPT data; and 2) the Bechtel Environmental Integrated Data Management System (BEIDMS) database, including measurements of concentration of 44 analytes and other wellbore parameters collected from 1990 through 2011 from 145 monitoring wells. Additional databases were also incorporated as part of the SRS F-Area Phase II Demonstration, including a hydrostratigraphic database (Smits et al. 1997); a geographic information system database of digital elevation models from topographic maps; and a hydrologic database. The hydrologic database includes hydraulic properties of saturated sediments extracted from a large-scale flow model (Smits et al. 1997; Flach et al. 1999) and unsaturated soil properties (water retention and relative permeability curves) (Phifer et al. 2006). The Akuna Data Management Toolset for the F-Area also incorporated meteorological data, contaminant source release data to the F-Area basins, and a series of relevant environmental and reports. A schematic diagram of the Data Management System implementation, developed as part of the Phase II Demonstration, is shown in Figure 1.4.

2.2.2.2 Visualization

Goals of the visualization component of the Phase II Demonstration were to provide two-dimensional and three-dimensional visualizations of plume migration, monitoring data, uncertainty simulations, and HPC predictions of basin seepage and other model outputs, including uranium concentration and pH evolution over space and time. For the Phase II F-Area Demonstration, several templates were generated for the display of structured (Boxlib format) and unstructured (XDMF and Exodus format) meshes, for model setup files (Tecplot format, lists of Tecplot files), and for HPC simulation output (Amanzi code, XDMF format). Examples of using VisIt with these templates for visualization are shown in the following sections.

2.2.2.3 High Performance Computing

The Phase II simulations of the SRS F Area applied a variety of capabilities in Amanzi. These advances included high-level capabilities of the Multi-Process Coordinator and Process Kernels (such as the new Richards Equation Process Kernel), as well as lower-level capabilities of the HPC Toolset and HPC Core Framework (such as new linear solvers). To capture the influence of the sloping topography and hydrostratigraphy at the F-Area site in the model predictions, unstructured meshes were used. These meshes were created with LaGriT using elevation data for the top surface and layers and then written in Exodus II format for Amanzi. The regions needed to define the initial and boundary conditions for the model were included in the unstructured mesh file. The new capabilities of Amanzi and their role in this demonstration are highlighted in the following paragraphs.

The F-Area demonstration used the new Richards Equation Process Kernel to simulate unsaturated flow in the vadose zone. The Discretization Toolset and mesh infrastructure used by the Richards Equation Process Kernel were enhanced to support polygonal (two-dimensional) and polyhedral (three-dimensional) cells. A seepage face boundary condition was implemented and used on the hill-slope approaching Fourmile Branch Creek. A new optimization capability to minimize non-monotone behavior due to mesh distortion was developed and used within the Mimetic Finite Difference (MFD) framework. The support of both two-dimensional and three-dimensional cells makes it possible to increase efficiency by using a two-dimensional quadrilateral mesh for this two-dimensional centerline simulation. These gains in efficiency are particularly important for UQ and PE studies. In addition, the reaction Process Kernel was enhanced to include the ion exchange and surface complexation reaction networks described in Appendix E. The initial condition for each F-Area run was set at January 1955, computed as part of the simulation using steady-state infiltration and a pseudo-time-stepping algorithm. For low values of the van Genuchten *m*-parameter (less than ~0.35), this proved to be a particularly challenging initialization, and a robust Picard nonlinear solver as well as an interface to the HYPRE libraries Algebraic Multigrid (AMG) solver were added to Amanzi.

The simulations took advantage of Amanzi's capabilities to manage subcycling of one or more process kernels in time. For example, shortly after the active period of waste disposal at the F-Area begins (approximately 1958) until it ends (approximately 1988), the flow rates in the model are relatively high but not varying rapidly in time. This makes it natural for the flow Process Kernel to take larger time steps (by a factor of 10 to 100) than the transport or

reaction Process Kernels. Because reaction and transport are coupled in the same conservation law, their relative subcycling must be much less, and are generally evolved synchronously.

A visualization of an Amanzi simulation for the F-Area model using representative parameter values is shown in Figure 2.32. This simulation of flow and reactive transport in a heterogeneous, multilayered hydrogeological system exercised the new features of Amanzi presented above. Figure 2.32, prepared with VisIt, illustrates the two-dimensional evolution of pH and uranium concentration over time. During the waste discharge operation, the low-pH plume front advanced in front of the uranium plume and thus increased its mobility. Despite the low permeability of the TCZ, both the acidic and uranium plumes reach the LUTRA, which are consistent with the observations. In the post-operational period, the pH values progressively start to rebound as the acidic plume mixes with uncontaminated groundwater, although the pH rebound is impeded by H^+ desorption from minerals. The groundwater pH values remain relatively low for a prolonged time period, and the uranium plume migrates towards the FMB as the uranium concentration decreases significantly. Due to capping of the basin, however, a significant amount of contamination is left in the vadose zone below the basin.

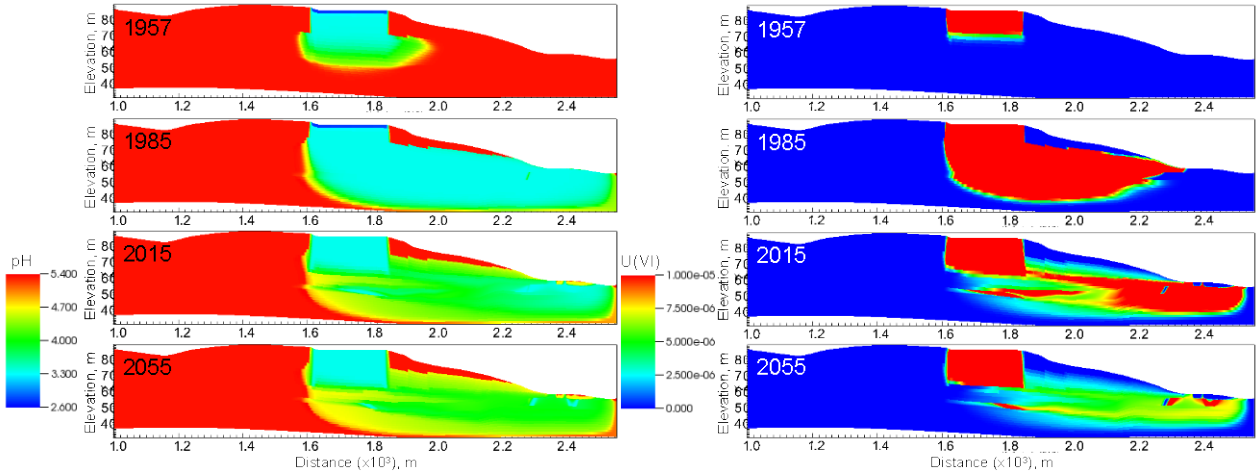

Figure 2.32. Results of two-dimensional Amanzi simulations of the pH (left column) and uranium concentration (right column) evolution over time at the SRS F-Area.

2.2.2.4 Uncertainty Quantification

The overall goal of the Phase II Demonstration UQ component was to demonstrate the application of Akuna and Amanzi to seamlessly integrate uncertainty analysis tools to assess the impact of the seepage from the basin (i.e., source of contamination), key uncertain hydraulic parameters, and geochemical reaction parameters on long-term acidic uranium plume transport at the SRS F-Area. Two steps were taken to accomplish this goal:

1. UQ using Agni coupled to TOUGHREACT, to test Agni prior to Amanzi geochemical model development and to screen the input parameters that would subsequently be used for Amanzi simulations

2. UQ using Agni-Amanzi.

Both the TOUGHREACT and the Amanzi UQ analyses were based on simulations along the two-dimensional centerline of the uranium plume shown in Figure 2.32 and included Monte Carlo uncertainty analysis and global SA. Agni generated multiple sets of parameters from the prescribed probability distribution, distributed the simulations over multiple processors, and analyzed the outputs.

Parameter screening was first conducted using Agni-TOUGHREACT. Agni-TOUGHREACT simulations were based on the application of the geochemical model of reactive transport processes identified through the LBNL SFA research (Dong et al. 2012 Sassen et al. 2012; Spycher et al. 2012; Bea et al. 2012). Although the geochemistry model used in the TOUGHREACT UQ analyses is different from that used with Amanzi, the goal was to obtain a general and qualitative evaluation of input parameters to be used for similar parameters/processes in the Amanzi UQ analysis. Agni and TOUGHREACT were coupled using the PEST protocol within Agni (Doherty 2008) as a pre- and post-processor for 1) sampling the varied parameter values, 2) creating the input files for TOUGHREACT, and 3) analyzing the simulation outputs for the global SA using the Morris method (Morris 1991). The base-case simulation results were compared with observations to validate the model (Bea et al. 2012).

For the UQ analysis, 24 parameters listed in Table 2.2 were selected and used as input to simulations, including flow, geochemical, and source parameters (for their uncertainty ranges and more details, see Appendix D). To assess which factors exerted the greatest control on plume mobility, the total aqueous U(VI) concentration was evaluated at the two wells along the two-dimensional transect (near the source and ~500 m downgradient near the injection zones) and at two times (40 years and at 60 years from the beginning of the waste discharge operations) using a total of 250 simulations.

Table 2.2. Agni-TOUGHREACT Uncertainty Quantification parameters and their symbols. The highlighted parameters are selected for Agni-Amanzi Uncertainty Quantification.

Flow Parameters			**Geochemical Parameters (Surface Area)**			**Source Parameters**	
k_ua	UA	Permeability	kao_ua	UA	Kaolinite reactive surf.	recharge	Natural recharge rate
k_tc	TC		geo_ua	UA	Goethite reactive surf.	basin_wt	Basin discharge rate
k_la	LU		koh_ua	UA	Kaolinite specific surf.	sc_h	Source H^+ conc.***
p_ua	UA	Porosity	koh_tc	TC		sc_no3	Source NO_3^+ conc.***
p_tc	TC		koh_la	LU		sc_so4	Source SO_4^{2-} conc.***
p_la	LU		hoh_ua	UA	Goethite specific surf.	sc_u	Source U conc.***
a_ua	UA	vG* m	hoh_tc	TC		sc_ca	Source Ca^{2+} conc.***
m_ua	UA	vG* m	hoh_la	LU		sc_na	Source Na^+ conc.***

* vG = van Genuchten; ** surf. = Surface; *** conc. = concentration.

The sensitivity of input parameters listed in Table 2.2 is shown in Figure 2.33. These UQ results suggest the key controls on system behavior vary as a function of distance relative to the source and time. Source parameters (such as seepage rate and source pH) tend to have

more influence at early times and near the source, whereas hydrological (such as permeability) and geochemical parameters tend to control plume behavior at distances from the source and at longer times. In terms of the significance of parameters, the geochemical parameters are important only in the UUTRA, which contains most of the plume mass, whereas the sensitivity to permeability is high also in the lower aquifers (TCCZ and LUTRA). This is because the lower hydraulic parameters affect flow in the entire system but the geochemical parameters have a more local impact in the presence of the plume. The porosity of the upper aquifer has an impact—however, not through flow, but through geochemistry because it directly affects sorption through the solid-to-water ratio. The source pH has a significant impact due to the effect of pH-driven reactions on the plume mobility. Based on these results, 12 parameters were selected for the Amanzi UQ analysis: permeability in all the aquifers (UUTRA, TCCZ, and LUTRA); porosity; mineral surface areas in the UUTRA; regional infiltration rate (recharge) and basin seepage rate; and basin discharge (source) pH and U concentration.

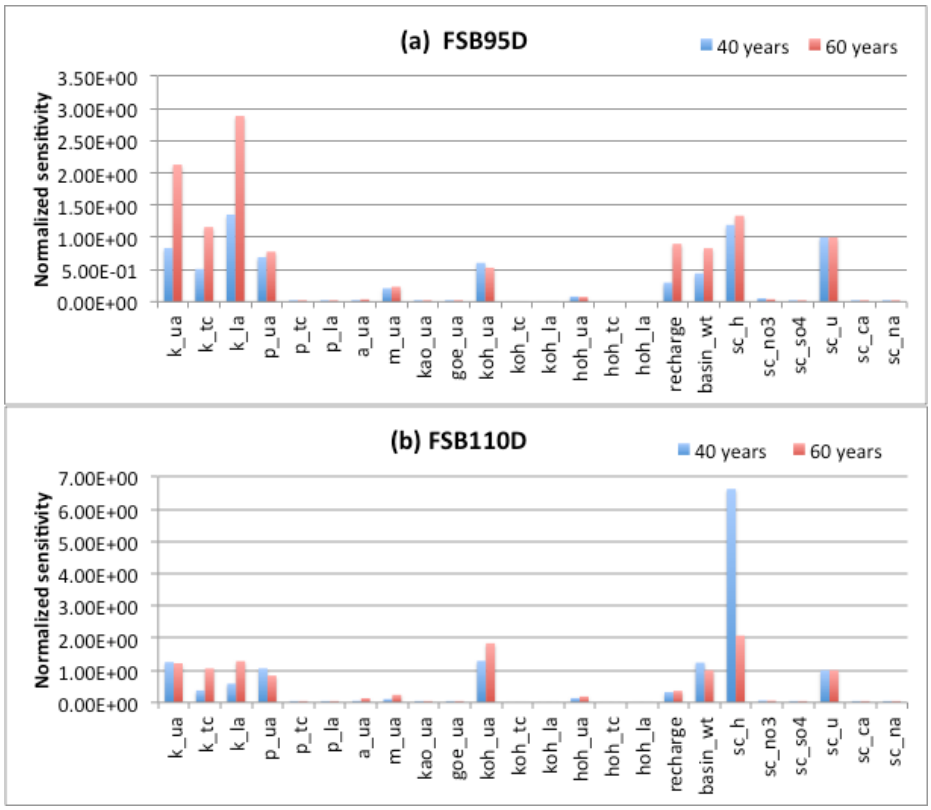

Figure 2.33. Normalized sensitivity relative to the source U(VI) concentration: (a) U(VI) concentration at FSB95D and (b) U(VI) concentration at FSB110D. The parameter symbols are listed in Table 2.2.

Uncertainty quantification was performed using Agni-Amanzi coupling, which used the input parameters selected as described above in addition to two sorption parameters described in Section 2.2.1.3. The use of a different sorption model in Amanzi effectively reduced the sensitivity of the results to the surface area of the sorbent phases (goethite and kaolinite) because this effect is captured directly in the sorption density. Agni distributed and initiated hundreds of Amanzi simulations in parallel, each of which ran on multiple processors on the

NERSC supercomputer, Hopper. Sorption site density was added later in the Amanzi UQ. The Monte-Carlo analysis included comparison of measured and simulated breakthrough curves of pH and the U(VI) concentrations at the downstream monitoring wells (the field data were obtained from the DM database).

The global SA results using Amanzi were compared to the TOUGHREACT results. The selected parameters are listed in Table 2.3 (for their uncertainty distributions and more details, see Appendix D). In the Monte Carlo analysis, Agni generated a total of 150 sets of different parameters from independent normal distributions, using the newly implemented Latin Hypercube sampling, and distributed the simulations over 3600 cores (24 cores per each simulation). All of the Monte Carlo simulations using Amanzi took approximately 4 hours in wall time (which was the longest simulation time among the runs) and approximately 14,400 computer hours. Figure 2.34 shows the Monte Carlo simulation results at the two observation wells for pH and uranium concentrations. The observed breakthrough curves are fairly close to the predicted mean breakthrough curves and within the confidence bounds (mean ± 2 standard deviations) except for some scattered observation points.

Table 2.3. Agni-Amanzi Uncertainty Quantification parameters and their symbols. The highlighted parameters were selected for Agni-Amanzi UQ, while additional sorption parameters that replaced those in the TOUGHREACT analysis were used (see Table 2.4).

Flow Parameters			**Geochemical Parameters**			**Source Parameters**	
k_ua	UA	Permeability	s_dens	UA	Sorption site density	recharge	Natural recharge rate
k_tc	TC		geo_ua	UA	CEC	basin_wt	Basin discharge rate
k_la	LU		koh_ua	UA	Kaolinite specific surf.**	sc_h	Source H^+ conc.***
p_ua	UA	Porosity	hoh_ua	UA	Goethite specific surf.*	sc_u	Source U conc.***
m_ua	UA	vG* m					

* vG = van Genuchten; ** surf. = surface area; *** conc. = concentration

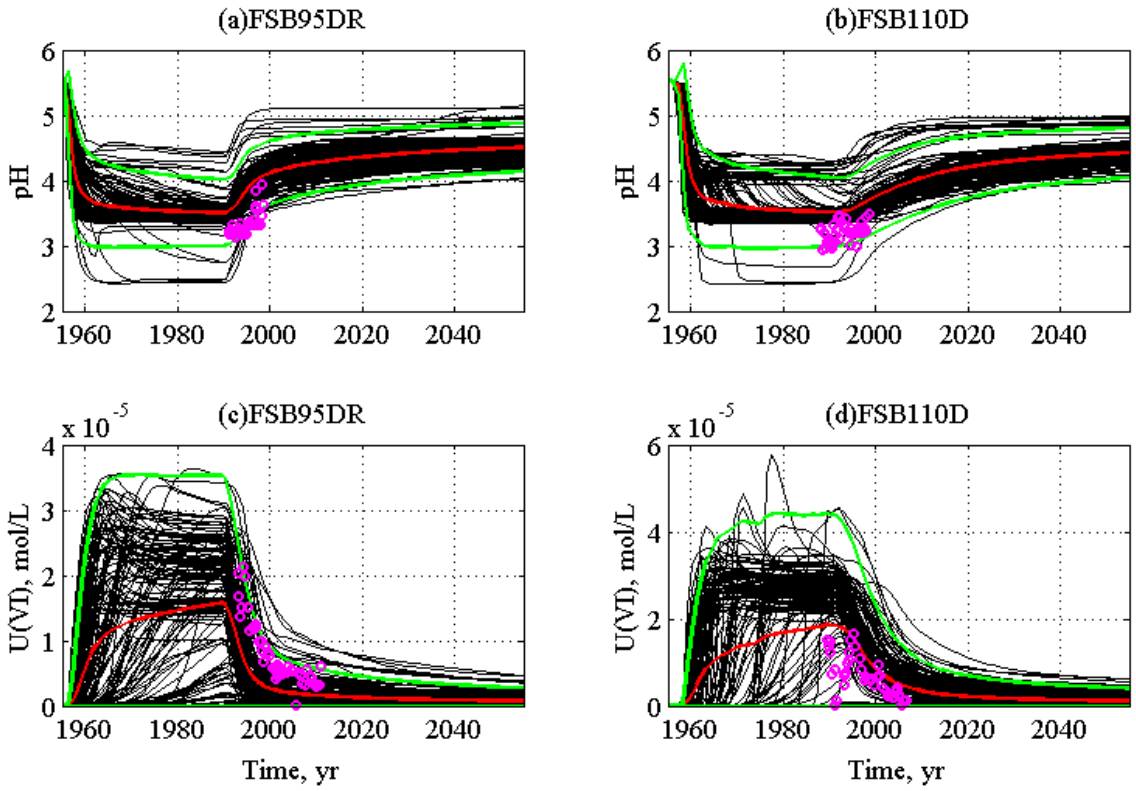

Figure 2.34. MC analysis results: breakthrough curves and their uncertainty ranges: a) pH at FSB95D, b) pH at FSB110D, c) U(VI) concentration at FSB95D, and d) U(VI) at FSB110D. The black lines are the predicted breakthrough curves, red lines are the mean predicted curves, green lines are the mean ± 2 standard deviations, and the magenta dots are observations.

The Amanzi simulations illustrate (Figure 2.34a, b) that during the basin operations, pH values rapidly decrease as the acidic plume arrives. All the pH curves reach a plateau due to saturation of the sorption sites. After the basin closure, the pH rebound is strongly delayed mainly due to the effect of hydrogen (H^+) buffering. Although some curves predict that the pH could exceed the value of 5 by the year 2055, the majority of curves predict a slower pH rebound. Figure 2.34c and 2.34d show that the breakthrough curves of U(VI) concentrations are the reverse of those for pH. Similar to pH, the plateau of U(VI) concentrations can be seen during the basin operation. After the basin closure, uranium concentrations decrease significantly, although the mean curve does not drop below the MCL of 1.3E-7mol/L.

The Agni global SA, using the Morris method, was performed in the same manner as in the Agni-TOUGHREACT simulations to 1) identify the key controls on the plume mobility and 2) evaluate the difference between Amanzi and TOUGHREACT, both of which showed good agreement with the observations. In addition to the two time slices evaluated in the Agni-TOUGHREACT UQ, the sensitivity of pH and U(VI) concentrations was evaluated over time at two locations shown in Figure 2.35.

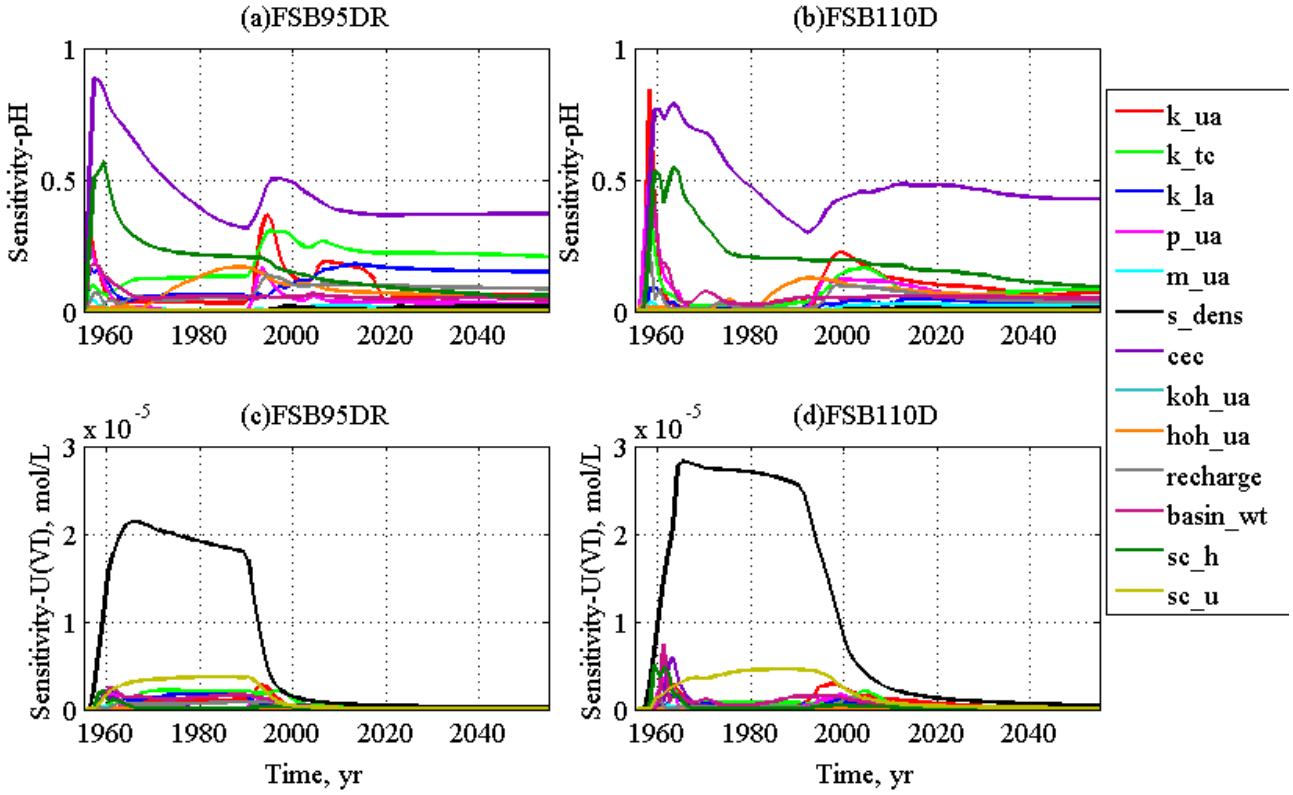

Figure 2.35. Global sensitivity analysis results using Agni-Amanzi: time profile of sensitivity: a) pH at FSB95D, b) pH at FSB110D, c) U(VI) at FSB95D, and d) U(VI) at FSB110D. The parameter symbols are listed in Table 2.3.

Figure 2.35 illustrates complex patterns of the impact of different parameters on pH and U(VI) concentrations during and following the basin closure. Table 2.34 provides a summary of the most influential parameters, including aquifer permeability, geochemical and source parameters. For pH, the CEC and source pH have a large impact at both locations during the operation, whereas after the basin closure, the permeability values become important. For the U(VI) concentrations, the sorption site density and the U(VI) source concentration are the dominant parameters during the basin operation, and the TCCZ permeability becomes important after basin closure. This kind of information is useful for managers and researchers involved in design of long-term monitoring, sampling, and remediation strategies needed for decision making at the site.

Although some interpretations are similar to the Agni-TOUGHREACT SA (e.g., large sensitivity to the source parameters during the basin operation), the sensitivity to the geochemistry parameters is much larger in the Agni-Amanzi results. These differences originate from the difference in both the geochemical system implemented in Amanzi and the parameter range. The global sensitivity depends on the range of parameters; the uncertainty range of the geochemical parameters in the Agni-Amanzi UQ is much larger than the one in the Agni-TOUGHREACT UQ. This is in part due to the fact that far fewer sorption parameters are used in the Agni-Amanzi UQ as compared to the Agni-TOUGHREACT runs,

implying the need for a larger range to capture the full range of uncertainty. This difference suggests the difficulty of interpreting the global sensitivity results but also the importance of having a robust code such as Amanzi to explore the large uncertainty range of geochemistry parameters.

Table 2.4. Three most important parameters controlling pH and U plume mobility at a location close to the basin and a second location far from the basin, assessed at two different times: 1985 (during basin operation) and 2055 (100 years from the beginning of the basin operation).

Location Close to Basin				**Remote Monitoring Well**		
		1985	2055		1985	2055
pH	1	CEC	CEC	1	CEC	CEC
	2	Source pH	TCCZ permeability	2	Source pH	Source pH
	3	Goethite specific surface area	LUTRA permeability	3	Goethite specific surface area	TCCZ permeability
U		1985	2055		1985	2055
	1	Sorption site density	Sorption site density	1	Sorption site density	Sorption site density
	2	Source U	TCCZ permeability	2	Source U	TCCZ permeability
	3	TCCZ permeability	Source U	3	Basin discharge	Source U

2.2.3 Discussion

The Phase II F-Area Demonstration focused on using the newly developed ASCEM HPC and UQ capabilities to assess how uncertainty associated with contaminant source, geochemical reactions, and flow characteristics can impact the predictions of the long-term behavior of pH and U plumes in the region upgradient of the injection barrier at the SRS F-Area. The Amanzi simulations of the unsaturated-saturated flow and contaminant transport (based on the numerical solution of the Richards equation and including a nonelectrostatic sorption model) compared well with field observations. The demonstration also met its main objective of using ASCEM to identify the key hydraulic and geochemical parameters that control plume behavior at different distances from the basin and over time. Gaining such an understanding is a critical prerequisite for making sound and sustainable risk management, remediation, and closure decisions. Note that Monte Carlo simulations of coupled vadose zone and groundwater flow along with reactive transport simulations that take into account complex geochemical reactions are rarely performed over large spatial extents and long time frames such as the simulations shown here. The Amanzi parallel processing capabilities have overcome this hurdle, thereby advancing capabilities to provide a stronger foundation upon which to make remediation decisions.

In addition to meeting the main goals of the Phase II Demonstration, several individual technical accomplishments were achieved. The input file format, based on Extensible Markup Language, accommodated a large number of input parameters in the F-Area model in a way that a user with some subsurface modeling knowledge could easily understand. The parallel implementation of Amanzi enabled the researchers to simulate the long-term plume evolution within a reasonable time frame. Amanzi's robustness allowed researchers to explore the large parameter ranges in UQ. The coupling between Agni and Amanzi

significantly improved the flexibility and usability of the ASCEM-UQ approach; for example, to change parameters and output variables. Agni includes various functions, such as different distributions, Latin hypercube sampling, $\log_{10}$ transform, and factor variation (i.e., changes a parameter by a varied factor), which are essential to perform UQ in a real site applications such as the SRS F-Area, involving a large number of parameters of different types. The ability of Agni to distribute multiple Amanzi simulations over a large number of processors is crucial when each simulation is computationally intensive involving a large domain and complex processes such as the F-Area model.

A number of technical accomplishments were also realized in the DM and Visualization toolsets. The web-based and linked Data Management and Visualization toolsets for the SRS F-Area were significantly expanded from Phase I. Because of the large volume and number of types of the SRS data sets that need to be considered for both building and assessing the synthetic model, this tool has become an essential capability for ASCEM developers and Site Application working group members. Quick access to, and visualization of, the borehole data sets and concentrations of various species helped modelers to efficiently develop a conceptual model. For example, the filtering tool was useful for locating a well with a specific name, wells in a particular geologic unit, or wells having a specific data set (e.g., U concentration). The plotting tool was improved significantly to include multiple curves so that modelers can compare the concentrations of different species and/or different wells in the same figure. The download tool enables modelers to obtain data sets at each well in formats used by Agni-Amanzi. The VisIt templates enabled quick transfer of data and model output into the Visualization Toolset.

In summary, the Phase II Demonstration showed that the ASCEM UQ Agni-Amanzi coupling could provide uncertainty ranges needed for decision-making, risk assessment, and site management. The SRS F-Area Demonstration provides an opportunity to develop and test ASCEM capabilities, which are needed to help EM and Savannah River National Laboratory (SRNL) provide an efficient and cost-effective transition from active to passive cleanup of uranium-contaminated groundwater, using the MNA and enhanced attenuation technologies, which will ultimately be useful throughout the DOE complex.

2.3 Waste Tank Performance Assessment Working Group

2.3.1 Background and Problem Description

The Waste Tank Performance Assessment Working Group provides an opportunity to test and demonstrate ASCEM capabilities needed for EM performance assessments of waste tank closures and low-level waste in engineered containment systems. These types of systems are a prominent component of the EM program across the DOE complex and relevant to many waste disposal, remedial action, decontamination and decommissioning, and long-term stewardship activities. Engineered barriers and waste forms also present unique process and software platform requirements in comparison to purely geologic systems in the form of geometries, materials and associated properties, and physical and chemical processes.

The Phase II Demonstration built upon the Phase I Demonstration and focused on the use of advanced mesh refinement (AMR) to efficiently and accurately resolve fine-scale features

such as steel liners and fast-flow paths that are routinely encountered in Performance Assessment (PA) of engineered containment systems for radiological waste disposal. AMR offers the prospect of increased computational efficiency and/or simulation accuracy by selectively refining only those regions of the domain occupied by small-scale features. Current practice typically involves a coarse uniform mesh resolution that cannot accurately resolve features or a nonuniform orthogonal mesh that introduces large grid cell aspect ratios and size disparities, both of which with corresponding numerical inaccuracies. The demonstration scenario involved radionuclide release from a closed waste tank that is representative of conditions at the SRS and Hanford Site.

2.3.2 Waste Tank Conceptual Model

The specific application is a representative closure scenario for an EM waste tank, similar to the Savannah River Type IV tank depicted in Figure 2.36. The deterministic analysis is intended to mimic the current state of PA modeling practice with respect to physical processes. For example, simple linear sorption will be adopted for contaminant transport modeling. More sophisticated treatment of physical and chemical processes is anticipated in future activities. Although not advancing modeling of processes, the demonstration seeks to advance the state of practice with respect to resolution of fine-scale features.

Waste tank closures and PAs thereof are most advanced in the EM complex at the SRS, where two tanks have been closed and PAs have been issued for the F-Tank and H-Tank Farms. Similar closures and PAs are planned for the Hanford Site. The modeling scenario chosen for the ASCEM Phase II Demonstration is representative of EM tank closure analyses but not tailored to any specific tank or facility. Nonetheless, various model inputs such as material properties are drawn from existing PAs, principally the recent SRS H-Tank Farm PA (SRR 2011). Simulation of the transport of plutonium-238 and its progeny is considered in the demonstration because plutonium-238 and its progeny constitute a significant dose driver (SRR 2011 [Table 5.5-3 and page 546]), and the long-lived members of the plutonium-238 decay chain (plutonium-238 → uranium-234 → thorium-230 →radium-226 → lead-210) have a variety of decay rates and sorption and solubility characteristics. Technetium-99 is an early dose driver (SRR 2011 [Table 5.5-3]) and also considered in the Phase II Demonstration.

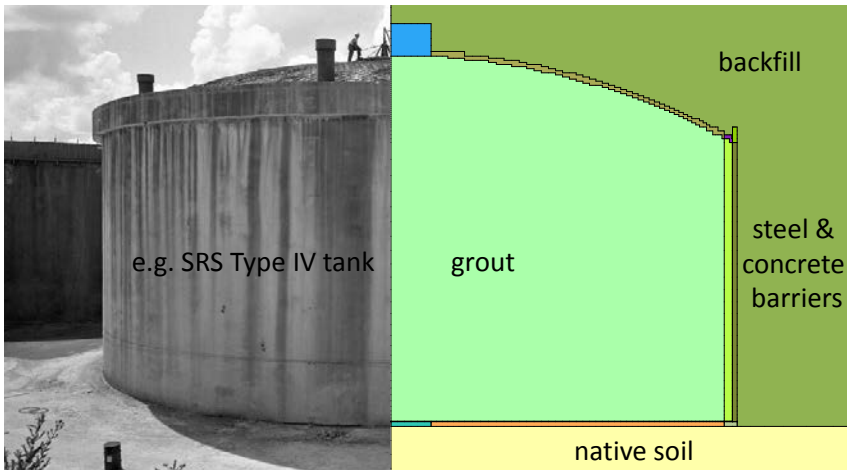

Figure 2.36. EM waste tank closure example.

The PA simulation begins after waste removal to the extent practicable, and the interior void space is filled with a reducing grout (Figure 2.36), leaving the residual waste contained within a nominal 1.3-cm-thick primary steel liner and perhaps partially intermixed with fill grout. Following facility closure, an engineered cover system will be emplaced and initially reduce infiltration to a small fraction of rainfall (Figure 2.37).

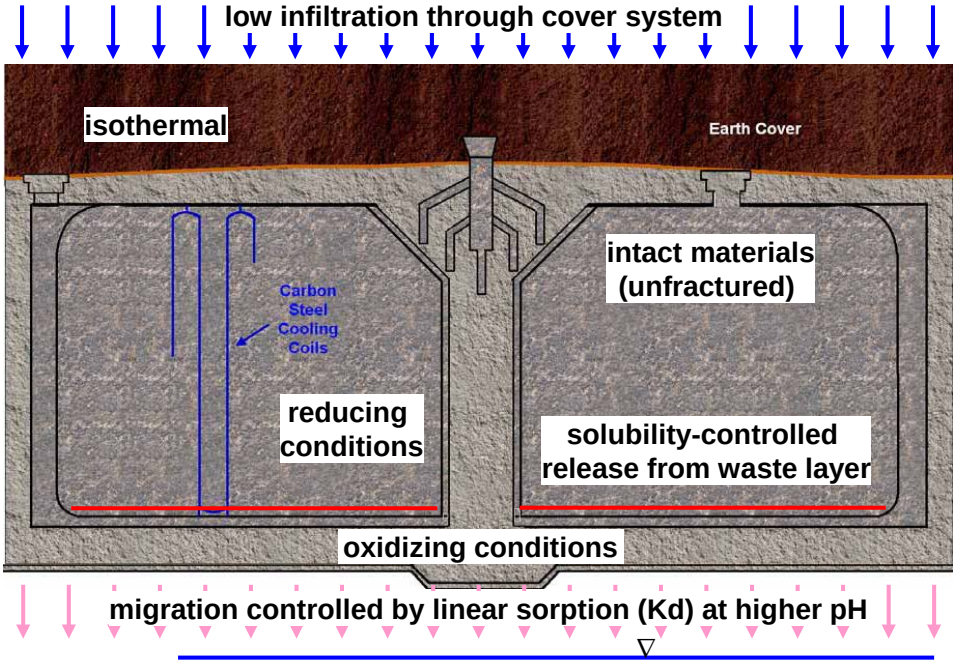

Figure 2.37. Concept for ASCEM Phase II Demonstration.

The regulatory framework for waste tank closure at the SRS is defined in the H-Tank Farm Performance Assessment document (SRR 2011 [Section 2.0]). The PA demonstrates expected compliance with performance objectives over a 10,000-year period following U.S.

Nuclear Regulatory Commission guidance (NRC 2007 [Section 4.1.1.1]). Over 10,000 years and beyond, engineered materials are expected to slowly degrade through a variety of known and potential physical and chemical mechanisms, including general and pitting corrosion influenced by carbonation (steel liners, cooling coils, and reinforcement bars), cracking due to shrinkage, corrosion-induced stresses, and seismic stresses (grout and concrete), and oxidation (grout). The engineered cover system is also expected to degrade through a variety of mechanisms, such that infiltration gradually increases to a level similar to no-cap conditions. Given significant uncertainty in long-range mechanistic predictions of material degradation, PAs often adopt nonmechanistic (postulated) assumptions for nominal and/or sensitivity simulations (e.g., barriers fail at 500 years).

The Phase II Demonstration mimics some of the typical elements of waste tank closure analyses, such as engineered materials, sharp permeability contrasts, fast-flow paths, and physical degradation of materials.

2.3.3 Demonstration Goals and Results

Key ASCEM components engaged in the Phase II Demonstration include the AMR and radioactive decay and progeny ingrowth capabilities within the HPC Toolset. The goal of AMR was to resolve fine-scale features of the selected tank closure scenario, including thin barriers and fast-flow paths, to avoid model simulation biases and uncertainties compared to typical practice. The objective of transport involving radionuclide decay and linear sorption was intended to demonstrate applicability to EM PAs and graded modeling approaches; the latter refers to using less sophisticated modeling of physical processes for screening, probabilistic analyses, or other purposes.

The demonstration effort focused on a benchmarking simulation of steady-state, unsaturated (Richards) flow through the tank geometry depicted in

Figure 2.38 using a uniform grid. Two scenarios were considered: an “Intact” case for which the fast-flow path is not present and a “Fast-Flow” case as depicted in

Figure 2.38. The fast-flow path required fine-scale discretization. Code-to-code benchmarking was performed using the PORFLOW code (http://www.acricfd.com/software/porflow). For the Intact case, Amanzi and PORFLOW produced practically identical saturation fields (Figure 2.39). For the Fast-Flow case, the results are nearly the same (Figure 2.40).

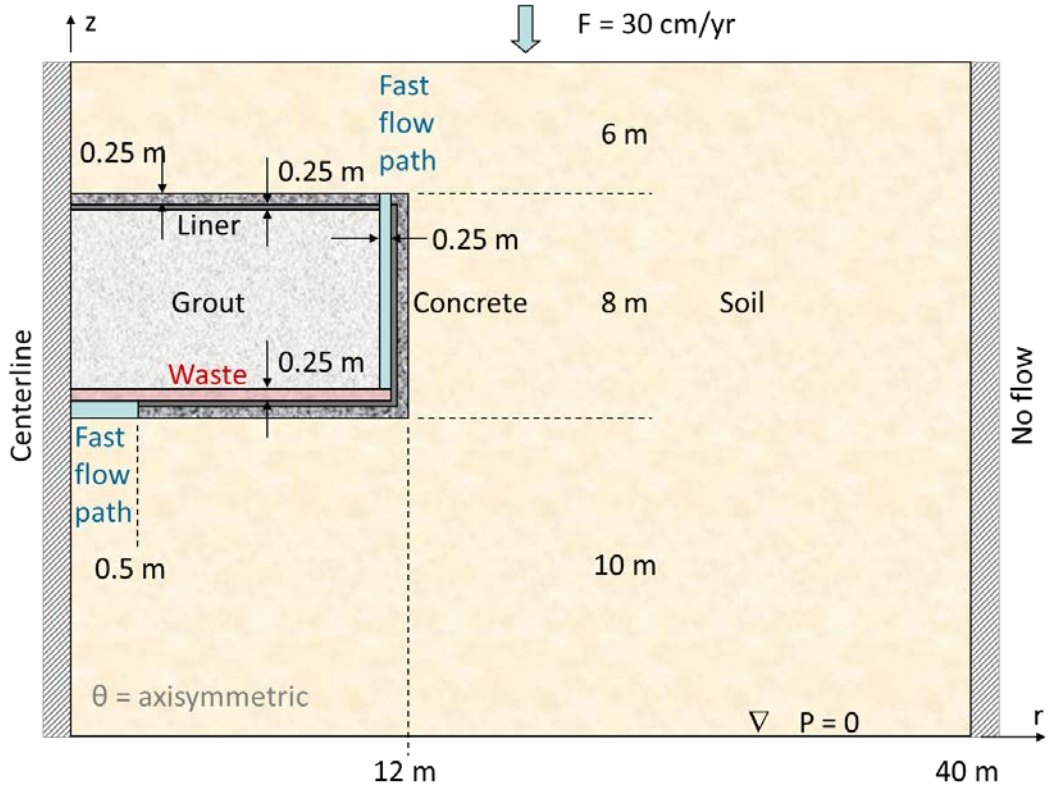

F***igure 2.38***. Tank geometry for benchmarking.

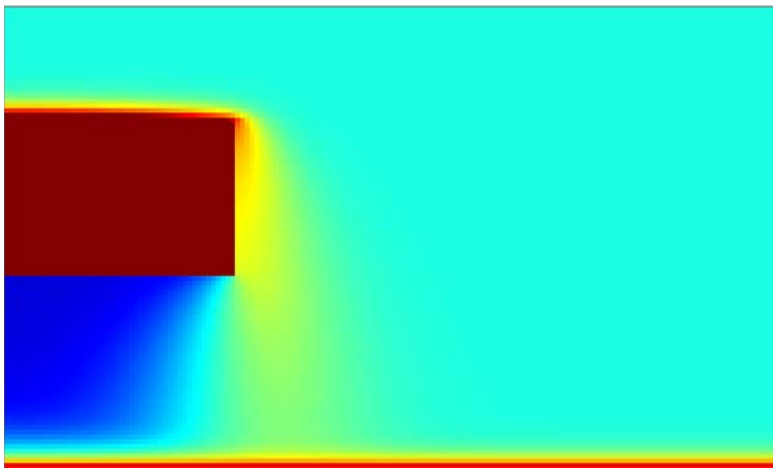

(a)

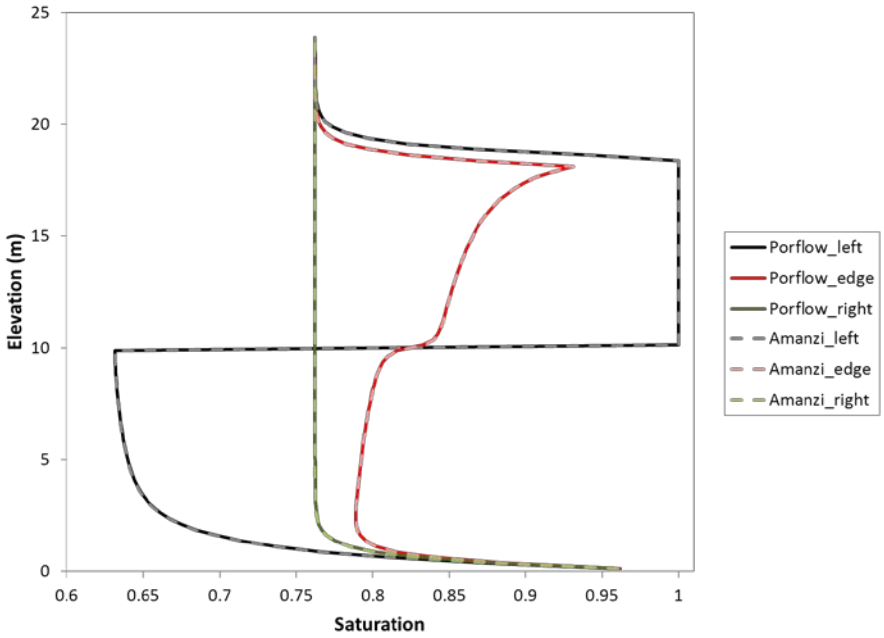

(b)

Figure 2.39. Amanzi simulated results for Intact case: (a) saturation field (saturated is red, unsaturated is blue) and (b) benchmarking comparison for selected vertical profiles.

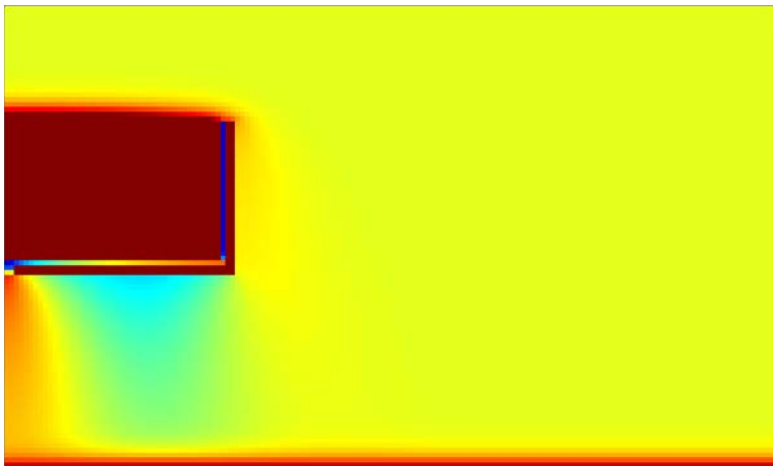

(a)

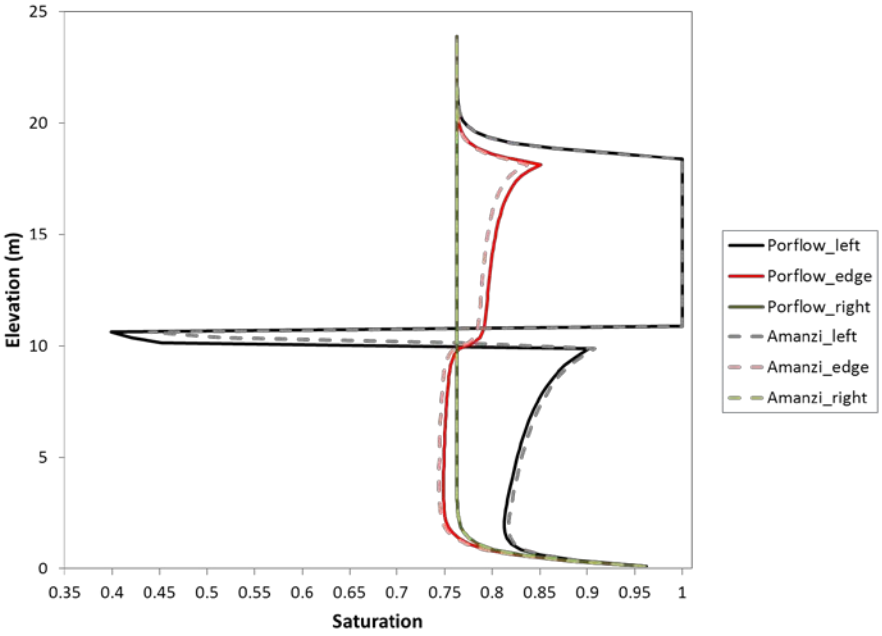

(b)

Figure 2.40. Amanzi simulated results for Fast-Flow case: (a) saturation field (saturated is red and unsaturated is blue) and (b) benchmarking comparison for selected vertical profiles.

The results in Figures 2.39 and 2.40 were generated using a uniform 0.25-meter computational mesh. To demonstrate the AMR capabilities of Amanzi, a similar benchmark simulation for the refined geometry depicted in Figure 2.41 was pursued. Although the two benchmarking problems share the same features, the second geometry was greatly refined to reflect the true physical dimensions of key features. In particular, the thick steel liner and fast-flow path were reduced to a thickness of 1 and 2 centimeters, respectively, from 25 cm, the resolution of the uniform grid. As anticipated, achieving convergence of unsaturated flow on an AMR grid for highly-contrasting fine-scale features was challenging. These challenges drove algorithm development for Amanzi during Phase II that focused primarily

on two key areas: problem geometry specification and computational efficiency through robust solver performance.

Currently, the HPC Thrust is pursuing numerical advances in solving the nonlinear coupled system that arises from representing the Richards equation on the AMR grid. These include a nonlinear multigrid strategy to better couple the AMR refinement levels together and a wider range of methods to solve the nonsymmetric linear systems that arise. Other areas for enhancement include the incorporation of time-dependent material properties (to better represent the transient system throughout the lifespan of the engineered systems) and incorporation of the radioactive decay models into Amanzi for solute transport.

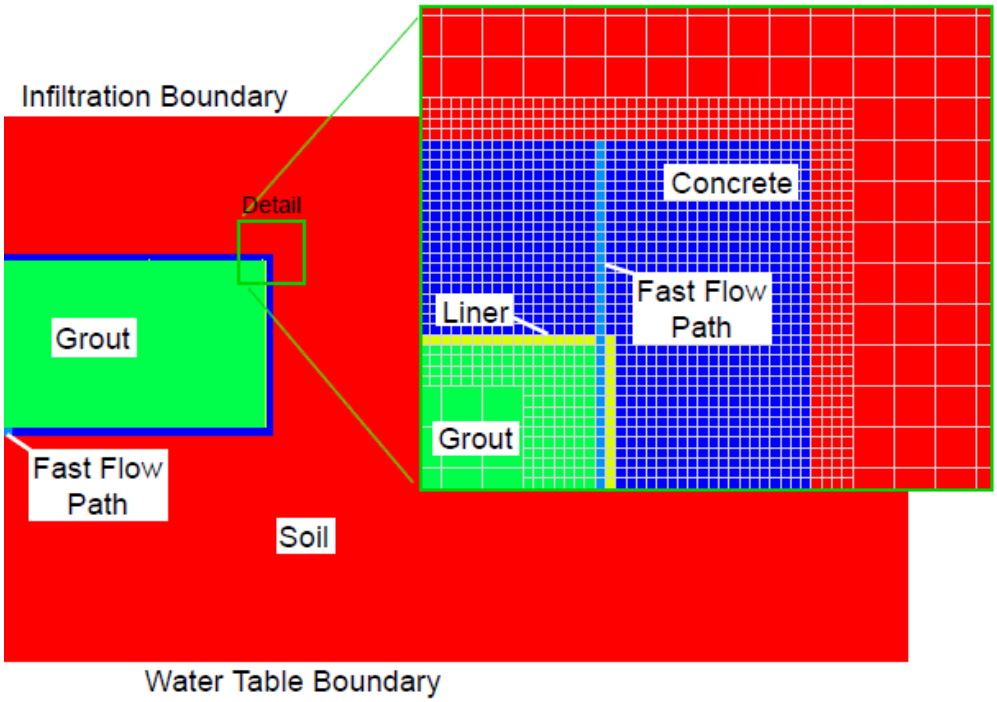

Figure 2.41. Tank geometry for Amanzi benchmarking using an AMR grid.

In anticipated future activity, Amanzi will be used to simulate flow and releases of radionuclides from a grouted waste tank to the underlying water table over hundreds to thousands of years to complete the primary Waste Tank PA demonstration begun in Phase II. Physical phenomena to be considered in the simulation include transient, variably saturated moisture transport using Richards equation, and transport of dissolved radionuclides through advection and diffusion. The transport simulation will incorporate first-order decay and progeny ingrowth, linear sorption (K_d), and solubility controls under isothermal conditions. Infiltration and selected material properties will be prescribed to vary through time. Parallel runs on up to 1000 cores are anticipated.

Another activity consisted of collaboration with the Cementitious Barriers Partnership (CBP) for development of loosely coupled near-field simulation of processes within a barrier, including ASCEM far-field simulation of processes in the surrounding geologic environment. The CBP simulation generated a data file of transient water and solute fluxes at the cement–soil interface that can be used as a static source term or boundary condition in an ASCEM simulation.

2.3.4 Discussion

The Waste Tank PA demonstration is motivated by the need to resolve fine-scale components of engineered containment systems and by the expectation that simulation of unsaturated flow through these systems presents a test of AMR numerical algorithms in Amanzi. Progress on the Phase II Demonstration and testing led to several implemented and pending algorithm advances, including a fully-coupled modified Newton solver for Richards equation on adaptive AMR grids. Further development of Amanzi is needed, including the development of more robust schemes to solve the nonlinear and poorly-conditioned linear systems that arise. Completion of the joint ASCEM–CBP demonstration will entail the development of an interface to enable detailed (flux-, or source-based) coupling.

3 DISCUSSION

Phase II Demonstration activities 1) used an end-to-end approach to illustrate integration of many ASCEM capabilities; 2) advanced many ASCEM-specific components, including Data Management, Model Setup, PE, UQ, HPC, and Visualization; and (3) illustrated how ASCEM toolsets can be used to address EM problems. The end-to-end demonstration showed the advantage of linking Akuna and Amanzi to facilitate linked model setup, execution, and analysis, including PE and uncertainty analysis. HPC allowed execution of a suite of mechanistic models that considered detailed information about uncertainties, heterogeneities, parameter distributions, and boundary conditions in high resolution and over plume-relevant spatial scales. The Phase II Demonstration followed a major development effort and relied more on the Site Applications Thrust working groups for implementation of ASCEM capabilities than Phase I.

During the Phase II Demonstration, new data management methodologies were developed, including a new design of the database infrastructure. The resulting unified database system can represent data from heterogeneous sources having different formats. This approach not only allows the data to be stored in a uniform format but also permits automatic generation of views that drive the same kind of interfaces for all relevant data types. This approach makes it easy for users to find data of interest, use filter functions to select subsets of interest, and browse data by visualizing plots, graphs, and plume extents.

The Phase II Demonstration showed that that the ASCEM HPC and UQ toolsets can be used for simulating complex geochemical reactions in heterogeneous systems over large spatial extents and long time frames. Amanzi simulations of unsaturated-saturated flow and contaminant transport (based on the numerical solution of the Richards equation) as well as reactive transport (using a complex nonelectrostatic geochemistry model) were conducted in

two and three dimensions and over large spatial extents. The model simulations compared well with field observations at two different sites: the Hanford Site BC Cribs and the SRS F-Area Seepage Basins. HPC also featured the availability of AMR, where localized regions of enhanced mesh refinement are generated automatically to represent combinations of fine-scale features (e.g., material interfaces) and representation of advancing fronts with contrasting properties. AMR was evaluated for the Waste Tank PA representative problem.

The Phase II Demonstration for both the DVZ and F-Area showed that the UQ Agni-Amanzi coupling can provide uncertainty ranges needed for decision making, risk assessment, and site management. At the F-Area, the UQ analysis identified the key hydraulic and geochemical parameters that control plume behavior as a function of the distance from the contaminant source and over time. At the BC Cribs, the UQ analysis captured uncertainty with respect to subsurface heterogeneities and recharge rates. In general, the coupling between Agni and Amanzi significantly improved the flexibility and usability of the ASCEM-UQ approach; for example, to change parameters and output variables. The ability of Agni to distribute multiple Amanzi simulations over large numbers of processors was crucial to such simulations, each of which was computationally intensive.

The Akuna Toolset was used to support a complete modeling workflow, from model setup to simulation execution and analysis through visualization. The demonstrations showed how Akuna tools can be used to manage environmental and simulation data sets and methods for individual simulations as well as PE and UQ analyses. Visualization of site data, conceptual and numerical models simulation outputs, and UQ and PE summary results are integrated into Akuna to support powerful visual exploration of environmental and simulation data sets. Although designed to work with Amanzi, Akuna can be used with any simulator as long as it is set up to read and write the file formats specific for that simulator. This flexibility was demonstrated using the TOUGHREACT and eSTOMP simulators in the Phase II Demonstration.

The Visualization Toolset was significantly expanded in the Phase II Demonstration. Methods and templates to enable quick access to and visualization of the borehole data sets and concentrations of various species were developed to facilitate generation of a site conceptual model, associated model domain for simulation, and comparison of simulated and measured data. The plotting tool was improved significantly to include multiple curves so that users can compare the concentrations of different species and/or different wells in the same graphical representation.

4 FUTURE WORK

The Phase III ASCEM Demonstration marks the beginning of the applied phase of the project, in which capabilities and quality assurance of the toolsets are refined to a point where they can be demonstrated to guide site cleanup efforts and be tested by end users. Working group activities and interactions with end users will be a new focus of the Site Applications Thrust in an effort to begin integrating ASCEM into the EM community and gaining broader feedback on needed performance and capabilities.

The Platform and Integrated Toolset will continue capability enhancements to interface with HPC simulation capabilities to provide support for model development and analysis tasks. The Data Management structure will continue to be enhanced and integrated with Visualization tools. A key focus will be on creation of interfaces to enable the data management system to be easily queried and data extracted to provide integration with other Platform toolsets. The Model Setup and Analysis Toolset will be enhanced with new capabilities to support conceptual/numerical model generation, with different mesh types, and enhanced geochemical models. Improvements to usability, robustness, and performance will also be made. Akuna will be enhanced for improved workflows, model management, and new algorithms available in the toolsets. Attention will be given to performance and usability of the environment. New capabilities will be added to the PE, UQ, and SA toolsets. Commonalities in the toolsets will be exploited to improve performance. An initial version of the Decision Support Toolset will be designed and implemented. The interface between Akuna and Amanzi, known as Agni, will be enhanced to improve robustness and performance.

HPC enhancements will continue to focus on improving performance. The flexibility of the Multi-Process Coordinator, which manages coupling of processes, will be enhanced to provide more robust and accurate simulation models. Features will be added that enhance integration with the Platform Toolset, such as model gradients for optimization and capabilities for computing parameter sensitivities. Solvers will be enhanced through design and implementation of pre-conditioners to support flexibility, robustness, and scalability. The HPC Core Framework Toolset will leverage an existing build process in conjunction with automated testing and reporting to improve reliability of all components. Together with the verification and validation activity, this capability will provide support for quality assurance.

The Site Applications Thrust working groups will continue efforts to implement model development to advance and refine capabilities and to test EM-relevant questions. The working groups will collaborate with the Platform and HPC thrusts to prepare a series of demonstration workshops based on Phase II Demonstration results that will be conducted at EM sites, such as the Hanford Site and SRS, as well as others.

The SRS F-Area Working Group will focus demonstration activities to include engineered treatments conducted to date at the site and evaluate remediation alternatives. The demonstration will evaluate the possibility of replacing active groundwater remediation with natural and enhanced attenuation strategies for final end-state decisions. The enhanced ASCEM components will be demonstrated in a final significant effort for this working group. The DVZ Working Group will focus efforts on making the Phase II Demonstrations more robust and providing test cases and expertise to support model development and testing. Future demonstrations will include explicit representation of soil desiccation and other remediation technologies, as well as exploring the concept of end states and options for site closure. The Waste Tank Performance Assessment Working Group will complete work on advancements in the areas of AMR implementation on structured grids, radioactive decay and progeny ingrowth, and collaboration with CBP on a joint demonstration. The waste tank problem set will be expanded with data from SRS and the Hanford Site, as appropriate, commensurate with ongoing code development. The Oak Ridge Mercury Working Group

will develop a detailed plan, including identification of crucial first steps and implementation of a surface–water component in the analysis.

The ASCEM capabilities are expected to help EM provide efficient and cost-effective transition to site closure end states. Through the working groups and end-user engagement, ASCEM will sequentially test and demonstrate capabilities that will enable it to be used to guide DOE site decision making to develop long-term paths to completing the DOE cleanup mission.

5 REFERENCES

Balakrishnan S, A Roy, MG Ierapetritou, GP Flach, and PG Georgopoulos. 2003. "Uncertainty Reduction and Characterization of Complex Environmental Fate and Transport Models: An Empirical Bayesian Framework Incorporating the Stochastic Response Surface Method." *Water Resources Research* 39(12):1350. doi:10.1029/2002WR001810.

Bea SA, H Wainwright, N Spycher, B Faybishenko, S Hubbard, and ME Denham. 2012. "Identifying Key Controls on Acidic-U(VI) Plume Behavior at the Savannah River Site, Using Reactive Transport Modeling." *Journal of Contaminant Hydrology* (In Press).

Cook JR, LB Collard, GP Flach, and PL Lee. 2002. *Development of Probabilistic Uncertainty Analysis Methodology for SRS Performance Assessments Maintenance Plan Activities*. WSRC-TR-2002-00121, Westinghouse Savannah River Corporation, Aiken, South Carolina.

Davis JA, JA Coston, DB Kent, and CC Fuller. 1998. "Application of the Surface Complexation Concept to Complex Mineral Assemblages." *Environmental Science & Technology* (32)19:2820-2828.

Diggle PJ and PJ Ribeiro. 2006. *Model-Based Geostatistics*. Springer, New York.

DOE – U.S. Department of Energy. 1992. *B-Plant Source Aggregate Area Management Study Report*. DOE-RL-92-05, Rev. 0, U.S. Department of Energy, Richland Operations Office, Richland, Washington.

Dong W, TK Tokunaga, JA Davis, and J Wan. 2012. "Uranium(VI) Adsorption and Surface Complexation Modeling Onto Background Sediments from the F-Area Savannah River Site." *Environmental Science & Technology* 46(3):1565-1571.

Doherty J. 2008. *PEST: Model-Independent Parameter Estimation*. Watermark Numerical Computing, Brisbane, Australia.

EarthVision. 2012. Accessed September 27, 2012, at http://www.dgi.com/earthvision/evmain.html.

Fenimore JW and JH Horton. 1973. *Operating History and Environmental Effects of Seepage Basins in Chemical Separations Areas of the Savannah River Plant*. DPST-72-548, E.I. du Pont de Nemours & Co, Savannah River Laboratory, Aiken South Carolina.

Flach G. 2004. *Groundwater Flow Model of the General Separations Area Using Porflow (U).* WSRC-TR-2004-00106, Westinghouse Savannah River Company, Aiken, South Carolina.

Flach GP, MK Harris, RA Hiergesell, AD Smits, and KL Hawkins. 1999. *Regional Groundwater Flow Model for C, K, L, and P Reactor Areas, Savannah River Site, Aiken, South Carolina (U).* WSRC-TR-99-00248, Rev. 0, Westinghouse Savannah River Company, Aiken, Aiken, South Carolina.

Gorton I, S Finsterle, K Schuchardt, C Gable, D Higdon, M Vessilinov, W McGinn, A Shoshani, and D Agarwal. 2010. *System Requirements for ASCEM Platform and Integrated Toolsets.* ASCEM-PIT-102610-Rev. 3, U.S. Department of Energy, Washington, D.C.

Gorton I, C Sivaramakrishnan, G Black, S White, S Purohit, M Madison, and K Schuchardt. 2011. "Velo: Riding the Knowledge Management Wave for Simulation and Modeling." In *Proceedings of the 4th International Workshop on Software Engineering for Computational Science and Engineering* (SECSE 2011), pp. 32-40. Association for Computing Machinery, New York.

Hammond GE, PC Lichtner, C Lu, and RT Mills. 2012. "PFLOTRAN: Reactive Flow and Transport Code for Use on Laptops to Leadership-Class Supercomputers. In *Ebook: Groundwater Reactive Transport Models*, F Zhang, GT Yeh, and JC Parker (eds.), Bentham Science Publishers, pp. 141-159, eISBN: 978-1-60805-306-.
doi: 10.2174/978160805306311201010141.

Hubbard S, B Faybishenko, M Freshley, D Agarwal, J Bell, W Bethel, M Denham, G Flach, V Freedman, G Hammond, D Higdon, J Horsman, E Keating, P Lichtner, L Monroe, P Monroe, P Moore, D Moulton, G Pau, D Schep, K Schuchardt, R Seitz, A Shoshani, N Spycher, and P Weber. 2010. *ASCEM Phase I Demonstration.* ASCEM-SITE-102010-0, U.S. Department of Energy, Washington, D.C.

Icenhower JP, N Qafoku, WJ Martin, and JM Zachara. 2008. *The Geochemistry of Technetium: A Summary of the Behavior of an Artificial Element in the Natural Environment.* PNNL-18139, Pacific Northwest National Laboratory, Richland, Washington.

Killian TH, NL Kolb, P Corbo, and IW Marine. 1986. *Environmental Information Document, F-Area Seepage Basins*. Report No. DPST 85-704, E.I. du Pont de Nemours & Co, Savannah River Laboratory, Aiken South Carolina.

Konikow LF and JD Bredehoeft. 1992. "Groundwater Models Cannot be Validated." *Advances in Water Resources* 15:75-83.

LaGriT. 2012. Accessed September 27, 2012, at https://lagrit.lanl.gov/.

Millings MR, BB Looney, and ME Denham. 2012. *Geochemical Modeling of F Area Seepage Basin Composition and Variability*. SRNL-STI-2012-00269, Rev. 0, Savannah River National Laboratory, Aiken, South Carolina.

Morris, MD. 1991. "Factorial Sampling Plans for Preliminary Computational Experiments." *Technometrics*, 33: 161–174.

Moulton D, M Berndt, M Buskas, R Garimella, L Prichett-Sheats, G Hammond, M Day, and J Meza. 2011. *High-Level Design of Amanzi, the Multi-Process High Performance Computing Simulator*. ASCEM-HPC-2011-030-1, U.S. Department of Energy, Washington, D.C.

U.S. Nuclear Regulatory Commission. 2007. *NRC Staff Guidance for Activities Related to U.S. Department of Energy Waste Determinations, Draft Final Report for Interim Use*. NUREG-1854, US Nuclear Regulatory Commission, Washington, D.C.

Petrel – Petrel E&P Software Platform. 2012. Accessed September 27, 2012, at http://www.slb.com/services/software/geo/petrel.aspx.

Phifer MA. 1991. "Closure of a Mixed Waste Landfill – Lessons Learned." In *Waste Management 1991*, pp. 517-525. Waste Management Symposia, Phoenix, Arizona.

Phifer MA, MR Millings and GP Flach. 2006. *Hydraulic Property Data Package for the E-Area and Z-Area Soils, Cementitious Materials, and Waste Zones*. Westinghouse Savannah River Company, Savannah River Site, Aiken, South Carolina.

Phifer MA, WE Jones, EA Nelson, ME Denham, MR Lewis, and EP Shine. 2007. *FTF Closure Cap Concept and Infiltration Estimates*. WSRC-STI-2007-00184, Rev. 2, Westinghouse Savannah River Corporation, Aiken, South Carolina.

Rucker DF and JB Fink. 2007. "Inorganic Plume Delineation Using High-Resolution Electrical Resistivity at the BC Cribs and Trenches Site, Hanford." *Vadose Zone Journal* 6(6):946-958.

Sassen DS, SS Hubbard, SA Bea, J Chen, N Spycher, and ME Denham. 2012. "Reactive Facies: An Approach for Parameterizing Field-Scale Reactive Transport Models Using Geophysical Methods." *Water Resources Research* (in press). doi:10.1029/2011WR011047.

Serne RJ, AL Ward, W Um, BN Bjornstad, DF Rucker, DC Lanigan, and MW Benecke. 2009. *Electrical Resistivity Correlation to Vadose Zone Sediment and Pore-Water Composition for the BC Cribs and Trenches Area*. PNNL-17821, Pacific Northwest National Laboratory, Richland, Washington.

Smits AD, MK Harris, KL Hawkins, and GP Flach. 1997. *Integrated Hydrogeological Model of the General Separations Area, Volume 1: Hydrogeological Framework*. WSRC-TR-96-0399, Rev. 0, Westinghouse Savannah River Company, Savannah River Site, Aiken, South Carolina.

Spycher N, S Bea, H Wainwright, S Mukhopadhyay, J Christensen, W Dong, S Hubbard, J Davis, and M. Denham. 2012. "Integrating Geochemical, Reactive Transport, and Facies-Based Modeling Approaches at the Savannah River F-Area." Goldschmidt, June 24-29, 2012, Montreal, Canada.

Savannah River Remediation. 2011. *Performance Assessment for the H-Area Tank Farm at the Savannah River Site*. SRR-CWDA-2010-00128, Rev. 0. Savannah River Remediation, LLC, Closure and Waste Disposal Authority, Aiken, South Carolina.

Strom RN and DS Kaback. 1992. *SRP Baseline Hydrogeologic Investigation: Aquifer Characterization, Groundwater Geochemistry of the Savannah River Site and Vicinity*. WSRC-RP-92-450 (DE93 003187), Savannah River Laboratory and Westinghouse Savannah River Company, Aiken, South Carolina.

Steefel C. 2012. *CrunchFlow, Software for Modeling Multicomponent Reactive flow and Transport, User's Manual*. Lawrence Berkeley National Laboratory, Berkeley, California. Accessed October 23, 2012, at http://www.csteefel.com/CrunchPublic/CrunchFlowIntroduction.html.

Steefel C, D Moulton, G Pau, K Lipnikov, J Meza, P Lichtner, T Wolery, D Bacon, N Spycher, J Bell, G Moridis, S Yabusaki, E Sonnenthal, G Zyvoloski, B Andre, L Zheng, and J Davis. 2011. *Mathematical Formulation Requirements and Specifications for the Process Models*. ASCEM-HPC-2011-01-0a, U.S. Department of Energy, Washington, D.C.

Truex MJ, M Oostrom, VL Freedman, C Strickland, and AL Ward. 2011. *Laboratory and Modeling Evaluations in Support of Field Testing for Desiccation at the Hanford Site*. PNNL-20146, Pacific Northwest National Laboratory, Richland, Washington.

VisIt. 2012. Accessed September 27, 2012, at https://wci.llnl.gov/codes/visit/.

Ward AL, M Oostrom, and DH Bacon. 2008. *Experimental and Numerical Investigations of Soil Desiccation for Vadose Zone Remediation: Report for Fiscal Year 2007*. PNNL-17274, Pacific Northwest National Laboratory, Richland, Washington.

Ward AL, RJ Serne, and MW Benecke. 2009. "Development of a Conceptual Model for Vadose Zone Transport of Tc-99 at Hanford's BC Cribs and the Screening of Remedial Alternatives." In *Waste Management 2009: Waste Management for the Nuclear Renaissance*, March 1-5, 2009, WM Symposia, Tucson, Arizona.

White MD and M Oostrom. 2000. *STOMP – Subsurface Transport Over Multiple Phases: Theory Guide*. PNNL-12030, Pacific Northwest National Laboratory, Richland, Washington.

White MD and M Oostrom. 2006. *STOMP – Subsurface Transport Over Multiple Phases, Version 4: User's Guide*. PNNL-15782, Pacific Northwest National Laboratory, Richland, Washington.

WorldWind. 2012. Accessed September 27, 2012, at http://worldwind.arc.nasa.gov/java/.

Xu T, E Sonnenthal, N Spycher, and K Pruess. 2006. *TOUGHREACT User's Guide: A Simulation Program for Non-Isothermal Multiphase Reactive Geochemical Transport in Variably Saturated Geologic Media*. LBNL-55460 (Revised 2006, V1.2), Lawrence Berkeley National Laboratory, Berkeley, California.

Xu T, N Spycher, E Sonnenthal, L Zheng, and K Pruess. 2012. *TOUGHREACT User's Guide: A Simulation Program for Non-Isothermal Multiphase Reactive Geochemical Transport in Variably Saturated Geologic Media, Version 2.0*. LBNL-DRAFT, Lawrence Berkeley National Laboratory, Berkeley, California.

Appendix A – LIST OF ASCEM PUBLICATIONS

PEER REVIEWED PUBLICATIONS

Bea SA, H Wainwright, N Spycher, B Faybishenko, S Hubbard, and ME Denham. 2012. "Identifying key controls on acidic-U(VI) plume behavior at the Savannah River Site, using reactive transport modeling." *Journal of Contaminant Hydrology* (submitted).

Faybishenko B. 2011. "Fuzzy-Probabilistic Calculations of Evapotranspiration." Chapter 5 in *Evapotranspiration - Remote Sensing and Modeling*, InTech Publisher, pp. 81-96. ISBN 978-953-307-808-3.

Meyer J, W Bethel, J Horsman, SS Hubbard, H Krishnan, EH Keating, L Monroe, R Strelitz, P Moore, G Taylor, B Torkian, TC Johnson, and I Gorton. 2012. "Visual Data Analysis as an Integral Part of Environmental Management." *IEEE Transactions on Visualization and Computer Graphics* 18(12):2088-2094.

Tokunaga TK, J Wan, and ME Denham. 2012. "Estimates of vadose zone drainage from a capped seepage basin, F Area, Savannah River site." *Vadose Zone Journal* (in press).

Williamson M, J Meza, D Moulton, I Gorton, M Freshley, P Dixon, R Seitz, C Steefel, S Finsterle, S Hubbard, M Zhu, K Gerdes, R Patterson, and YT Collazo. 2011. "Advanced Simulation Capability for Environmental Management (ASCEM): An Overview of Initial Results. *Technology and Innovation* 13(2):175-199, 1949-8241. DOI: 10.3727/1949822411Z13085939956625.

ABSTRACTS

Agarwal D, A Wiedmer, B Faybishenko, J Hunt, G Kushner, A Romosan, A Shoshani, and T Whiteside. 2012. "A Methodology for Management of Heterogeneous Site Characterization and Modeling Data." Accepted for the oral presentation at the *XIX International Conference on Computational Methods in Water Resources* (CMWR 2012, June 2012).

Faybishenko B and G Flach. 2012. "Uncertainty Quantification of Evapotranspiration and Infiltration from Modeling and Historic Time Series at the Savannah River F-Area." *Fall 2012 American Geophysical Union Meeting*, San Francisco, California, December 2012.

Freshley MD, JD Moulton, I Gorton, SS Hubbard, VL Freedman, G Flach, CI Steefel, SA Finsterle, and P Dixon. 2012. "Advanced Simulation Capability for Environmental Management (ASCEM): Development and Demonstrations." *Subsurface Biogeochemical Research Annual Meeting*, April 30 - May 2, 2012, Wardman Park Hotel, Washington, D.C.

Meyer J, EW Bethel, J Horsman, S Hubbard, H Krishnan, A Romosan, E Keating, L Monroe, R Strelitz, P Moore, G Tayler, B Torkian, TC Johnson, and I Gorton. 2012. "Visual Data Analysis as an Integral Part of Environmental Management." *IEEE Visualization 2012*, Seattle, Washington, October 14-20, 2012.

Moulton JD, CI Steefel, I Gorton, V Freedman, and P Dixon. 2012. "Amanzi: A Parallel Open-Source Flow and Reactive-Transport Simulator for Environmental Applications." *InterPore*, May 14-16, 2012, Purdue University, West Lafayette, Indiana.

Schuchardt KL, DA Agarwal, SA Finsterle, CW Gable, I Gorton, LJ Gosink, EH Keating, CS Lansing, J Meyer, WAM Moeglein, GSH Pau, EA Porter, S Purohit, ML Rockhold, A Shoshani, and C Sivaramakrishnan. 2012. "Akuna - Integrated Toolsets Supporting Advanced Subsurface Flow and Transport Simulations for Environmental Management." *XIX International Conference on Computational Methods in Water Resources* (CMWR 2012), University of Illinois at Urbana-Champaign, June 17-22, 2012.

Wiedmer A, JR Hunt, B Faybishenko, D Agarwal, GP Flach, T Whiteside, P Bennet, L Bagwell, A Romosan, and SS Hubbard. 2011. "Mass Balances and Uncertainty in Radionuclide Transport at the SRS F-Area Seepage Basins Groundwater Plume." *American Geophysical Union*, Fall Meeting, December 5-9, 2011, San Francisco, California.

Wiedmer A, JR Hunt, B Faybishenko, and D Agarwal. 2012. "Data-Driven Modeling of Radionuclide Inventory at the Savannah River Site F-Area Seepage Basins and Implications for Long-Term Behavior." *American Geophysical Union Meeting*, San Francisco, December 3-7, 2012.

CONFERENCE PROCEEDINGS

Dixon P, M Williamson, M Freshley, D Moulton, I Gorton, E Keating, Y Collazo, K Gerdes, and J Meza. 2011. "Advanced Simulation Capability for Environmental Management (ASCEM)." *Proceedings of the 14th International Conference on Environmental Remediation and Radioactive Waste Management*, ICEM2011, September 25-29, 2011, Reims, France.

Freshley M, V Freedman, S Hubbard, I Gorton, D Moulton, and P Dixon. 2012. "Advanced Simulation Capability for Environmental Management: Development and Demonstrations." *Waste Management Symposium*, February 26 – March 1, 2012, Phoenix, Arizona.

Gorton I, C Sivaramakrishnan, G Black, S White, S Purohit, M Madison, and K Schuchardt. 2011. "Velo: Riding the Knowledge Management Wave for Simulation and Modeling." In *Proceedings of the 4th International Workshop on Software Engineering for Computational Science and Engineering* (SECSE 2011), pp. 32-40. Association for Computing Machinery, New York.

Meza JC, JD Moulton, I Gorton, SS Hubbard, M Freshley, and P Dixon. 2011. "Advanced Simulation Capability for Environmental Management." *SciDAC*, July 10-14, 2011, Denver, Colorado.

Meza JC, SS Hubbard, MD Freshley, I Gorton, JD Moulton, and ME Denham. 2011. "Advanced Simulation Capability for Environmental Management (ASCEM): Early Site Demonstration." W*aste Management Symposium*, February 27-March 3, 2011, Phoenix, Arizona.

Seitz R, M Freshley, P Williamson, K Dixon, Y Gerdes, and Y Collazo. 2011. "Identification and Implementation of End-User Needs During Development of a State-of-the-Art Modeling Toolset." *Proceedings of the 14th International Conference on Environmental Remediation and Radioactive Waste Management*, ICEM2011, September 25-29, 2011, Reims, France.

Seitz RR, MD Freshley, P Dixon, SS Hubbard, V Freedman, B Faybishenko, G Flach, I Gorton, S Finsterle, JD Moulton, CI Steefel, and J Marble. 2013. "Advanced Simulation Capability for Environmental Management – Current Status and Phase II Demonstration Results." *Waste Management Symposium*, February 24-28, 2013, Phoenix, Arizona.

Zhu M, J Meza, D Moulton, I Gorton, M Freshley, P Dixon, R Seitz, J Wengle, R Patterson, and R Nelson. 2010. "A New Initiative for Developing Advanced Simulation Capabilities for Environmental Management (ASCEM)." *Proceedings Waste Management Conference*, March 7-11, Phoenix, Arizona.

DOE REPORTS

DOE – U.S. Department of Energy. 2010. *Advanced Simulation Capability for Environmental Management (ASCEM): Independent Peer Review and Assessment Team Report*. Office of Environmental Management, U.S. Department of Energy, Washington, D.C.

Freshley M, S Hubbard, V Freedman, and G Flach. 2012. *Phase II Demonstration Plan*. ASCEM-SITE-11-02, U.S. Department of Energy, Washington, D.C.

Gorton I, S Finsterle, K Schuchardt, C Gable, D Higdon, M Vessilinov, W McGinn, A Shoshani, and D Agarwal. 2010. *System Requirements for ASCEM Platform and Integrated Toolsets*. ASCEM-PIT-102610-Rev. 3, U.S. Department of Energy, Washington, D.C.

Hubbard S, B Faybishenko, M Freshley, D Agarwal, J Bell, W Bethel, M Denham, G Flach, V Freedman, G Hammond, D Higdon, J Horsman, E Keating, P Lichtner, L Monroe, P Monroe, P Moore, D Moulton, G Pau, D Schep, K Schuchardt, R Seitz, A Shoshani, N Spycher, and P Weber. 2010. *ASCEM Phase I Demonstration.* ASCEM-SITE-102010-0, U.S. Department of Energy, Washington, D.C.

Millings MR, BB Looney, and ME Denham. 2012. *Geochemical Modeling of F Area Seepage Basin Composition and Variability*. SRNL-STI-2012-00269, Rev. 0, Savannah River National Laboratory, Aiken, South Carolina.

Moulton D, M Berndt, M Buskas, R Garimella, L Prichett-Sheats, G Hammond, M Day, and J Meza. 2011. *High-Level Design of Amanzi, the Multi-Process High Performance Computing Simulator*. ASCEM-HPC-2011-030a, U.S. Department of Energy, Washington, D.C.

Seitz R, M Freshley, B Faybishenko, S Hubbard, D Watson, R Roback, J Blink, and A Armstrong. 2010. *User Suggestions and State of Practice for Development of ASCEM Requirements*. ASCEM-PM-10-05, U.S. Department of Energy, Washington, D.C.

Seitz R, M Freshley, P Dixon, and M Williamson. 2011. *ASCEM User Needs Report – FY 2011*. ASCEM-SITE-11-02, U.S. Department of Energy, Washington, D.C.

Steefel C, D Moulton, G Pau, K Lipnikov, J Meza, P Lichtner, T Wolery, D Bacon, N Spycher, J Bell, G Moridis, S Yabusaki, E Sonnenthal, G Zyvoloski, B Andre, L Zheng, and J Davis. 2011. *Mathematical Formulation Requirements and Specifications for the Process Models*. ASCEM-HPC-2011-01-0a, U.S. Department of Energy, Washington, D.C.

Appendix B – CURRENT AKUNA AND AMANZI CAPABILITIES

Table B.1. Akuna features and capabilities.

Feature/Capability	Description
Akuna Modeling Platform	A graphical user interface (GUI) tool for subsurface modeling and simulation • User environment for model creation and analysis • Model and simulation data and metadata management • Private and public workspaces • Simulation launching and monitoring for platforms ranging from desktops to HPC • Windows, Linux, and Mac platform support • Workflow dependency tracking and simulation management
Model Setup	Model setup including semi-automated structured and unstructured mesh generation • NASA World Wind interface for visualizing geographic locations, topography, and other site attributes • Object (region)-based material property and initial and boundary condition specifications • Semi-automated generation of structured and unstructured meshes with three-dimensional visualization
Parameter Estimation (PE)	Inverse modeling methods for automatically calibrating models to measured data • Levenberg-Marquardt algorithm with parallel evaluation of Jacobian matrix or Broyden update • Particle Swarm Algorithm (currently only serial) • Downhill Simplex Algorithm (currently only serial) • Automatic selection of relevant parameter combinations and estimation of super-parameters • Analysis of residuals • Determination of estimation uncertainty (linear/Gaussian) and prediction uncertainty
Uncertainty Quantification (UQ)	UQ tools to generate simulation input and analyze model results • Monte Carlo analysis using random parameter distributions or Latin-Hypercube sampling • Model runs launched in parallel; result read into Akuna or other software (e.g., MATLAB) • Statistical analysis and visualization of results • Markov-chain Monte Carlo analysis • Ensemble Kalman Filter

Feature/Capability	Description
Sensitivity Analysis (SA)	Local and global sensitivity analysis methods, executed in parallel • Local methods with user defined specific parameter perturbations • Robust and efficient global methods • Visualization of parameter design and sensitivity coefficients
Agni	Coupling of Akuna with Amanzi and other simulators • Drives simulations for PE and UQ • Unified interface for specification of analysis parameters and outputs • Common utilities and framework on which model analyses are built • Executes multiple simulations simultaneously using different parallelization methods • Creates simulator-specific input file, launches simulation, and extracts outputs • Executed as a standalone or driven by Akuna • Performs high-performance analyses of model results
Data Management	The ASCEM Observational Data Management System (AODMS) provides data management capabilities to • Import, organize, retrieve, and search various types of observational data sets supporting simulations • Browse data sets using map-based user interfaces • Search data using filters • Interface with visualization

Table B.2. Amanzi features and capabilities.

Feature/Capability	Description
Process Models/Kernels	
Single-Phase Saturated Flow	Darcy flow in steady-state or transient modes, with rock/soil compressibility
Single-Phase Unsaturated Flow	Richards equation for variably saturated steady-state and transient flow • Anisotropic-intrinsic permeability • Pressure, hydrostatic, flux, and seepage face boundary conditions • Dynamic water table • Mualem and Burdine relative permeability models • van Genuchten and Brooks–Corey water retention models
Nonreactive Transport	Advective transport in transient or steady-state variably saturated flow fields
Reactive Transport	Wide variety of geochemical reactions including • First-order aqueous reactions and aqueous complexation • Radioactive decay of aqueous and sorbed species • Mineral dissolution and precipitation • Ion exchange, equilibrium surface complexation • Sorption with K_d or Freundlich and Langmuir isotherms
Advanced Numerical Methods	
Flexible Model Specification	Modular design of Multi-Process Coordinator (MPC) • Process Kernels can be selectively turned on and off • Details of each Process Kernel specified in XML input file • Time evolution managed by sub-cycling process kernels in time if necessary • State object provides flexible data management capability for the simulation
Dual Unstructured/Structured Mesh Infrastructure	General unstructured polyhedral meshes readily capture complex geometries and natural features of the geologic framework models • Reads Exodus II meshes in serial (and partitions/distributes the mesh) or in parallel. • Supports 2D/3D polygonal/polyhedral meshes in large distributed settings. • Uniform API to external mesh frameworks, e.g., STKmesh(SNL), and MSTK (LANL) Block-Structured Adaptive Mesh Refinement (AMR) efficiently model engineered structures and barriers • Uses the BoxLib block-structured Adaptive Mesh Refinement (AMR) framework. • Structured patches enhance efficiency and are ideal for emerging architectures. • Dynamic refinement is based on fine-scale structural features (e.g., geometry of material interfaces and evolving solution features (e.g., contaminant plume)

Feature/Capability	Description
Advanced Discretizations	Mimetic Finite Difference (MFD) methods on unstructured meshes • No limitations on element shapes (e.g., capture pinch-outs with polyhedral elements), and no degeneracies at refinement interfaces. • Family of methods including second-order Finite Volume Methods • Design is open to various optimization criteria (e.g., monotonicity) • For block-structured Adaptive Mesh Refinement meshes, finite volume based methods are used with second-order Godunov treatment of nonlinear hyperbolic components
Adaptive Time Integration	Dynamic flow and reactive-transport conditions with rapid transients are captured efficiently through adaptive time stepping in the time integration of the model equations • Time control periods manage discontinuous changes in source or boundary conditions • Implicit time stepping with backward difference formulae for flow • Explicit time stepping is used for advective transport
Nonlinear/Linear Solvers	Variety of linear and nonlinear solvers available in Amanzi • Newton based nonlinear iteration strategies, including Newton-Krylov (NK) from Trilinos or PETSc, and Nonlinear Krylov Acceleration (NKA) • Preconditioners use either Jacobian-Free or semi-analytic Jacobian evaluation • Multilevel solvers from Trilinos (ML) or Hypre (AMG) for large-scale flow problems
HPC Core Infrastructure	Portable build system and automated testing framework • Mac OSX, and most Linux distributions (Windows is planned) • Builds Amanzi and all required third party libraries on a wide range of systems • Parallel input/output for restarts, visualization, and check pointing • Hierarchical testing framework supporting automated execution and reporting

Appendix C – GEOSTATISTICAL GENERATION OF DVZ CONCEPTUAL MODELS

The lithofacies used in mapping the BC Cribs area were identified based on K-means clustering of the spectral gamma ray data from four deep wells in the BC Cribs area. K-means clustering is an unsupervised classification method that partitions observations into a predefined number of groups, or clusters, by minimizing the differences between the observations and cluster centroids, which are iteratively updated. This was done outside the Akuna framework, but was necessary for the conceptual model descriptions. The four wells were the 299-E13-1, 299-E13-2, 299-E13-3, and 299-E13-6. The spectral gamma ray data used in the cluster analysis were averaged over 5-ft intervals for comparison with Rocsan particle size data, which was sampled at 5-ft intervals. Three lithofacies were identified by clustering of the thorium-232 (^{232}Th) and potassium-40 (^{40}K) data, and good separation occurs for the spectral gamma data for the three lithofacies (Table C.1). Facies 1 is dominantly sand, facies 2 is a sandy gravel, and facies 3 is a muddy sand (Figure C.1). After identification of the spectral gamma ray characteristics of the four wells used for classification, the lithofacies were estimated for an additional deep well, the 299-E13-62, using the thorium-232 and potassium-40 data from that well. Rocsan data were not available for the E13-62 well, so it was not included in the cluster analysis used to develop the lithofacies classification but was used in the variogram development

Table C.1. Indicator variogram models for the three lithofacies.

Spectral Gamma Data	Lithofacies	Proportion	Nugget	Sill	Vertical Range (m)	Horizontal Range (m)
^{40}K and ^{232}Th	1: S	0.494	0.13	0.87	28	280
	2: GS	0.408	0.35	0.65	30	300
	3: MS	0.098	0.35	0.23	10	100
				0.42	55	550

Variogram analysis and modeling (Goovaerts 1997) included identifying vertical indicator variograms for the five deep wells. Spherical variogram models (Goovaerts 1997) were fit to all of the experimental variograms and the relevant modeling parameters are listed in Table C.1. The five well locations did not provide sufficient data for establishing horizontal variograms across the simulation domain. Therefore, a 10:1 horizontal to vertical anisotropy ratio was assumed so that the horizontal variogram models could be developed (Table C.1).

One hundred three-dimensional realizations of the lithofacies were generated using sequential indicator simulation (Deutsch and Journal 1998). The simulation grid was based on a 60.1-degree rotation of the original coordinates around a pivot point of northing 573508.31, easting 134185.0, with an offset of -56.69 m in the easting, and 127 m in the northing to define the origin in the rotated space (Figure C.2). The horizontal grid resolution was 5 m with 1-m resolution in the vertical. There were 343,488 nodes in the simulation grid (Table C.2). Because wells were sparsely located within the domain of interest (only five deep wells within the simulation area), copies of lithofacies data from nearby wells were added at unsampled locations between existing wells to provide additional constraints on the

horizontal layering of the system. The extra conditioning locations are shown in Figure C.2. The block diagrams of the first two realizations are shown in Figure C.3, with the block cut near the locations of the 299-E13-62 and 299-E13-65 well locations.

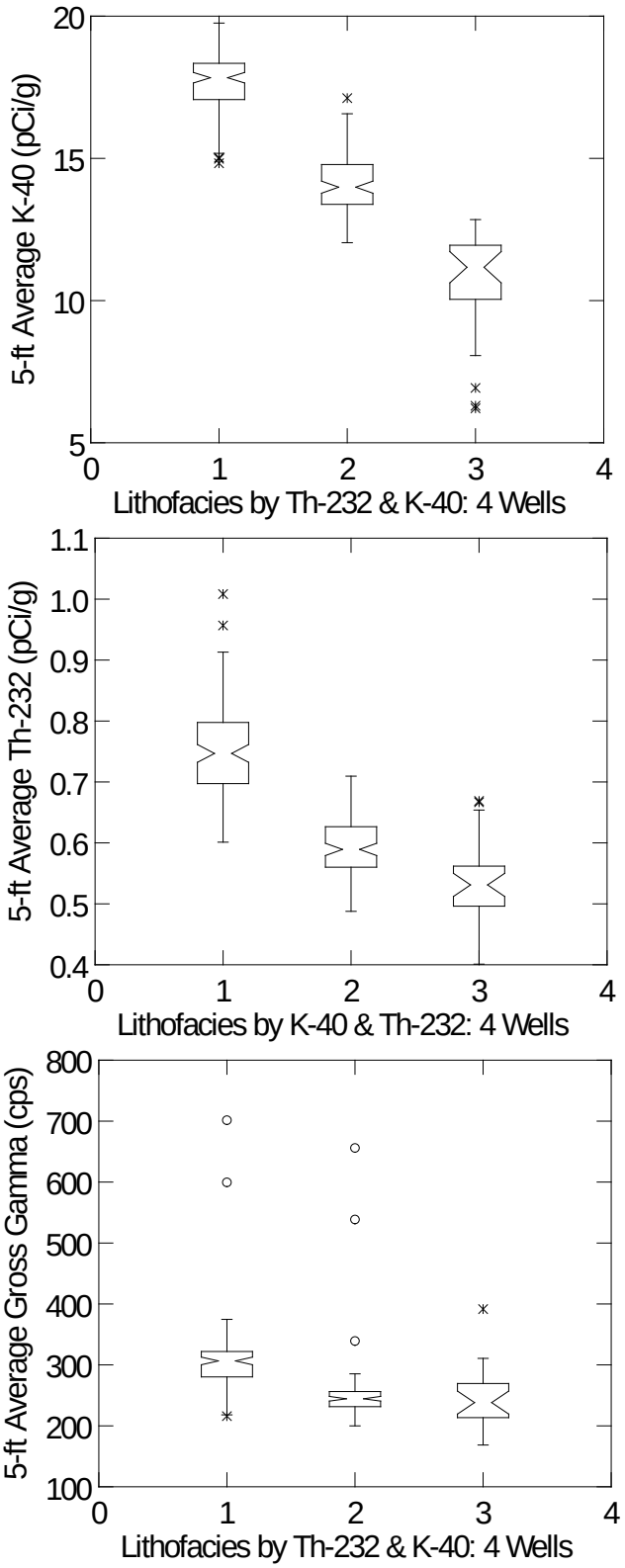

Figure C.1. Box plots of 5-ft average potassium-40, thorium-232 and gross gamma test data vs. lithofacies.

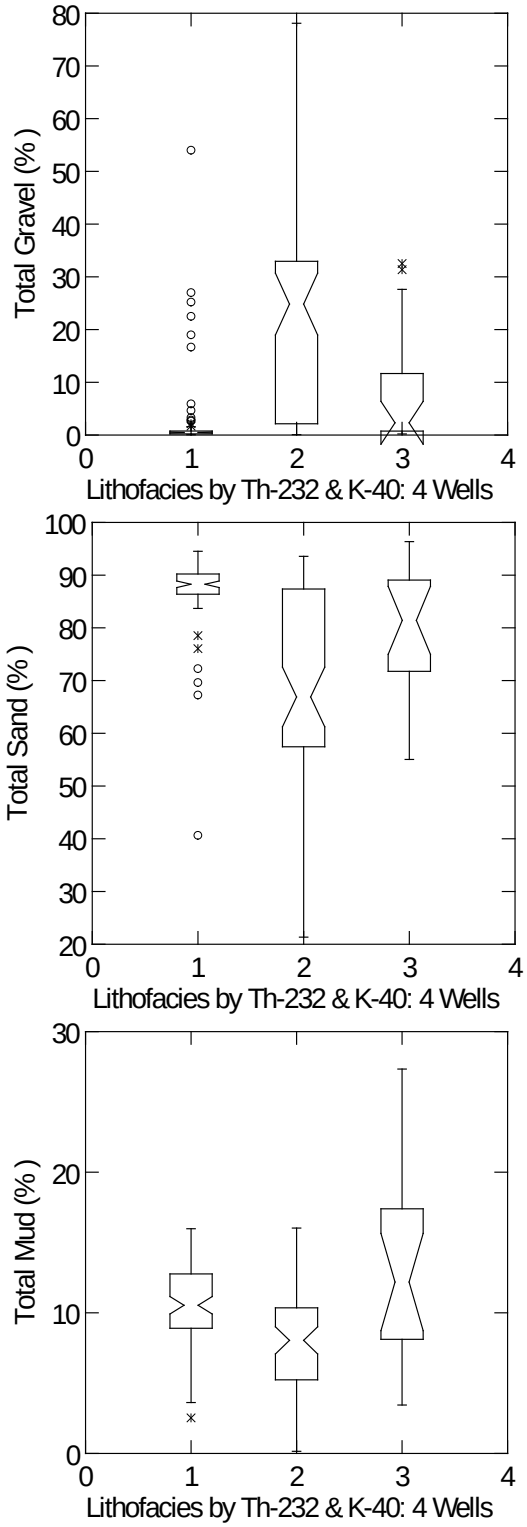

Figure C.2. Box plots of Rocsan grain size by lithofacies.

Table C.2. Grid dimensions in the rotated coordinate system.

Unit: m	Boundary Minimum	Boundary Maximum	Grid Node Minimum	Grid Node Maximum	Spacing	Number
X	0	320	2.5	317.5	5	64
Y	0	280	2.5	277.5	5	56
Z	120	227	120.5	226.5	1	107

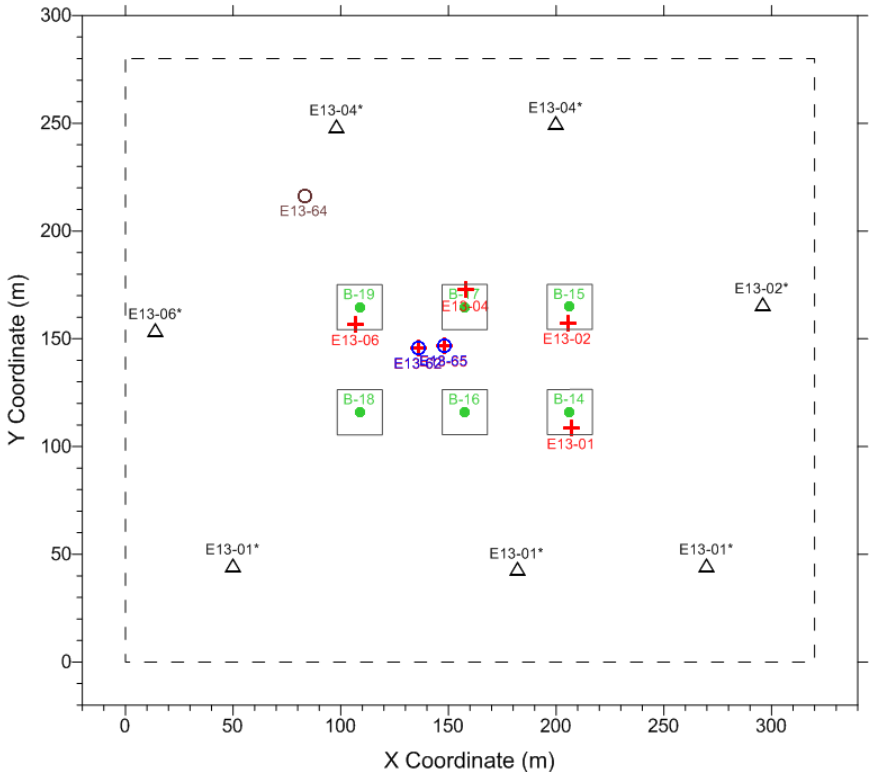

Figure C.3. Deep well locations (red), added conditioning wells (black), test wells (blue), and centers of cribs (green) in the rotated coordinate system. The boundary of the three-dimensional grid is marked in dashed lines.

References:

Deutsch CV and AG Journel. 1998. *GSLIB: Geostatistical Software Library and User's Guide, Second Edition.* Oxford University Press, New York.

Goovaerts P. 1997. *Geostatistics for Natural Resources Evaluation.* Oxford University Press, New York.

Appendix D – INPUT PARAMETERS AND ASSOCIATED UNCERTAINTIES FOR F-AREA UNCERTAINTY QUANTIFICATION AND HIGH-PERFORMANCE COMPUTING MODELS

Table D.1. General matrix of uncertain input parameters.

Input	Nominal Value (e.g., best-estimate or deterministic)	Uncertainty (e.g., distribution or range)	Comments/Basis
Boundary conditions			
Groundwater recharge	38 cm/y (15 in/y) per SRNL-STI-2009-00512, Rev. 0, Section 3.2.8.2, Table 3-13 (SRNL 2010); WSRC-TR-99-00248, Rev. 0, Table 4-1 (Flach et al. 1999);WSRC-TR-96-0399, Rev. 1, Vol. 2 (Flach and Harris 1999)	95% confidence interval = 30 to 46 cm/y (12 to 18 in/y) Mean/median = 38 cm/y (15 in/y) per SRNL-STI-2009-00512, Rev. 0, Table 3-13 (SRNL 2010); WSRC-TR-99-00248, Rev. 0, Table 4-1 (Flach et al. 1999); WSRC-TR-96-0399, Rev. 1, Vol. 2 (Flach and Harris 1999)	Long-term average net infiltration in General Separations Area under natural/nominal conditions. Confidence interval is consistent with posterior from Figure 6 of Balakrishnam et al. (2003); however, mean/median is lower. Field lysimeter studies produced best-estimates clustered around 15 in/yr (SRNL-STI-2009-00512,SRNL 2010). Calibrated groundwater flow models use recharge rates varying from around 12 in/yr at the low end (e.g., Young and Pohlmann (2003) cited in SRNL-STI-2009-00512 (SRNL 2010); WSRC-TR-99-00248 (Flach et al. 1999) to around 18 in/yr at the high end (e.g., WSRC-TR-96-0399, Rev. 1, Vol. 2 (Flach and Harris 1999). These observations suggest a symmetric distribution with a mean/median = 15 in/yr and a 95% confidence interval = +/- 3 in/yr.

Table D.1. (contd)

Input	Nominal value (e.g., best-estimate or deterministic)	Uncertainty (e.g., distribution or range)	Comments/basis
Lateral BCs	TBD	95% confidence interval = ± 0.9 m (3 ft) Calibration targets are typically screened at this level of uncertainty, and r.m.s. model agreement to targets is typically at this level WSRC-TR-96-0399, Rev. 1, Vol. 2, p. 9 and Table 7 (Flach and Harris 1999) WSRC-TR-2004-00106, Rev. 0, Table 3-1 (Flach 2004) WSRC-TR-99-00248, Rev. 0, p. 19 and Table 4-2 (Flach et al. 1999)	Prescribed head/pressure for a 2D model transect. Values assumed to be taken from potentiometric maps or model simulations based on long-term average well water levels (for hand contouring or model calibration).
Basin seepage during operations	Table 1 in SRNL-L6200-2010-00024 compiled from WSRC-RP-91-684 (Cummins et al. 1991)	±25% based on professional judgment	Net infiltration beneath basins (inflow plus rainfall minus evaporation/evapotranspiration) from 1955 through 1988. Uncertainty in evaporation is primary source of overall uncertainty?
Source loading – timing, composition, concentrations			
Radionuclide discharge to basins	Table 1 in SRNL-L6200-2010-00024 compiled from WSRC-RP-91-684 (Cummins et al. 1991)	±25% based on professional judgment	Uncertainty in evaporation is primary source of overall H-3 uncertainty? See Horton et al. (1971) and SRNL-L6200-2010-00024 for further discussion (Flach 2010a).
Chemical (bulk) composition of aqueous waste stream	Average values after Killian et al. (1986, DPST-85-704 Table 1) Reassessment of waste chemistry concentrations in SRNL-STI-2012-00269 (Millings et al. 2012)	2.7 < pH < 3.4 See SRNL-STI-2012-00269 (Millings et al. 2012) for further detail	SRNL-STI-2012-00269 (Millings et al. 2012), REVISION 0 provides a reassessment of waste chemistry concentrations.

Table D.1. (contd)

Input	Nominal value (e.g., best-estimate or deterministic)	Uncertainty (e.g., distribution or range)	Comments/basis
Base injection (funnel and gate system)			Base injection from 2004 to present. Actual injection not considered in Phase II Demonstration
Material properties			
Cover system (cap) physical properties - timing, layering, and hydraulic properties	Hydraulic conductivity: Attachments 1 and 9 in "F-Area HWMF Closure Plan Vol IV Book 1.pdf" (DOE 1991) Other properties: "Sand" or "Clay" in Tables 5-18 through 5-22 in WSRC-STI-2006-00198 (Phifer et al. 2006)	Hydraulic conductivity: 95% confidence interval = 0.5 to 1.0e-7 cm/s for clay layer based on data variability. For other layers, similarly assume a 95% c.i. range for log10K of 0.5 (half order of magnitude) Other properties: Tables 5-15 through 5-17 in WSRC-STI-2006-00198 (Phifer et al. 2006)	
Vadose soil physical and hydraulic (unsaturated hydraulic conductivity and water retention curves) properties	Tables 5-18 through 5-22 in WSRC-STI-2006-00198 (Phifer et al. 2006)	Tables 5-15 through 5-17 in WSRC-STI-2006-00198 (Phifer et al. 2006)	Updated with additional data from E-area report SRNL-STI-2011-00095 (Millings et al. 2011).
Aquifer hydraulic conductivity	See Table 2 below SRNL-L6200-2010-00025 for GSA-wide values (Flach 2010b)	Used facsimiles of the posterior distributions in Figure 6 of Balakrishnan et al. (2003)	The calibrated model described in WSRC-TR-2004-00106 (Flach 2004) may be useful for more localized nominal values.
Other aquifer physical properties	Section 5.6 of WSRC-STI-2006-00198 (Phifer et al. 2006)	Based on surrogate vadose zone materials and Tables 5-15 through 5-17 in WSRC-STI-2006-00198 (Phifer et al. 2006)	

Table D.1. (contd)

Input	Nominal value (e.g., best-estimate or deterministic)	Uncertainty (e.g., distribution or range)	Comments/basis
Reactive chemistry properties	Sorption-related parameters (site-specific surface area, site density, and surface complexation constant data are in Table D.2 and **Notes:** 1 Mean from Bea et al. (2012), STD= +/- 2(mean) 2 Mean from Bea et al. (2012), STD =11%. Covers the range of Table 5.9 in WSRC-STI-2006-00198 (Phifer et al. 2006) 3 Mean from Bea et al. (2012), STD = 1/2 perm. based on Levett scaling 4 Mean from Bea et al. (2012), STD =15% mean 5 STD = 10% Uncertainty range is +/- 20% (increased compared to Table D.1) 6 Uncertainty range is +/- 25% (increased compared to Table D.1) 7 (STD) = (range)/2 (based on SFA data and expert judgment) 8 Table D.3.	Sorption-related parameters (site-specific surface area, site density, and surface complexation constant data are in Table D.2 and **Notes:** 1 Mean from Bea et al. (2012), STD= +/- 2(mean) 2 Mean from Bea et al. (2012), STD =11%. Covers the range of Table 5.9 in WSRC-STI-2006-00198 (Phifer et al. 2006) 3 Mean from Bea et al. (2012), STD = 1/2 perm. based on Levett scaling 4 Mean from Bea et al. (2012), STD =15% mean 5 STD = 10% Uncertainty range is +/- 20% (increased compared to Table D.1) 6 Uncertainty range is +/- 25% (increased compared to Table D.1) 7 (STD) = (range)/2 (based on SFA data and expert judgment) 8 Table D.3.	Uncertainties provided by the Analytical Lab and statistical analysis of time series of concentration data.
Lithology and Facies			
Stratigraphy	Lithology from boreholes and CPT	+/- 1.5 m (5 ft)	Based on professional judgment of SRS geologists
Facies/interfacies analysis	Statistical analysis of lithological and CPT data--variogram analysis and kriging	+/- 1.5 m (5 ft)	
Inverse modeling data			

Table D.1. (contd)

Input	Nominal value (e.g., best-estimate or deterministic)	Uncertainty (e.g., distribution or range)	Comments/basis
Contaminant discharge to Fourmile Branch and wetlands	WSRC-RP-91-684 (Cummins et al. 1991)	TBD	Not included in Phase II Demonstration
Contaminant concentrations from wells, CPT, etc.	BEIDMS database	TBD	

TBD = To be determined.

Table D.2. Parameters used for TOUGHREACT simulations.

Flow parameters					Distribution				Notes
Parameter	Index	Unit	Ref.	Unit	Par_name	Distribution	Mean	std	
Permeability	1	UAZ	5.00E-12	[m^2]	k_ua	log10norm	-11.30	0.150	1
	2	TCCZ	1.98E-14	[m^2]	k_tc	log10norm	-13.70	0.500	
	3	LAZ	5.00E-12	[m^2]	k_la	log10norm	-11.30	0.150	
Porosity	4	UAZ	0.39	[-]	p_ua	norm	0.39	0.0468	2
	5	TCCZ	0.39	[-]	p_tc	norm	0.39	0.0468	
	6	LAZ	0.39	[-]	p_la	norm	0.39	0.0468	
Van Genuchten (alpha)	7	UAZ	4.00E-04	[$kg^{-1}\ m^{-1}\ s^2$]	a_ua	log10norm	-3.40	0.0750	3
Van Genuchten (m)	8	UAZ	0.27	[-]	m_ua	norm	0.27	0.0405	4
Geochemical parameters					Distribution				
Parameter	Index	Unit	Ref.	Unit	Par_name	Distribution	Mean	std	
Kaolinite reactive surface area (diss./prec.)	9	UAZ	2.07E+05	[$cm^2\ g^{-1}$]	kao_ua	norm	2.07E+05	2.07E+04	5
Goethite reactive surface area (diss./prec.)	10	UAZ	1.62E+05	[$cm^2\ g^{-1}$]	goe_ua	norm	1.62E+05	1.62E+04	
Kaolinite specific surface area (sorption)	11	UAZ	2.07E+05	[$cm^2\ g^{-1}$]	koh_ua	norm	2.07E+05	2.07E+04	
	12	TCCZ	2.07E+05	[$cm^2\ g^{-1}$]	koh_tc	norm	2.07E+05	2.07E+04	
	13	LAZ	2.07E+05	[$cm^2\ g^{-1}$]	koh_la	norm	2.07E+05	2.07E+04	
Goethite specific surface area (sorption)	14	UAZ	1.62E+05	[$cm^2\ g^{-1}$]	hoh_ua	norm	1.62E+05	1.62E+04	
	15	TCCZ	1.62E+05	[$cm^2\ g^{-1}$]	hoh_tc	norm	1.62E+05	1.62E+04	
	16	LAZ	1.62E+05	[$cm^2\ g^{-1}$]	hoh_la	norm	1.62E+05	1.62E+04	
Source parameters					Distribution				
Parameter	Index	Unit	Ref.	Unit	Par_name	Distribution	Mean	std	
Groundwater recharge factor	17		1	[-]	recharge	norm	1	0.1	6
Basin seepage rate factor	18		1	[-]	basin_wt	norm	1	0.125	7
Basin seepage chemical composition	19	pH	2.05	[-]	sc_h	norm	2.05E+00	2.56E-01	7
	20	nitrates	1.00E-02	[mol kgw^{-1}]	sc_no3	norm	1.00E-02	1.25E-03	7
	21	SO_4	4.80E-05	[mol kgw^{-1}]	sc_so4	norm	4.80E-05	6.00E-06	
	22	U(VI)	3.01E-05	[mol kgw^{-1}]	sc_u	norm	3.01E-05	3.76E-06	
	23	Ca	1.00E-05	[mol kgw^{-1}]	sc_ca	norm	1.00E-05	1.25E-06	
	24	Na	6.80E-05	[mol kgw^{-1}]	sc_na	norm	6.80E-05	8.50E-06	

Notes:

1 Mean from Bea et al. (2012), STD= +/- 2(mean)

Mean from Bea et al. (2012), STD =11%. Covers the range of Table 5.9 in WSRC-STI-2006-00198 (Phifer et al. 2006)

Mean from Bea et al. (2012), STD = 1/2 perm. based on Levett scaling

Mean from Bea et al. (2012), STD =15% mean

STD = 10%

Uncertainty range is +/- 20% (increased compared to Table D.1)

Uncertainty range is +/- 25% (increased compared to Table D.1)

(STD) = (range)/2 (based on SFA data and expert judgment)

Table D.3. Parameters used for Amanzi simulations

Flow parameters					Distribution			Notes
Parameter	Index	Unit	Ref.	Unit	Distribution	Mean	std	
Permeability	1	UAZ	5.00E-12	[m^2]	log10norm	-11.30	0.150	1
	2	TCCZ	1.98E-14	[m^2]	log10norm	-13.70	0.500	
	3	LAZ	5.00E-12	[m^2]	log10norm	-11.30	0.150	
Porosity	4	UAZ	0.39	[-]	normal	0.39	0.0468	2
Van Genuchten (m)	5	UAZ	0.27	[-]	normal	0.29	0.029	4
Geochemical parameters					Distribution			
Parameter	Index	Unit	Ref.	Unit	Distribution	Mean	std	
Site density	6	UAZ	0.15	[mol/m^3]	log10norm	-0.82	1.00	8
Cation exchange capacity	7	UAZ	2.75	[mol/m^3]	log10norm	0.44	1.00	
Kaolinite bulk surface area	8	UAZ	5.91E+04	[cm^2 mineral/cm^3 bulk]	log10norm	4.77	1.00	
Goethite bulk surface area	9	UAZ	1.11E+04	[cm^2 mineral/cm^3 bulk]	log10norm	4.04	1.00	
Source parameters					Distribution			
Parameter	Index		Ref.	Unit	Distribution	Mean	std	
Groundwater recharge factor	10	-	1.00	[-]	normal	1.00	0.100	6
Basin seepage rate factor	11	-	1.00	[-]	normal	1.00	0.125	7
Source pH	12	-	2.05	[-]	normal	2.05	0.125	7
Source U(VI)	13	-	3.01E-05	[mol kgw^{-1}]	normal	3.01E-05	3.76E-06	

Notes:

1 Mean from Bea et al. (2012), STD= +/- 2(mean)

2 Mean from Bea et al. (2012), STD =11%. Covers the range of Table 5.9 in WSRC-STI-2006-00198 (Phifer et al. 2006)

3 Mean from Bea et al. (2012), STD = 1/2 perm. based on Levett scaling

4 Mean from Bea et al. (2012), STD =15% mean

5 STD = 10%

6 Uncertainty range is +/- 20% (increased compared to Table D.1)

7 Uncertainty range is +/- 25% (increased compared to Table D.1)

8 (STD) = (range)/2 (based on SFA data and expert judgment)

Phase II Demonstration

References:

Balakrishnan S, A Roy, MG Ierapetritou, GP Flach, and PG Georgopoulos. 2003. "Uncertainty Reduction and Characterization of Complex Environmental Fate and Transport Models: An Empirical Bayesian Framework Incorporating the Stochastic Response Surface Method." *Water Resources Research* 39(12):1350. doi:10.1029/2002WR001810.

Bea SA, H Wainwright, N Spycher, B Faybishenko, S Hubbard, and ME Denham. 2012. "Identifying Key Controls on Acidic-U(VI) Plume Behavior at the Savannah River Site, Using Reactive Transport Modeling." *Journal of Contaminant Hydrology* (In Press).

Cummins CL, CS Hetrick, and DK Martin. 1991. *Radioactive Releases at the Savannah River Site 1954-1989 (U)*. WSRC-RP-91-684, Westinghouse Savannah River Company, Aiken, South Carolina.

DOE. 1991. *Closure Plan for F Area Hazardous Waste Management Facility, Savannah River Site*. Volume IV, Book 1, Revision 10, U.S. Department of Energy, Washington, D.C.

Flach G. 2004. *Groundwater Flow Model of the General Separations Area Using Porflow (U).* WSRC-TR-2004-00106, Westinghouse Savannah River Company, Aiken, South Carolina.

Flach G. 2010a. Letter to Mark Freshley et al. (PNNL) from Greg Flach (SRNL), "Source Term for ASCEM Phase I F-Seepage Basins Modeling Demonstration," July 29, 2010. SRNL-L6200-2010-00024, Savannah River National Laboratory, Aiken, South Carolina.

Flach G. 2010b. Letter to Mark Freshley et al. (PNNL) from Greg Flach (SRNL), "Input Data for a Phase I ASCEM F-Seepage Basins Flow Simulation," August 24, 2010. SRNL-L6200-2010-00025, Savannah River National Laboratory, Aiken, South Carolina.

Flach GP and MK Harris. 1999. *Integrated Hydrogeological Model of the General Separations Area (U); Volume 2: Groundwater Flow Model (U).* WSRC-TR-96-0399, Rev. 1, Westinghouse Savannah River Company, Aiken, South Carolina.

Flach GP, MK Harris, RA Hiergesell, AD Smits, and KL Hawkins. 1999. *Regional Groundwater Flow Model for C, K, L, and P Reactor Areas, Savannah River Site, Aiken, South Carolina (U).* WSRC-TR-99-00248, Rev. 0, Westinghouse Savannah River Company, Aiken, South Carolina.

Horton JH, JC Corey, and RM Wallace. 1971. "Tritium loss from water exposed to the atmosphere." *Environmental Science & Technology* 5:338-343.

Killian TH, NL Kolb, P Corbo, and IW Marine. 1986. *Environmental Information Document, F-Area Seepage Basins*. Report No. DPST 85-704, E.I. du Pont de Nemours & Co, Savannah River Laboratory, Aiken South Carolina.

Millings M, L Bagwell, M Amidon, and K Dixon. 2011. *Sediment Properties: E Area Completion Project, Savannah River Site*. SRNL-STI-2011-00095, Revision 0, Savannah River Laboratory, Aiken South Carolina.

Millings MR, BB Looney, and ME Denham. 2012. *Geochemical Modeling of F Area Seepage Basin Composition and Variability*. SRNL-STI-2012-00269, Rev. 0, Savannah River National Laboratory, Aiken, South Carolina.

Phifer MA, MR Millings, and GP Flach. 2006. *Hydraulic Property Data Package for the E-Area and A-Area Soils, Cementitious Materials and Waste Zones*. WSRC-STI-2006-00198, Rev. 0, Westinghouse Savannah River Company, Aiken, South Carolina.

SRNL. 2010. *Integrated Hydrogeological Model of the General SRNL, 2010, Savannah River Site DOE 435.1 Composite Analysis*. SRNL-STI-2009-00512, Savannah River National Laboratory, Aiken, South Carolina.

Young M H and KF Pohlmann. 2003. *Analysis of Vadose Zone Monitoring System: Computer Simulation of Water Flux under Conditions of Variable Vegetative Cover: E-Area Disposal Trenches.* Publication No. 41188, Division of Hydrologic Sciences, Desert Research Institute, Las Vegas, Nevada.

Appendix E – SURFACE COMPLEXATION MODEL AND GEOCHEMISTRY INPUT PARAMETERS FOR F-AREA AMANZI SIMULATIONS

This appendix provides information about the surface complexation model and geochemistry input used for modeling in the SRS F-Area Phase II Demonstration.

E.1. Surface Complexation Model

A new complexation model was developed to demonstrate the performance of coupling of the Agni-Amanzi capabilities for the UQ analysis. This model replaces the more complicated electrostatic model, which was previously used for F-Area simulations with the TOUGHREACT code (Xu et al. 2006) based on LBNL SFA research (Bea et al. 2012; Dong et al. 2012). The new form is a nonelectrostatic surface-complexation model, which is based on an assumption that the geochemical processes controlling the uranium migration rate in groundwater are described by combination of a single-site surface complexation model and an ion exchange model. The sorption reaction provides a direct pH effect on the mobility of uranium according to the reaction

$$>\mathrm{SOH} + \mathrm{UO_2^{2+}} \leftrightarrow >\mathrm{SOUO_2^{+}} + \mathrm{H^{+}} \qquad \text{(E-1)}$$

where $>\mathrm{SOUO_2^{+}}$ refers to the uranium-bearing surface complex developed on sediment grain surfaces.

To determine the stoichiometry and associated equilibrium constant for the reaction, James Davis of LBNL (as part of the LBNL SFA project) used experimental data from six contaminated sand sediments collected at the Savannah F-Area. These six sediment samples were used to carry out a total of 36 batch experiments. These represent a set of contaminated sediments that are not the same as the uncontaminated sediments investigated by Dong et al. (2012). Only experiments in the pH range of 3–6 were used in determining a best fit of 0.44 for the log Ks. In his analysis, Davis assumed that the site density is 3.84×10^{-6} mol_sites/m^2 sediment (~2.3 sites/nm^2), which is a generally agreed canonical value (Davis and Kent 1990), and used 2.36 m^2/g for the average sediment specific surface area (Dong et al. 2012). The resulting estimate of the site density is 9.1×10^{-6} mol sites/g sediment. Assuming a sediment density of 2.65 cm^3/g and a porosity of 35%, a bulk site concentration of 15.61 mol/m^3 porous medium is calculated. However, preliminary one-dimensional simulations with the Amanzi, PFLOTRAN (Hammond et al. 2012) and CrunchFlow codes showed that this value of the bulk site concentration resulted in virtually no U(VI) mobility over a transport distance of 1 m or less after 50 years. Because the batch experiments were conducted using the <2-mm size fraction, the results are likely biased toward a higher value for the equilibrium constant than is applicable at the field scale. To adjust the site concentration value, the reference value in the UQ analysis was decreased by 2 orders of magnitude to 0.156 mol/m^3 (see Table D.3 in Appendix D).

The mineral phases used to represent the geochemical system were kaolinite, goethite, and quartz. Secondary phases are schoepite, gibbsite, basalaluminate, jurbanite, and opal, which are allowed to form if supersaturated. The other important geochemical effect is pH buffering by sorption on the mineral surfaces. The pH evolves as a function of time because of buffering by the surface complexation and mineral reactions. Cation exchange reactions were considered in the Amanzi UQ runs to capture the pH buffering via sorption on mineral surfaces (in addition to pH buffering by mineral dissolution and precipitation reactions); see Table E.1. Preliminary Amanzi simulations using an initial CEC of 24.9 equivalents/m^3 bulk sediment (Table D.3) resulted in almost no pH buffering from sorption reactions, in contrast with the results obtained with TOUGHREACT. A bulk CEC value of about 12.5 μequivalents/g is reasonable for kaolinite-dominated sediment but low for typical sediments (e.g., a CEC of 50–120 μequivalents/g was determined for sediments from the Hanford 200 Area (Steefel et al. 2003). Therefore, for the Agni-Amanzi UQ simulations, the average CEC was adjusted to slightly higher values (Table D.3) to capture the pH, while the surface complex site concentration was lowered so as to provide reasonable base case for the simulation.

D.2. Geochemistry Input for Amanzi F-Area Simulations.

The geochemical system used by Amanzi is based on a preliminary version of the system described by Bea et al. (2012), which was used for the TOUGHREACT UQ study at the F-Area as described in Section 2.2.1.3. However, as described above, the electrostatic surface complexation and pH buffering model used in Bea et al. (2012) system was replaced with a single nonelectrostatic surface complexation reaction (Equation E-1) and a set of cation exchange reactions on a single bulk sediment site (as shown in Table E.2). The geochemical processes considered for the Phase II Demonstrations include aqueous complexation, mineral dissolution and precipitation, and adsorption/desorption. We considered a system with

thirteen primary species (H^+, Al^{3+}, Ca^{2+}, Cl^-, Fe^{3+}, $CO_2(aq)$, K^+, Mg^{2+}, Na^+, $SiO_2(aq)$, SO_4^{2-}, NO_3^-, UO_2^{2+}) and eight minerals. A tritium tracer subject to radioactive decay was also included. A detailed list of aqueous complexation reactions is included in Table E.3. The same uranium aqueous complexes used by Bea et al. (2012) were used in the Amanzi simulations, with the same dissociation constants and reaction stoichiometries before corrections to account for different carbonate basis species. The detailed mineral reactions are included in Table E.2. The kinetic rate constants for mineral dissolution and precipitation (Table E.4) are the "neutral" rate constants from Bea et al. (2012). Although Amanzi allows for varying some geochemical parameters on a material-by-material basis, these parameters were not available, so the initial mineral volume fractions and surface areas were applied uniformly across the domain (Table E.5). The geochemical constraints, Table E.6, consist of a pH 2 waste infiltration and a pH 5.4 solution applied uniformly across the domain as the background initial condition and as fresh water infiltration at the boundaries.

Table E.1. Surface complexation and cation-exchange reactions implemented in the Amanzi simulations.

Reaction	$\log_{10}$ K (25° C)
[(1)]Equilibrium Surface Complexation	
	-0.44
[(2)]Cation Exchange	K (25 C)
	1.0
	0.316
-	1.71
	0.025

[(1)]Bulk site concentration 0.1801 [moles sites m^{-3}], based on estimate from Davis (personal communication, 2012).
[(2)]Cation-exchange, Gaines-Thomas convention

Table E.2. Mineral dissolution/precipitation reactions considered in the Amanzi simulations.

Reaction	$\log_{10}$ K (25° C)	Ref.
$\text{Quartz} \leftrightarrow \text{SiO}_2(\text{aq})$	-3.7501	(1)
$\text{Kaolinite} \leftrightarrow 2\text{Al}^{+3} + 2\text{SiO}_2(\text{aq}) + 5\text{H}_2\text{O} - 6\text{H}^+$	7.57	(2)
$\text{Goethite} \leftrightarrow \text{Fe}^{+3} + 2\text{H}_2\text{O} - 3\text{H}^+$	0.1758	
$\text{Schoepite} \leftrightarrow \text{UO}_2^{+2} + 3\text{H}_2\text{O} - 2\text{H}^+$	4.8443	(1)
$\text{Gibbsite} \leftrightarrow \text{Al}^{+3} + 3\text{H}_2\text{O} - 3\text{H}^+$	7.738	(3)
$\text{Jurbanite} \leftrightarrow \text{Al}^{+3} + \text{SO}_4^{-2} + 6\text{H}_2\text{O} - \text{H}^+$	-3.8	(4)
$\text{Basaluminite} \leftrightarrow 4\text{Al}^{+3} + \text{SO}_4^{-2} + 15\text{H}_2\text{O} - 10\text{H}^+$	22.251	(4)
$\text{Opal} \leftrightarrow \text{SiO}_2(\text{aq})$	-3.005	(5)

[(1)] SNL [2007], within error margins of Guillaumont et al. [2003].
[(2)]Yang and Steefel [2008].
[(3)]Pokrovskii and Helgeson [1995].
[(4)]Nordstrom [1982].
[(5)]Sonnenthal and Spycher [2000].

Table E.3. Aqueous complexes considered in the Amanzi simulations. Equilibrium constants are taken from the default PFLOTRAN database.

Reaction	$\log_{10}$ K (25° C)
$OH^- \leftrightarrow H_2O - H^+$	13.99
$AlOH^{2+} \leftrightarrow Al^{3+} + H_2O - H^+$	4.96
$Al(OH)_2^+ \leftrightarrow Al^{3+} + 2H_2O - 2H^+$	10.59
$Al(OH)_3(aq) \leftrightarrow Al^{3+} + 3H_2O - 3H^+$	16.16
$Al(OH)_4^- \leftrightarrow Al^{3+} + 4H_2O - 4H^+$	22.88
$CaOH^+ \leftrightarrow Ca^{2+} + H_2O - H^+$	12.85
	5.3
	13.35
	16.67
	6.34
	16.16
	6.19
$NaOH(aq) \leftrightarrow Na^+ + H_2O - H^+$	14.78
-	13.69
$Mg(OH)^+ \leftrightarrow Mg^{+2} + H_2O - H^+$	11.79
	5.31
$(UO_2)_2(OH)_2^{2+} \leftrightarrow 2UO_2^{2+} + 2H_2O - 2H^+$	5.63
	17.57
$(UO_2)_2OH^{3+} \leftrightarrow 2UO_2^{2+} + H_2O - H^+$	2.71
	46.13
$(UO_2)_3(OH)_4^{2+} \leftrightarrow 3UO_2^{2+} + 4H_2O - 4H^+$	11.93
$UO_2(OH)_4^{2-} \leftrightarrow UO_2^{2+} + 4H_2O - 4H^+$	33.03
$(UO_2)_3(OH)_5^+ \leftrightarrow 3UO_2^{2+} + 5H_2O - 5H^+$	15.59
$(UO_2)_3(OH)_7^- \leftrightarrow 3UO_2^{2+} + 7H_2O - 7H^+$	31.05
	16.06
$(UO_2)_4(OH)_7^+ \leftrightarrow 4UO_2^{2+} + 7H_2O - 7H^+$	21.95
$UO_2NO_3^+ \leftrightarrow UO_2^{2+} + NO_3^-$	-0.28
$UO_2(OH)^+ \leftrightarrow UO_2^{2+} + H_2O$	5.21
$UO_2(OH)_2(aq) \leftrightarrow UO_2^{2+} + 2H_2O - 2H^+$	10.31
$UO_2(OH)_3^- \leftrightarrow UO_2^{2+} + 3H_2O - 3H^+$	19.22
	7.01

	16.44
	28.46
	22.84
	19.32
	23.91
$UO_2SiO(OH)_3^+ \leftrightarrow SiO_2(aq) + UO_2^{2+} + 2H_2O - H^+$	2.48

Table E.4. Mineral kinetic parameters(1) used in the Amanzi simulations.

Mineral	k_i	p
Quartz	$10^{-13.345}$	0.0
Kaolinite	$10^{-12.967}$	0.777
Goethite	$10^{-7.94}$	0.0
Schoepite	$10^{0.301}$	0.0
Gibbsite	$10^{-11.5}$	0.0
Jurbanite	10^{-8}	0.0
Basaluminite	10^{-8}	0.0
Opal	$10^{-12.135}$	0.0

(1) Reaction rate expression:

$$R_i = \left[k_i a_{H+}^{p}\right](1-\Omega)$$

Table E.5. Initial mineral volumetric fractions and mineral properties considered in the Amanzi simulations.

Mineral	vol. frac. [-]	surface area [$cm^2\ cm^{-3}$]	molar volume [$cm^3\ mol^{-1}$]
Quartz	0.88	3262.3	22.68
Kaolinite	0.11	59093.9	99.52
Goethite	0.016	11076.3	20.82
Schoepite	0	0.1	66.08
Gibbsite	0	0.1	31.95
Basaluminite	0	0.1	218.93
Opal	0	0.1	29.0
Jurbanite	0	0.1	126.0

Table E.6. Chemical composition for the background and seepage solutions used in the Amanzi simulations.

Component	Background and Infiltration	Seepage	Units
pH	5.4	2.05	[-]
Na	2.78×10^{-4}	$^{(1)}3.05 \times 10^{-4}$	[mol kgw^{-1}]
Cl	$^{(1)}9.98 \times 10^{-3}$	3.39×10^{-5}	[mol kgw^{-1}]
CO_2(aq)	$^{(2)}1.23 \times 10^{-5}$	$^{(2)}1.07 \times 10^{-5}$	[mol kgw^{-1}]
Al	$^{(5)}2.2 \times 10^{-8}$	10^{-8}	[mol kgw^{-1}]
Fe(III)	$^{(3)}2.5 \times 10^{-16}$	$^{(3)}2.41 \times 10^{-6}$	[mol kgw^{-1}]
K	3.32×10^{-5}	1.72×10^{-6}	[mol kgw^{-1}]
Ca	10^{-5}	10^{-5}	[mol kgw^{-1}]
Mg	5.35×10^{-3}	2.47×10^{-6}	[mol kgw^{-1}]
U(VI)	1.25×10^{-10}	3.01×10^{-5}	[mol kgw^{-1}]
Nitrates	10^{-3}	10^{-2}	[mol kgw^{-1}]
SO_4	2.25×10^{-5}	4.8×10^{-5}	[mol kgw^{-1}]
SiO_2(aq)	$^{(4)}1.77 \times 10^{-4}$	1.18×10^{-4}	[mol kgw^{-1}]
^3H	10^{-15}	2.17×10^{-9}	[mol kgw^{-1}]
$P_{CO2(g)}$	$10^{-3.5}$	$10^{-3.5}$	[atm]

(1) Charge Balance
(2) Equilibrium with CO_2(g)
(3) Equilibrium with Goethite
(4) Equilibrium with Quartz
(5) Equilibrium with Kaolinite

References:

Bea SA, H Wainwright, N Spycher, B Faybishenko, S Hubbard, and ME Denham. 2012. "Identifying Key Controls on Acidic-U(VI) Plume Behavior at the Savannah River Site, Using Reactive Transport Modeling." *Journal of Contaminant Hydrology* (In Press).

Davis JA and DB Kent. 1990. "Surface Complexation Modeling in Aqueous Geochemistry." *Reviews in Mineralogy and Geochemistry* 23:177-260.

Dong W, TK Tokunaga, JA Davis, and J Wan. 2012. "Uranium(VI) adsorption and surface complexation modeling onto background sediments from the F-Area Savannah River site." *Environmental Science & Technology* 46(3):1565-1571.

Guillaumont R, T Fanghanel, J Fuger, I Grenthe, V Neck, DA Palmer, and MH Rand. 2003. "Update on the Chemical Thermodynamics of Uranium, Neptunium, Plutonium, Americium, and Technetium." *Chemical Thermodynamics 5*, OECD Nuclear Energy Agency, etd., Elsevier, Amsterdam.

Hammond GE, PC Lichtner, C Lu, and RT Mills. 2012. "PFLOTRAN: Reactive Flow and Transport Code for Use on Laptops to Leadership-Class Supercomputers. In *Ebook: Groundwater Reactive Transport Models*, F Zhang, GT Yeh, and JC Parker (eds.), Bentham Science Publishers, pp. 141-159, eISBN: 978-1-60805-306-.
doi: 10.2174/978160805306311201010141.

Nordstrom DK. 1982. "Aqueous Pyrite Oxidation and the Consequent Formation of Secondary Iron Minerals." In *Acid Sulfate Weathering*, JA Kittrick, DS Fanning, and LR Hossner (eds.), *Soil Science Society of America* Publication 10:37-56.

Pokrovskii VA and HC Helgeson. 1995. "Thermodynamic properties of aqueous species and the solubilities of minerals at high pressures and temperatures: The system Al_2O_3-H_2O-NaCl." *American Journal of Science* 295, 1255–1342.

SNL – Sandia National Laboratories. 2007. *Qualification of Thermodynamic Data for Geochemical Modeling of Mineral-Water Interactions in Dilute Systems*. ANL-WIS-GS-000003, Rev. 01, TJ Wolery and CF Jove Colon (eds.), Sandia National Laboratories, Las Vegas, Nevada. ACC: DOC.20070619.0007.

Sonnenthal E and N Spycher. 2000. *Drift-Scale Coupled Processes Model, Analysis and Model Report (AMR) N0120/U0110*. Yucca Mountain Nuclear Waste Disposal Project, Lawrence Berkeley National Laboratory, Berkeley, California.

Steefel CI, S Carroll, P Zhao, and S Roberts. 2003. "Cesium Migration in Hanford sediment: A multi-site cation exchange model based on laboratory transport experiments." *Journal of Contaminant Hydrology* 67:219-246.

Xu T, E Sonnenthal, N Spycher, and K Pruess. 2006. *TOUGHREACT User's Guide: A Simulation Program for Non-Isothermal Multiphase Reactive Geochemical Transport in Variably Saturated Geologic Media*. LBNL-55460, Lawrence Berkeley National Laboratory, Berkeley, California.

Yang L and CI Steefel. 2008. "Kaolinite dissolution and precipitation kinetics at 22°C and pH 4." *Geochimica Cosmochimica Acta* 72(1):99-116.